MICROWAVE SYNTHESIS AND OCCLUSION REACTIONS OF ZEOLITES

by

ANN ELIZABETH TAYLOR

A thesis submitted to
The University of Birmingham
for the degree of
DOCTOR OF PHILOSOPHY

UNIVERSITY OF BIRMINGHAM

School of Chemistry
The University of Birmingham
July 2007

UNIVERSITY OF
BIRMINGHAM

University of Birmingham Research Archive

e-theses repository

This unpublished thesis/dissertation is copyright of the author and/or third parties. The intellectual property rights of the author or third parties in respect of this work are as defined by The Copyright Designs and Patents Act 1988 or as modified by any successor legislation.

Any use made of information contained in this thesis/dissertation must be in accordance with that legislation and must be properly acknowledged. Further distribution or reproduction in any format is prohibited without the permission of the copyright holder.

Synopsis

The work presented in this volume covers two distinct fields of zeolite chemistry. The first section of this thesis is dedicated to the synthesis of zeolites A (LTA), X (FAU), Y, (FAU) and rho (RHO) in a microwave oven. Results have demonstrated that when zeolitic gels are heated in a microwave oven they yield zeolite crystals far quicker than when heated in a conventional oven. This is in part a consequence of the rapid heating of the zeolitic gel caused by the microwave radiation, however, this alone is not responsible for such dramatic reductions in synthesis times. An examination of the effect of reagents on the crystallisation of zeolites in a microwave oven is undertaken.

The other portion of this thesis focuses on the ion exchange and occlusion reactions undergone by zeolites A (LTA), ZK-4 (LTA) and rho (RHO) in the presence of monovalent metal nitrates. In some cases non-framework peaks are seen in the powder X-ray diffraction patterns of occluded samples. These peaks are attributed to the formation of a superlattice within the zeolite cavities. Particular attention is given to the structural identification of the silver nitrate superlattice formed within zeolite A.

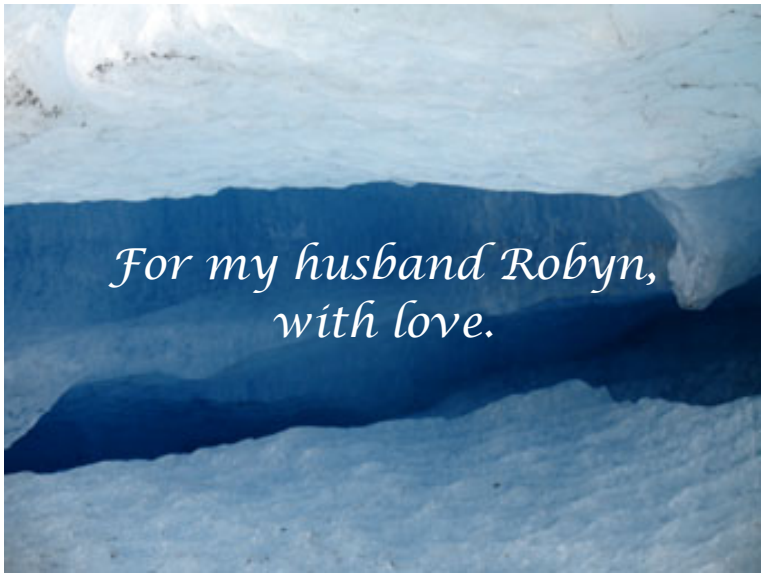
For my husband Robyn,
with love.

Acknowledgements

I extend thanks to my supervisor, Dr Paul Anderson, whose advice and guidance throughout my PhD and undergraduate project have been invaluable. Thank you for seeing me through my crises of (chemical) faith and putting up with my many piles of X-ray data. Thank you to EPSRC for funding throughout my PhD studies.

My greatest debt is owed to my husband Robyn, without whose encouragement, motivational speeches and chauffeuring ability none of this would have been possible. Thanks are also due to my family for their support throughout my university career.

Dr Martin Viertelhaus and Dr Ian Gameson have also been a great help and source of knowledge – thank you both for being so patient with my questions about space groups! I must also thank Martin for his assistance with dehydrated zeolites.

Thanks to the students in the Anderson group, especially Phil for his assistance with last minute bits and bobs. I must also thank the staff and students of Level 5 for helping me with the use of new or unfamiliar equipment. For assistance and training in all things microwave, I send my gratitude to Dr Martin Jones and Pete Wilkinson.

It is also necessary to thank the staff of the Department of Metallurgy and Materials for training me to use the electron microscopy equipment. Thanks are due to Dr Simon Kitchin for running my ^{29}Si NMR samples and his assistance in their interpretation.

I would also like to say a big “thank you” to Michael Pedley who found, photocopied and forwarded me an obscure reference which I had trouble locating.

The help of Emma Mansley at the Geology Department in The University of Leicester with zeolite sample analysis was also of importance. My thanks to you.

I would like to thank my former chemistry teachers, Dr K. Hodge and Dr S. Banks, for inspiring me to enjoy and study chemistry at each stage of my secondary education. Your enthusiasm for the subject you taught encouraged my interest in chemistry.

Thanks also to my friends for helping me through my time here in Birmingham and making these past few years such a happy time: Simon, Lynn, Chris and Mel – your company on (too many!!!) tea breaks has been a valuable part of keeping me sane and motivated.

My final thanks go to all the ALS gang and all my virtual friends at FT.

CONTENTS

Chapter 1: Introduction to Zeolites

Chapter 2: Experimental Techniques

Chapter 1: Introduction to Zeolites

1. Introduction to Zeolites

The Swedish mineralogist, Cronstedt, was the first to discover zeolites, and their name derives from the Greek meaning 'boiling stone' – so called because their behaviour, when strongly heated alone, gave the appearance of boiling as water within the material left the structure. Since their first discovery in 1756, many different structures have been identified – some naturally occurring and some purely synthetic.

1.1 Structure

Zeolites are aluminosilicates with a regular microporous framework. They consist of $[SiO_4]^{4-}$ and $[AlO_4]^{5-}$ tetrahedra which are corner-linked in three dimensions. When connected in such a manner the $[SiO_4]^{4-}$ units form a neutral framework of formula SiO_2. However, the substitution of aluminium (with one less nuclear charge compared to silicon) into the structure creates a negative charge, thus making the overall framework negative. A consequence of this is the presence of non-framework cations located in the channels and pores of the zeolite. These cations are most commonly from the alkali metal and alkaline earth groups due to the high pH at which zeolites are synthesised. A further result of the formal negative charge associated with the aluminium tetrahedra is Lowenstein's Rule, which states that there may be no Al-O-Al linkages present in a hydrothermal synthesis. This is because it is not as favourable to have clusters of negative charge as having them distributed evenly throughout the framework. Also to be found in the zeolite cages is a large amount of water. This information is best represented by the general formula for a zeolite:

$$M^{n+}_{x/n}[Al_xSi_yO_{2x+2y}]^{x-}.zH_2O$$

The M signifies the cations of charge *n* to balance the framework charge, *x*. As can be seen, more siliceous zeolites will have fewer cations present, which results in their increased hydrophobic character.

It is also possible for other elements to take the place of silicon or aluminium tetrahedra in the framework. These elements are typically phosphorous, gallium and germanium. This class of materials, is referred to as *zeotypes*[1].

As has previously been mentioned, the cations are not a physical part of the framework. In hydrated zeolites, the cations are weakly bonded to the framework and intrapore water, whereas in dehydrated zeolites, the cations are more strongly bound to the framework structure. This means it is possible to exchange these ions for different cations, either by stirring the zeolite in an aqueous solution or, less commonly, via solid state ion exchange (SSIE) which involves grinding and heating the zeolite with an appropriate salt[2]. Care must be taken to avoid degradation of the zeolite structure through use of acid salts or solutions. Ion exchange will be discussed in more detail later in this chapter (see page 5) and in chapter 4.

The charge, size and location of the cations within the zeolite framework affect the properties of the zeolite, particularly in relation to ion exchange and catalysis. The dimensions of the zeolitic channels and oxygen windows dictate what can or cannot enter the zeolite framework. However, some positions within the zeolite may still be inaccessible due to cations obstructing openings. Due to vibrations of the crystal, particularly at elevated temperatures, and framework flexibility, some molecules with a notional size slightly larger than the zeolite ring openings may sometimes enter the structure. A fascinating example of the influence of temperature on molecule absorption into a zeolite is illustrated by the sieving properties of zeolite A (LTA structure type) at temperatures below –100°C. Despite a difference in size of only 0.2 Å between O_2 and N_2 (critical dimension ~2.8 Å and ~3.0 Å respectively[3]), oxygen can be selectively taken up by zeolite A. As temperatures are increased the lattice vibrates more and the selectivity is lost as the aperture allows both oxygen and nitrogen through[4].

There are many crystallographically distinct sites which can be occupied by cations – indeed there are usually many more sites than necessary for charge neutrality of the zeolite. Cations therefore have a variety of locations to occupy, and factors such as their charge, size and distance from each other dictate where they will be most stably sited.

1.2 Uses of Zeolites

Zeolites have many important industrial applications. The regular network of channels and cavities provide an excellent means of separating species (hence their other name "molecular sieves").

1.2.1 Catalysis

The large internal surface area of zeolites can be exploited for catalytic purposes and they can be highly selective, especially when the pore sizes are manipulated, for example by ion exchange. The role of zeolites in catalysis encompasses three different areas of selectivity which make use of the pore size[1,5]:

1. Reactant selective catalysis: here reagents can only enter the zeolite, and hence gain access to the catalytic site, if their size is less than the pore diameter.
2. Product selective catalysis: only products of the appropriate size may leave the cavity. Different products have different diffusion rates out of cavities.
3. Transition state catalysis: due to the limited room in the cavity, some transition states cannot occur, this limits the reactions which may take place, and ultimately affects the product.

There are many advantages of zeolites over other high surface area catalysts: they can be

made to be very selective (and hence give fewer by-products and a purer product), have a large number of catalytic sites per unit volume, and a more regular structure, which produces more reproducible results. The reproducibility and selectivity is dependent on zeolite sample purity, as other products could form in any zeolite impurities present (as these would have different cavity sizes, allowing different reagents in and products out).

Maxwell[6] discusses the use of zeolite Y (FAU) as a catalyst in the petrochemicals industry. Its use in Fluid Catalytic Cracking (FCC) processes is advantageous for five reasons:

1. High activity levels
2. Low coke forming tendency
3. High organic nitrogen and NH_3 resistance
4. Regenerability
5. Molecular shape selectivity.

1.2.2 Ion Exchange

Zeolites can also function as ion exchangers. As previously mentioned, the cations associated with the tetrahedral aluminium ions are not part of the framework, and are available for exchange. This principle is applied in water filters, water softeners and detergents, where Na^+ ions in zeolite A are put into the water, as Ca^{2+} and Mg^{2+} ions from the hard water are taken up in their place[5]. Ion exchange is also applied to clean up of nuclear waste: for example, clinoptilolite can pick up ^{137}Cs [1].

Ion exchange is limited by the pH of the solution, as below pH 3-4 the aluminium in the framework is attacked, and the structure destroyed. Hence high Si/Al ratios are more stable at low pH.

1.2.3 Other Uses

Dehydrated zeolites can be used as drying agents because they will absorb moisture[1,5]. This is a result of the cation, which was co-ordinated to the water, having moved to a less stable, lower co-ordination site. The zeolite drying agent can be re-dehydrated and reused. When dehydrated, zeolites can also act as adsorbents, with hydrophobic zeolites having the potential ability to remove organic molecules from aqueous solutions[5].

Zeolites have found many agricultural applications[7], the majority using the natural zeolite, clinoptilolite. These include use in removing harmful heavy metals and PCBs (poly-chlorinated biphenyls) from soil on farmland. The use of zeolites as slow release fertilisers has been reported[7,8]. The fertiliser is stored within the zeolite and is applied to the area required. During rain or watering the fertiliser is released from the zeolite into the soil gradually over a period of time. This prevents the sudden release of fertiliser into the environment, which can then result in its being washed away into rivers and groundwater, causing pollution. The same principle can be applied to weed killers[3] and insecticides[7]. Zeolites can also be used as part of animal litter, and can then be used as fertilisers to release the beneficial nutrients evenly into the soil.

The addition of 1–2% by weight of zeolites to animal feed has been shown to provide benefits[7,9,10]. It is reported that the zeolites in the feed can degrade natural toxins formed by fungus in the crop being fed to the animals. This led to better health and an increase in animal body mass.

Ozin[11] has reviewed some more unusual potential uses of zeolites, including in electrical and optical applications, such as lasers, batteries and sensors. The zeolite laser, for example, consists of zeolite ZSM-5 hosting guest molecules to increase the frequency of incident

radiation.

As can be seen from the many examples, zeolites have wide ranging uses in everyday life. With so many industrial applications, there is great demand for zeolites. Therefore, rapid and efficient syntheses which yield products of high purity are of paramount importance.

1.3 Synthesis

The manner in which zeolite syntheses are carried out has a bearing upon the products yielded and their quality. It is therefore important to examine the factors which influence the outcome of zeolite synthesis reactions.

1.3.1 Reagents

The reagents are the most obvious and significant factor in any synthesis[1,12]. Purity of reagents is key to forming the appropriate product free from impurities.

Zeolites, being aluminosilicates, require a source of silicon, aluminium and oxygen. Charge balancing cations are also necessary, and are usually supplied in the form of a hydroxide. Aluminium is often supplied in the form of alumina or sodium aluminate, although other sources are available. Silica sources are wide ranging, but most commonly used are fumed silica, colloidal silica and sodium metasilicate. Details of literature studies into the effect of the silica source are outlined in chapter 3: "Microwave Synthesis", where experiments examining the influence of silica source were carried out. Another consideration is whether to use seed crystals (see Section 1.3.4 below) to aid the formation of the desired zeolite.

Some zeolites are only formed in the presence of a template or structure-directing agent that

promotes a particular structure. For a true template the zeolite should only form in the presence of the cation, for example, offretite (OFF) and zeolite Ω (MAZ) only form if the tetramethylammonium (TMA^+) cation is present in the gel[13]. It is believed that the TMA^+ ion directs the formation of the gmelinite cage common to both the OFF and MAZ structures.

1.3.2 pH

Gel pH also plays an important role in determining the composition and structure of the zeolite formed[14]. Zeolites are crystallised from gels with a high pH, often over 12. The pH influences the quantity of species in solution, and therefore available for reaction, and this impacts on the rate of product formation[15]. Research examining the effects of gel pH is discussed in more detail in chapter 3: "Microwave Synthesis".

1.3.3 Reaction Vessels

As a consequence of the high pH used, standard borosilicate glass is an inappropriate reaction vessel. Leaching of silicon from the glass may occur, altering the quantity of silicon in the gel and hence affecting not only the Si/Al ratio, but perhaps the product formed. Durable plastic containers are more commonly used. It is necessary to thoroughly clean the containers between use, or at least use them for one zeolite type only, as any crystals remaining from previous reactions may act as seed crystals.

1.3.4 Ageing and Seeding

Once the gel is made, it can either be heated straight away, or left to age at room temperature prior to use. The ageing process is said to provide a period for nuclei to form, which are the building blocks of the final crystals. Traditionally nucleation takes place in the initial heat up period of the gel to reaction temperature. However, if microwave heating is employed, the slow heat up phase is effectively eliminated, and the ageing step is beneficial. If the

precursor nuclei are present already then the crystallisation stage can occur sooner and reduce the heating time necessary.

As an alternative to ageing, seed crystals, or even 10% by weight of aged gel, can be added to the zeolite gel[16]. After adding the aged gel or seed crystals, the rate of crystallisation was found to be enhanced compared to unaged zeolite gels.

1.3.5 Stirring

Stirring during the ageing process or reaction can cause an increase in collisions between species in solution, and prevents a local depletion of reagents around the forming crystals. In some instances this may be beneficial and lead to a reduction in reaction time, through increased rates of nucleation. However, stirring may also break down existing species and stimulate production of undesired structures. For example, in the synthesis of zeolite Na-X (FAU), Freund[17] performed the same reaction with differing stirring speeds ranging from 0 to 350 rpm. Whilst the time taken to yield crystalline products decreases with increasing stirring speed, the purity is compromised by the co-crystallisation of zeolite Na-P (GIS).

1.3.6 Nucleation and Crystal Growth

Barrer described the processes involved in crystallisation of a zeolitic product[3]. Firstly, small aggregates form unstable nuclei, some of which grow large enough to become stable nuclei, whilst the others redissolve. Material in the solution is deposited on the stable nuclei, and these form crystallites. This process is relatively slow, as the crystals form by a condensation polymerisation[3].

1.3.7 Heating Conditions

The heating conditions for the precursor gel tend to mimic those which form zeolites in

nature. Naturally occurring zeolites are often found in lava flows or volcanic sediments, and so temperatures over 200°C and high pressures (> 100 bar) were typically used in early syntheses. With the use of reactive alkali-metal aluminosilicate gels, however, lower temperatures and pressures can be used enabling synthesis to take place at around 100°C and under autogenous pressure.

Ostwald's Law of successive transformation is very important in the consideration of zeolite synthesis. According to the law, the first phase formed during a reaction is thermodynamically the least stable, and is replaced by ever more stable phases until the most stable product is formed. However, in some instances, thermodynamically unfavourable products may persist if there is a significant activation energy barrier to the more stable phase[18]. All zeolite structures are metastable with respect to more dense phases.

Due to these transformations, if a relatively unstable product is desired, it is essential that the reaction be stopped at the appropriate time and the product isolated by filtration. This removes the structure from the reaction medium, and therefore it can no longer be broken down and further transformed as solid-state rearrangements have a prohibitively large energy barrier[3].

Finally, there is the choice of whether to heat the gel in a microwave oven or conventional oven. As will be discussed in chapter 3: "Microwave Synthesis", there are many advantages in opting to use a microwave oven.

1.4 Introduction to the Zeolite Structures

A number of different zeolites have been investigated in the course of this research. A brief outline of the structures, syntheses and uses of each is given below.

1.4.1 Zeolite A and ZK-4 - LTA

The structure of zeolite A can be viewed in two ways. It can be seen as either face-sharing α-cages linked by the 8 ring, or sodalite (β) cages linked by a double 4 ring. The size of the unit cell is sometimes given as ~12.3 Å (depending on the cations within the structure and the exact Si/Al ratio), as this is the size of the smallest repeating unit, and the space group is $Pm\bar{3}m$ (number 221). The silicon to aluminium ratio is ~1, so in order for Lowenstein's rule to be obeyed the Si and Al atoms must alternate to prevent Al-O-Al linkages, but the $Pm\bar{3}m$ space group does not take this silicon and aluminium ordering into account. When the regular alternation of Si and Al is to be considered, the 12.3 Å unit cell must be doubled, so the true unit cell is 24.6 Å. This new, larger, unit cell has a higher symmetry space group of $Fm\bar{3}c$ (number 226).

The formula of zeolite A is known to be $[Na_{96}(H_2O)_{216}][Si_{96}Al_{96}O_{384}]$ with the sodium ions being available for exchange. This leads to its most common use as an ion exchanger in products such as washing powders where the sodium is swapped for calcium. Typical zeolite A syntheses take 3.5 hours at 99°C.

On the next page, Figure 1.1 shows a representation of the LTA structure. For clarity, only the tetrahedral Si and Al atoms are shown, and these are located at the intersection of the bonds. The oxygen atoms are found approximately half way along the bonds, depicted by the lines. No cations, salts or intrapore water are shown in the interests of maintaining a clear diagram.

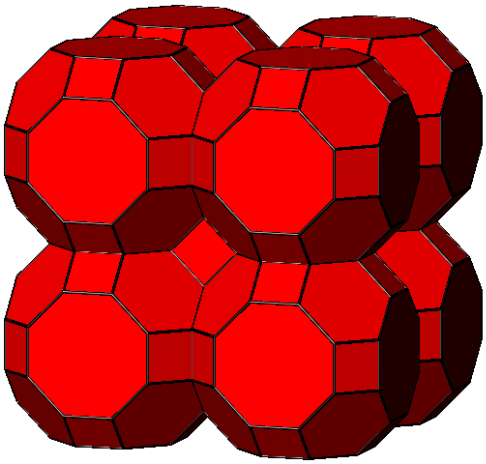

Figure 1.1: Representation of the LTA structure

Zeolite ZK-4 also has the LTA structure and was first synthesised and developed by Kerr[19,20]. Due to the use of the large cation tetramethylammonium hydroxide (TMAOH) in the synthesis, the quantity of aluminium present in the zeolite framework is far lower than in zeolite A. The proportion of silicon to aluminium present in the structure is over 1 and can reach values as high as 3[21].

Resulting from the increased level of silicon in the framework, relative to zeolite A, is a reduction in the lattice parameter for zeolite ZK-4. Bonds between silicon and oxygen are shorter than those between aluminium and oxygen, hence there is a contraction in the unit cell size for zeolite ZK-4, which depends upon the exact Si/Al ratio of the sample.

A consequence of the use of a bulky cation in the production of ZK-4, is that the as-synthesised zeolite will not undergo ion exchange as the TMAOH has a diameter of ~6.0-6.5 Å, compared to the channel opening of ~5 Å. To remove the TMAOH cation, it is necessary to calcine the zeolite at 500°C under flowing oxygen for 24 hours. Once calcined and ion-exchanged to the sodium form, zeolite ZK-4 can adsorb a greater quantity of

n-paraffins than sodium zeolite A[19]. This is because there are fewer Na^+ per unit cell in zeolite ZK-4 than in zeolite A, as a result of the reduced level of aluminium in the framework, which means there is a greater volume available to adsorb molecules.

1.4.2 Zeolites X and Y – FAU

Zeolites X and Y are iso-structural, both belonging to the faujasite (FAU) class of zeolites. The difference between these two forms is the silicon to aluminium ratio. Zeolite X has the lower ratio with Si/Al between 1 and 1.5. The ratios commonly encountered for zeolite Y are between 1.5 and 3, although it is possible to have a greater proportion of Si present. Zeolite X was the first to be synthesised and was patented in 1959[22], with the patent for zeolite Y following in 1964[23].

The FAU structure consists of sodalite cages linked by double 6 rings, with a space group of $Fd\bar{3}m$ (number 227). The lattice parameter for zeolite X is a = 24.86 – 25.02 Å and for zeolite Y, a = 24.61 – 24.85 Å[4].

Zeolite Y has found use in the petrochemical industry in the process of fluid catalytic cracking[6].

The synthesis of zeolite X is often performed at 80°C over 24–48 hours. Zeolite Y has a marginally shorter heating period of 19 hours, and this is undertaken at 90°C.

Figure 1.2 on the following page is a representation of the FAU structure. As before, the Si and Al atoms are found at the intersection of the black bonds. Oxygen atoms (which are not shown) are located approximately half way along the bonds.

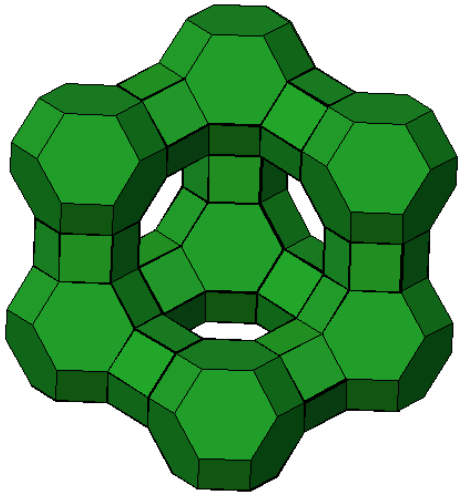

Figure 1.2: Representation of the FAU Structure

1.4.3 Zeolite Rho (RHO)

The structure of zeolite rho is similar to that of zeolite A (LTA) in that there are α-cages linked via 8-rings. In zeolite rho, however, the linkages are *double* 8 rings. The space group of the RHO structure is $Im\bar{3}m$ (number 229). The framework is fairly flexible and when dehydrated the round 8-ring oxygen windows become elliptical and the volume of the unit cell decreases by approximately 10 %[24]. This results in the structure adopting the lower symmetry space group $I\bar{4}3m$. When hydrated, zeolite rho typically has a lattice parameter of ~15.03 Å, although this of course depends on the Si/Al ratio, which usually lies between 2 and 5.

The depiction of the RHO structure on the following page was drawn using the same conventions as previously used. The lines which represent bonds intersect, and at the intersection is the Si or Al atom. Approximately midway between the Si or Al atoms, is the position of the oxygen, which for clarity has not been included.

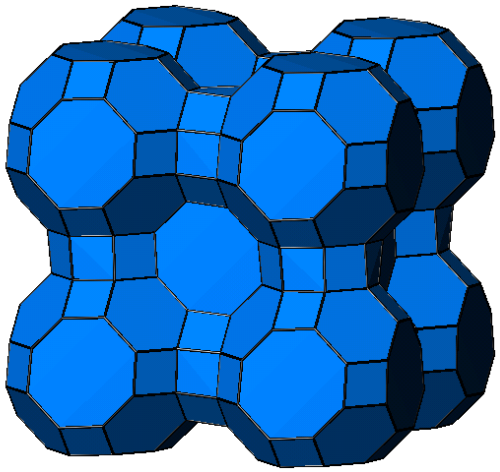

Figure 1.3: Representation of the RHO structure

The synthesis of zeolite rho is a delicate art, and conditions can vary. In his patent, Robson describes reactions as taking between 7 and 21 days at temperatures from 70 to 80°C[25]. Work by Edmondson studied the optimum conditions for ageing and heating of zeolite rho gels[26]. The results demonstrated that a successful synthesis required ageing of the gel at room temperature for 24 hours prior to heating at 80°C for 5–6 days.

Zeolite rho contains caesium in addition to sodium as a counter ion. The level of caesium present in the synthesis mixture determines the purity of the final product[27]. An excess of caesium can favour the formation of chabazite or pollucite, whereas a low concentration can cause faujasite to be produced. Due to the variable success rate of the synthesis, few commercial uses have been found for zeolite rho. One proposed use is in the methanol amination reaction[28].

1.4.4 Pollucite - ANA

Whilst not directly a focus of research in the present work, circumstances arose which gave cause to study pollucite and its uses.

Pollucite, $CsAlSi_2O_6$, which has the analcime structure, is denser than typical zeolites, but is still classed as such. Pollucite has found industrial importance as a result of its high melting point (>1900°C) and low thermal expansion coefficient. These uses include high temperature applications, for example in combustors or nozzle flaps in aircraft engines[29], as well as the ability to take up the radioactive isotope ^{137}Cs.

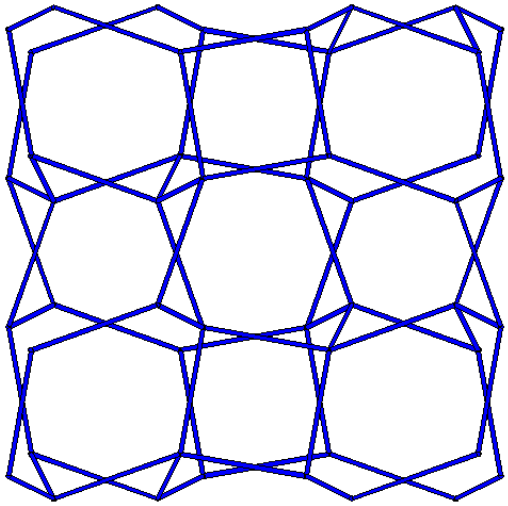

Figure 1.4: Representation of the ANA structure

Pollucite synthesis has been outlined in various journals[29-31], and the routes used are diverse – all have used different reagents and heating conditions. MacLaren's group synthesised pollucite in autoclaves under hydrothermal conditions at 220°C for 24 hours[29]. Yanagisawa *et al*[30] used induction heating, a method similar to microwave synthesis. The reactions were most successful when carried out at 200 and 300°C for 10 minutes.

The synthesis route used by Gallagher and McCarthy[31] was far more complex and involved high temperature solid-state reactions. Most samples were ground and pressed into pellets before heating in furnaces at temperatures between 600 and 1200°C, depending on the reagents. Synthesis tended to involve 4 grinding and heating stages, which means that a reaction could take up to 4 days to yield a single pollucite pellet.

Chapter 2: Experimental Techniques

2. Experimental Techniques

Many methods can be used to determine the structure and composition of materials, including ^{29}Si MAS NMR, EDX, SEM and X-ray diffraction. By far the most commonly undertaken of these for routine analysis is powder X-ray diffraction. EDX and NMR can be used to find the Si/Al ratio of the zeolite, while SEM can give images of the powder formed.

2.1 Powder X-ray Diffraction

2.1.1 Diffraction Criteria

For diffraction to occur, the wavelength of the incident radiation must be comparable to the separation of the objects through which it passes. In the case of X-ray diffraction techniques, the object must be crystalline, i.e. have a regular repeating structure. For diffraction effects to be seen the diffracted waves must be in phase, and therefore create constructive interference.

A crystal is composed of atoms linked in a repeating pattern, with the smallest repeating unit referred to as the unit cell. The separation of atoms is of the same order of magnitude as the wavelength of X-rays, which is why X-ray diffraction is an appropriate analytical tool.

2.1.2 Production of X-rays

To produce X-rays, electron beams are fired at a metal target, most commonly copper or molybdenum[1]. The beam knocks out an electron from the 1s (K) orbital of the metal atom. An electron from the 2p (L) or 3p (M) orbital drops down to the 1s level to fill the vacancy. The 2p → 1s transition gives the Kα line and the 3p → 1s gives rise to the Kβ line. Due to spin multiplicity in the p orbital the spin state of the electron determines whether the lines are $K\alpha_1$ or $K\alpha_2$. These lines both have distinctive energies, and their wavelengths depend on the

element used, and lie in the X-ray region of the electromagnetic spectrum. To form a monochromatic beam, the radiation is passed through a filter or diffracted by a crystal monochromator[1].

2.1.3 Data Collection

The X-ray beam is aimed at the powder sample and is scattered by the crystal lattice. Due to the presence of an effectively infinite number of randomly orientated crystallites, the X-rays are scattered through 2θ in all directions. The detector moves through a range of 2θ values, commonly between 5° and 50° for zeolites, and intersects these 'cones' of intensity. Depending on the structure, there will be peaks of scattered intensity in various 2θ positions which are related to the lattice spacing. Figure 2.1 below illustrates this set up.

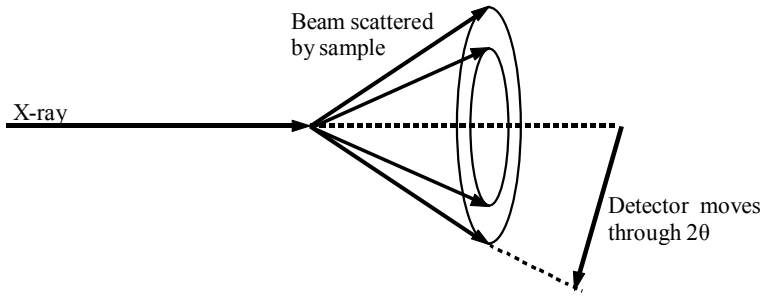

Figure 2.1: Sample set up in the X-ray beam

The atoms can be considered as lattice points which lie on lattice planes. The parallel and equally spaced lattice planes of a particular (hkl) are separated by a fixed distance known as the d-spacing. The planes intercept the axes of the unit cell at (a,b,c) dividing it into equal amounts. The fraction at which this occurs is 1/h, 1/k and 1/ℓ on the a, b and c axes respectively. The reciprocal of these fractions (h,k,l) are the Miller Indices. These relate to the peaks in the X-ray diffraction pattern.

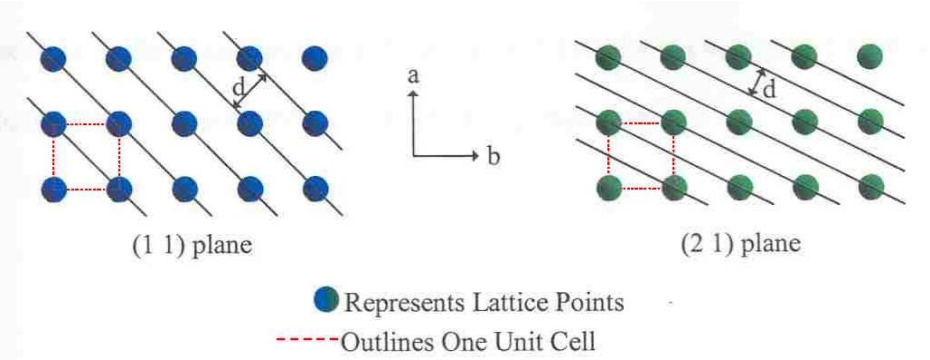

Figure 2.2: Lattice planes in 2 dimensions

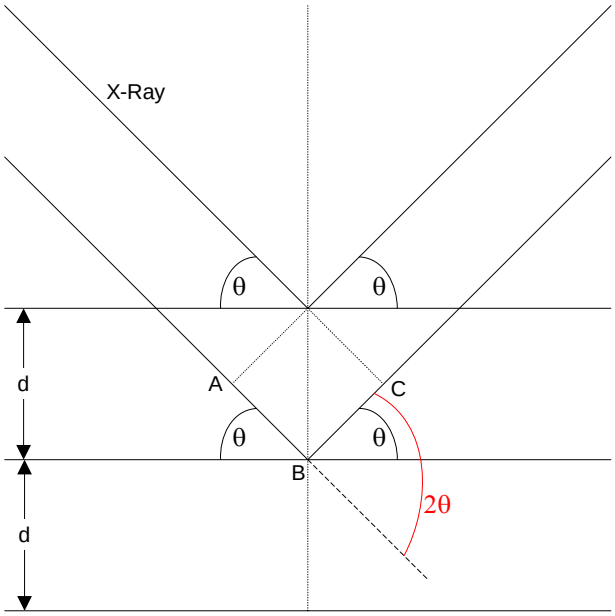

Figure 2.3: Reflection from Lattice Planes.

The beam is diffracted by 2θ relative to its original path, and it is this value recorded by the X-ray diffractometer.

The diagram in Figure 2.3 above, illustrates the interaction of X-rays with lattice planes. The difference in path length between the two X-rays shown is equal to AB + BC, and this must be equal to a whole number for the wavelengths (nλ) to create constructive interference, and hence contribute to a peak of intensity in the X-ray diffraction pattern.

i.e.:

$$AB + BC = n\lambda$$

One of the right-angled triangles (taken from Figure 2.3) is shown in Figure 2.4 below. From simple trigonometry it is possible to derive the Bragg equation.

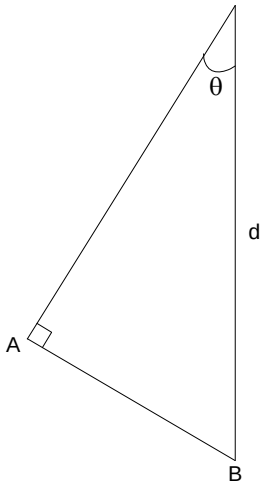

Figure 2.4: Detail of a right-angled triangle from Figure 2.3

$$\sin\theta = \frac{O}{H} = \frac{AB}{d}$$

Rearranging this gives:

$$AB = d\sin\theta$$

The same equations are true for BC, therefore:

$$AB + BC = 2d\sin\theta$$

As stated earlier, AB plus BC must be equal to an integer number of wavelengths (nλ) for constructive interference to occur. Substituting this into the above equation gives Bragg's equation:

$$n\lambda = 2d\sin\theta \qquad \text{Equation 2.1}$$

where n is an integer, λ is the wavelength of the X-ray, *d* the spacing of the planes and θ is the

angle between the X-ray and the lattice plane.

From the diffraction pattern, various pieces of information allow the lattice parameter, a, to be determined. All peaks in the X-ray diffraction pattern must be assigned their (hkl) values. The d-spacing for each peak is known and so equation 2.2 below (which is only valid for cubic structures) can be used to find the size of the unit cell.

$$a = \sqrt{d^2\left(h^2 + k^2 + l^2\right)} \qquad \text{Equation 2.2}$$

where *a* is the lattice parameter and *d* the spacing of the planes. There are other equations for non cubic lattices, but these are not relevant to the structures studied in this work.

The positions of the peaks can yield information about the size, symmetry and ultimately Si/Al ratio of the unit cell (this requires calculation of the lattice parameter, see above and page 28). This enables us to identify the structure as well as determining whether any impurities are present. Peak widths provide a clue as to the crystal size (see section 2.1.4) – narrow peaks are due to large crystals in the sample. Peak intensities can yield information about unit cell contents (see section 2.1.5).

2.1.4 Estimation of Crystal Size from Peak Widths

The width of a peak in an X-ray diffraction pattern is inversely proportional to the size of the crystal, i.e. the smaller the crystal, the broader the peak. Figure 2.5 on the next page illustrates how peak broadening can occur.

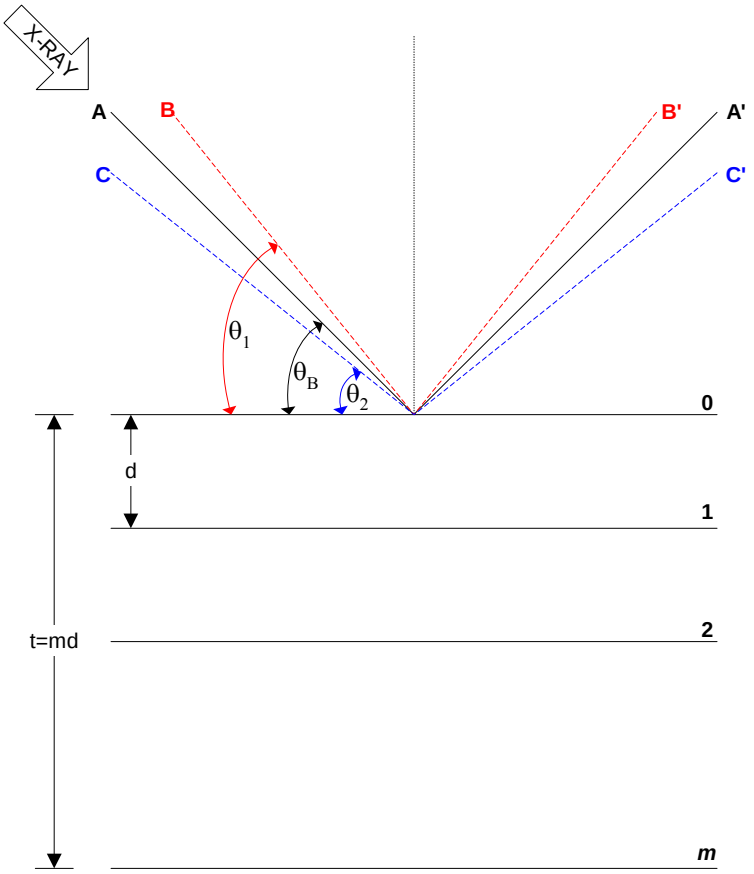

Figure 2.5: Origin of peak broadening (adapted from Cullity[2])

X-ray A makes the Bragg angle, θ_B, X-rays B and C make the angles θ_1 and θ_2, respectively. The diffraction process seen for these three rays is repeated for all layers of the crystal.

The thickness of the crystal, t (Å) is equal to the number of layers, *m*, multiplied by the d-spacing (Å).

For diffracted X-rays, such as A', which make the Bragg angle, the waves are in phase and constructively interfere to contribute to the peak maxima. The angles θ_1 and θ_2, which are close to the Bragg angle, are made by the X-rays B and C. These diffracted X-rays are slightly out of phase causing incomplete destructive interference. This creates smaller intensity peaks (i.e. broadening) around the peak at θ_B. The broad peaks are not seen for large crystals because there are sufficient layers that waves at θ_1 and θ_2 from deeper within the crystal will be exactly out of phase with θ_1 and θ_2 at the surface of the crystal, and thus the

waves are cancelled out leaving narrow peaks. However, small crystals lack the layers deep within the crystal to cancel out the rays at θ_1 and θ_2. Therefore, the peaks are broader in a small crystal[2]. The broad peaks have a shape similar to that shown in Figure 2.6 below.

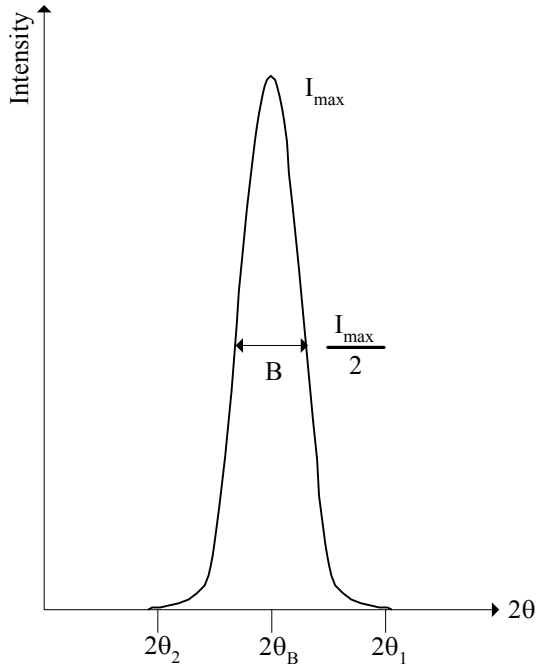

Figure 2.6: An example of a broad peak obtained in a powder X-ray diffraction pattern.

I_{max} is the maximum peak intensity and $\frac{I_{max}}{2}$ is half the value of I_{max}.

The θ values are as defined in Figure 2.5.

By finding the value 'B' (in radians) – known as the full width half at maximum height (FWHM) – it is possible to estimate the thickness of the crystals which gave rise to the peak. However, it should be noted that even large crystals would give rise to a peak of finite width. Therefore, it is the *broadening* relative to a "normal" peak that needs to be considered, rather than the actual peak width. This means that peak widths should be measured in an X-ray diffraction pattern considered to be of good quality, and the average peak width found. This value should then be deducted from that of the wide peaks whose broadening needs to be determined. The Scherrer Equation (2.3) can then be used for the calculation of crystal size.

$$t = \frac{0.9\lambda}{B\cos\theta}$$ Equation 2.3

t is the thickness of the crystal in Angstroms (Å), λ is the wavelength of the X-rays (Å) and θ is the value of the Bragg angle (i.e. the angle of the peak maximum). B is the FWHM of the broad peak after correcting for intrinsic instrumental line broadening and must be in radians, not degrees.

The determination of crystal size by this means is a useful way of judging how well formed a sample is, in the absence of SEM images.

2.1.5 Peak Intensity

Each atom in the unit cell has a scattering factor, f_j, which is proportional to the atomic number, as f_j is derived from the total scattering of all the electrons of the atom[3]. The sum of these scattering factors is F_{hkl} and is termed the structure factor. When F_{hkl} is squared, it is proportional to the intensity of the (hkl) reflection. Thus, the intensity of a reflection in the X-ray diffraction pattern can ultimately yield information about the unit cell contents. This is a complex process and a full mathematical treatment of this subject can be found in Atkins[4].

2.1.6 Equipment

The X-ray diffractometer used in this work was a Siemens D5000 diffractometer, which used the copper $K\alpha_1$ line of wavelength 1.5406 Å, and had a germanium monochromator. Scans up to half an hour in duration were used for simple zeolite identification. For work looking at zeolites containing occluded salts, scans lasting for 12 hours were necessary.

2.2 ^{29}Si MAS NMR

The information provided by ^{29}Si MAS NMR can be used to find the Si/Al ratio of the sample. This can be deduced by the chemical shifts and intensities of peaks.

Nuclear Magnetic Resonance methods involve a sample being placed in a magnetic field. The interaction between the magnetic field and the nuclear magnetic moment causes the energy levels in the nucleus to split – this is known as the Zeeman interaction[1]. The specimen is then subjected to a radio frequency field. The atoms will absorb radiation only at the energy equal to the difference in energy between the two spin states. This energy absorption is seen in the NMR spectrum as a peak.

When NMR spectroscopy of zeolites is performed, it is important to note that this is done in the solid state, so the full powder structure may be seen. Interactions result in line broadening in the solid state, making the peaks poorly defined. There are two main reasons why linewidth broadening occurs[4]. The first cause is local magnetic fields from atomic nuclei interacting. The field created, B_{local}, is proportional to the angle, θ, of the sample to the incident field according to:

$$B_{local} \propto \left(1 - 3\cos^2\theta\right)$$

In a solution, molecular motion would average these local fields to zero, but in solid state NMR the field remains and contributes to the field the nuclei experience. The sample, therefore, has a range of different fields arising from the local environment.

The second cause of line broadening is chemical shift anisotropy. This is also related to the angle between the sample and the incident field, again involving the relationship $(1–3\cos^2\theta)$. Electron currents within the atomic electron clouds cause chemical shift. The production of these currents depends on the sample orientation with respect to the applied field. In a

solution an average chemical shift is produced due to the random motion of the molecules. However, in a solid, the position of the sample is fixed, and the shift is spread over a broader range of frequencies.

The answer to this problem is to spin the sample at an angle, such that these effects are minimised. Both effects are related to the term $(1–3\cos^2\theta)$. By setting this term to zero:

$$\left(1-3\cos^2\theta\right)=0 \qquad \text{Equation 2.4}$$

$$\cos^2\theta = 1/3$$

$$\theta = 54.74°$$

Therefore, spinning the sample at 54.74° to the applied magnetic field reduces the effects to zero[4]. This angle is the "magic angle" referred to in the name of the technique.

The determination of the silicon to aluminium ratio is based on the fact that the five different silicon environments appear at slightly different chemical shifts to each other. The five silicon environments relate to the number of neighbouring aluminium atoms, ranging from 4 to 0[5-8]. This is written as Si(4Al) to Si(0Al). The approximate range of shifts for these different environments is from –83 to –108 ppm from TMS, for Si(4Al) to Si(0Al) respectively. A 5 ppm shift towards low-field for each additional aluminium atom is seen. It has been reported in the literature[7,8] that these values can be very different if the bonds or angles are strained.

It is possible to determine the population of each type of environment by the area under the peak. To find the ratio of silicon to aluminium Equation 2.5 below is used[6,8].

$$\left(\frac{Si}{Al}\right)_{NMR} = \frac{\sum_{n=0}^{4} I_{Si(nAl)}}{\sum_{n=0}^{4} 0.25 n I_{Si(nAl)}} \qquad \text{Equation 2.5}$$

This equation is valid assuming Lowenstein's rule is obeyed.

2.2.1 Silicon to Aluminium Ratio From Lattice Parameters

Owing to a difference in the radii of silicon and aluminium it is possible to calculate the composition of the unit cell. Breck[9] has shown that an estimate of the ratio of silicon to aluminium can be determined from lattice parameters for zeolites X and Y, which contain 192 $(Si,Al)O_4$ tetrahedra. Chemical analysis determined the silicon to aluminium ratio of 37 samples and a graph of N_{Al} against lattice parameter was plotted. The equation of this graph is known and it is therefore possible, when the lattice parameter has been found from X-ray diffraction data, to use Breck's equation[9] (see Equation 2.6 below) to find an estimate of the Si to Al ratio.

$$\frac{N_{Si}}{N_{Al}} = \left(\frac{192b}{a_0 - 24.191}\right) - 1 \qquad \text{Equation 2.6}$$

When data of silicon to aluminium ratio was plotted on a graph, a straight line was formed with a gradient of b=0.00868, and Breck estimated an error of ±0.005. The accuracy of the result depends on the quality of the X-ray data. If peaks are broad, then errors in the calculated lattice parameters can be large, leading to errors in the Si/Al ratio.

Where NMR data was unavailable for samples of zeolite X and Y, the calculation above was used, after checking the peak indexing with the program CELL. Any mislabelled peaks, or those with large errors, were not included in the final Si/Al ratio determination.

2.3 Scanning Electron Microscopy

Scanning electron microscopy uses electrons to generate a surface image. As electrons are easily scattered, SEM must be performed in an ultra high vacuum to avoid collisions with air molecules. Upon reaching the sample, there are several different interactions which can occur between the electrons and the sample surface. Figure 2.7 below illustrates some of the possible outcomes of an electron collision which are of significance in scanning electron microscopy.

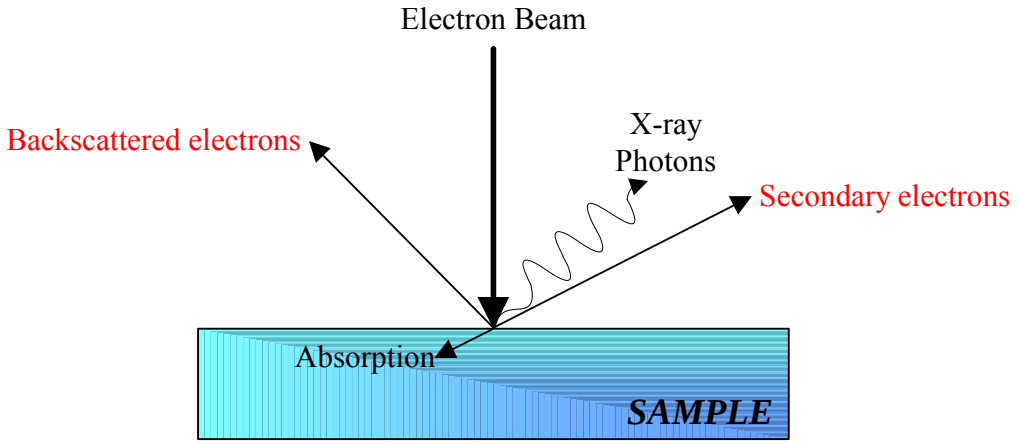

Figure 2.7: Some of the processes which occur when electrons interaction with matter. Red text indicates the electrons detected by an SEM in image generation.

To best understand a scanning electron microscope, it is necessary to see how the components are arranged. A simplified diagram of the parts of an SEM is shown in Figure 2.8 and a discussion of the function of these parts follows.

2.3.1 Electron Gun

The electron gun generates the electrons necessary to make up the electron beam. There are many different electron sources, the most common of these being thermionic emission. A filament is heated, and this increases the kinetic energy of the electrons until they have enough energy to escape the surface. The filament is usually made of tungsten, although

lanthanum and cerium hexaborides are also used, and have a greater brightness when compared to tungsten. An alternative electron source is field emission, which applies a strong electric field to the tungsten filament surface. This generates electrons and is a brighter source compared to thermionic methods. The field emission source can be further brightened by heating[10].

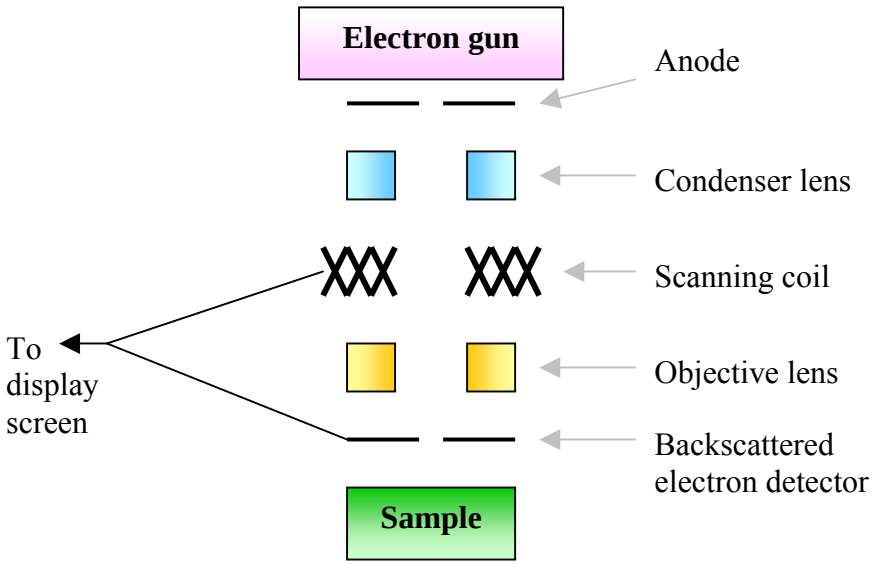

Figure 2.8: A schematic diagram of a scanning electron microscope

2.3.2 Anode

This electrode is positive, and hence the electrons in the beam leaving the gun are accelerated towards this electrode.

2.3.3 Condenser Lens and Objective Lens

With the exception of when electrons are parallel to a field, their direction of travel can be altered by an electric or magnetic field. Therefore, electromagnets, which consist of a coil of wire carrying an electric current (solenoid), make excellent lenses. By altering the current in the coil, the magnetic field strength is affected and this adjusts the focal length of the lens[10].

Both the condenser and objective lens are electromagnetic lenses which focus the electron beam[10,11]. The resulting beam is between 20 and 100 Å, much larger than the few Å diameter of atoms, and so atomic resolution cannot be achieved.

2.3.4 Scanning Coil

The scanning coils are responsible for scanning the beam across the sample surface at a constant rate[11]. The surface in question must be conducting to prevent a build up of charge, and if not can be coated with a thin layer of gold without affecting the morphology (see notes below on sample preparation).

2.3.5 Backscattered Electron Detector

The main way in which the image is generated is by collecting backscattered electrons (BSE)[10], which are electrons deflected by surface collisions. The BSE are collected by the detector, which must be close to the sample, to collect as many electrons as possible. The electrons are accelerated onto a phosphor, which emits a flash of light per electron. The light signal is amplified by a photomultiplier tube, to give a better image. The image is then displayed on a cathode ray tube.

As mentioned previously, many processes can occur when electrons hit a surface. An inelastic collision results in a small amount of relatively low energy secondary electrons being ejected from the immediate area of the collision – these electrons are representative of a small area and are therefore used to generate high resolution images[10]. Another result of electron impacts is the production of X-ray photons, which are used for EDX (see Section 2.4).

2.3.6 Sample Preparation

All samples to be placed in the electron microscope sample chamber were fixed on a metal

stub using thin adhesive pads. To prevent a build up of surface charge it was necessary to coat non-conducting samples, such as the zeolites examined in this work, with gold. If the surface charge is not conducted to earth, the sample will charge up in a similar manner to a capacitor and this can affect the scanning beam, and have repercussions for image resolution[10]. The coating process was carried out using a sputterer. Once there is a vacuum in a sputterer, argon gas fills the chamber and is ionised. The ions bombard gold foil, and the gold is deposited on the sample surface. The gold layer should be at least 5 nm on all parts of the sample, but can be a few tens of nanometres thick – it is better to have a slight excess than an insufficient coating[10].

The SEM used was a JEOL JSM 6300. This uses a tungsten electron gun for electron beam generation. Photographs of samples could be taken and stored on a computer connected to the electron microscope.

2.4 Energy Dispersive Analysis with X-rays

The X-rays produced from the collision of electrons with the sample (see Figure 2.7) can be used in Energy Dispersive Analysis with X-rays (abbreviated to EDX or EDAX). This is a method of determining which elements are present in a sample, and in what ratio. This is done by analysing the X-ray spectrum of the sample, and sorting these X-rays with respect to their energy. Certain X-ray energies are characteristic of particular elements, due to the difference between the energy levels in the atom which gave rise to the X-ray.

The detector used is a single crystal disc composed of "lithium-drifted silicon", written Si(Li)[10]. This detector and the pre-amplifier must be kept cool with liquid nitrogen to achieve a low signal-to-noise ratio. The EDX detector converts the X-ray energy into a current, proportional in size to the X-ray energy. The pulse, in turn, is translated into a

voltage before being amplified and separated from the other pulses. Each pulse is plotted according to its energy, and this forms the spectrum of energy versus counts.

2.5 IR Spectroscopy of Occluded Zeolites

The infrared region of the electromagnetic spectrum lies between the microwave and visible regions, and has wavelengths ranging between $7x10^{-7}$ and $1x10^{-3}$ m. The unit of wavenumbers ($\tilde{\nu}$, measured in cm^{-1}) is most commonly used for IR spectra, and the relationship between wavelength and wavenumbers is given in Equation 2.7 below. Most infra red spectrometers operate between 4500 and 500 cm^{-1} wavenumbers.

$$\tilde{\nu} = \frac{1}{\lambda} \qquad \text{Equation 2.7}$$

Photons of IR radiation are absorbed by a molecule or solid only if their frequency exactly corresponds to the energy separation of the vibrational states of the material. These energy separations are characteristic of particular bonds. The IR spectrum is seen as a percentage transmission, ranging from the maximum (where no radiation is absorbed by the sample) to the bottom of the absorbance peaks where a particular amount of radiation has been absorbed to cause vibrations within the sample.

When performing infra red analysis of zeolite samples the KBr disc method was employed. In this technique, very small quantities of the sample were ground with potassium bromide powder and then pressed into a disc less than 1 mm thick which was placed in the path of the IR beam. The spectrometer used was a Perkin Elmer FT-IR Spectrometer Paragon 1000.

The IR spectra of zeolites has been reported in the literature[12,13]. Wavenumbers of key

vibrations and stretches have been recorded: Table 2.1 lists the main regions where peaks can be expected for a zeolite sample.

The work in this volume has focused on zeolites with occluded metal nitrates, and consequently extra peaks were observed in the IR spectra arising from the nitrate ions present. Table 2.2 lists the wavenumbers typically seen for nitrate groups within zeolites[12,13].

Table 2.1: Zeolite vibrations in IR spectra

Wavenumber (cm^{-1})	Assignment
3450	water
1640	water
1000	T–O_4 stretch
550	D4R
460	T–O bend

Table 2.2: Nitrate vibrations within zeolites in IR spectra

Wavenumber (cm^{-1})
1400–1450
1384
830

There is a drawback to the KBr disc method and that is the reaction between potassium bromide and silver nitrate to form silver bromide. As a result, IR analysis of any silver-containing samples was not possible by this technique.

2.6 Thermogravimetric Analysis (TGA)

The technique of thermogravimetric analysis involves heating small quantities (c. 10 – 20 mg) of sample and monitoring the weight loss as a function of temperature. It is possible to perform such experiments in various atmospheres, but in the work presented, all were carried out in air.

The apparatus consists of a small alumina crucible which contains the sample, and this is encased in a furnace. A computer controls the temperature and heating duration, as programmed by the user, and a graph is produced which shows the time on the x-axis, temperature on the left hand y-axis and the weight loss (in mg or as a weight percent) on the right hand y-axis. A typical TGA plot encountered in this work is shown in Figure 2.9.

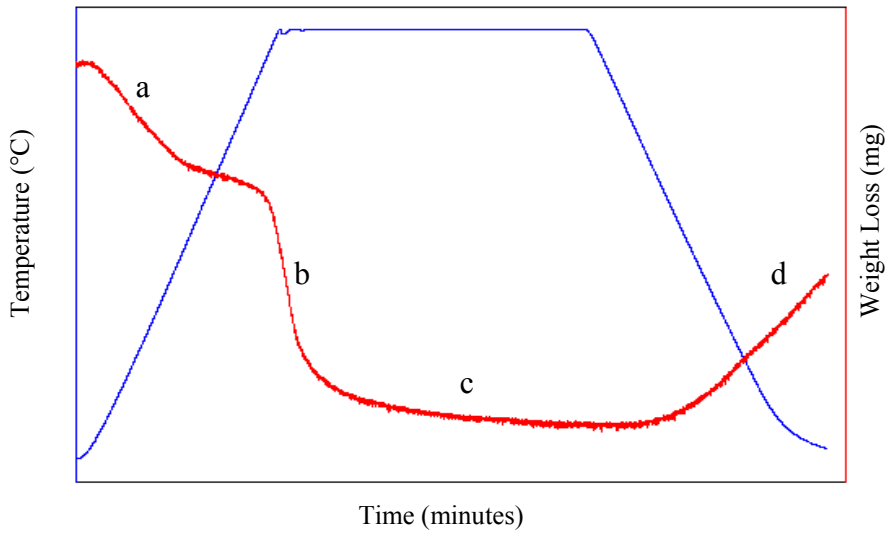

Figure 2.9: A Typical TGA Plot

Red line represents weight of sample

Blue line represents temperature (°C)

a: shows a weight loss. The first loss is water.

b: shows a second weight loss stage, distinct from the first. This is NO_3^- decomposition.

c: Shows a period of nearly constant weight.

d: a slight rise upon cooling – this is reabsorption of some water from the air.

In the context of occluded and ion-exchanged zeolites, TGA is a useful tool in estimating the amount of salt present in the sample. The first weight loss seen in such samples is water from the pores of the zeolite. If a large amount of salt has been occluded into the pores, this

will have driven out some of the water, hence there will be less water present to be lost upon heating in TGA relative to samples containing no salt. The second step seen in TGA graphs from samples containing occluded salt is due to the decomposition of the NO_3^- ion, as nitrate salts were used. Therefore the size of this step should give an indication of how much salt was present.

The equipment used was a Stanton Redcroft STA 1500 TGA, which is sensitive to ±0.0005 g.

2.7 Experimental

It is customary for the reactions carried out to be detailed in a stand-alone experimental chapter. However, much of the work carried out in this thesis was concerned with the refinement of particular reactions subject to the results obtained, i.e. the outcome of a reaction dictated what further work was necessary. It is therefore more logical to outline the reactions performed alongside the results in their own chapter. Below is a summary of the nature of the work and typical reaction conditions, but particulars of all reactions shall be reported in the relevant chapters, i.e. Chapter 3: "Microwave Synthesis" and Chapters 4 & 5: "Occlusion Reactions with Silver Nitrate" and "Occlusion Reactions with Other Nitrates", respectively.

2.7.1 Microwave and Conventional Heating Experiments

A typical synthesis experiment involved preparation of the zeolite gel from reagents which included a source of silicon, aluminium, group (I) hydroxide and deionised water. The gel was either heated directly or left to age prior to use, usually for 24 hours at room temperature.

A 10 ml portion of the gel was poured into each of the Teflon reaction vessels for microwave heating. The remainder of the gel was heated in a conventional oven so that direct comparisons could be made between the two heating methods.

The microwave oven, a MARS CEM 5000, was programmed with several pieces of information, regarding the heating of the gel. Firstly, the heating profile was set to "ramp", i.e. heat up to a temperature a little over the target temperature in short period, most commonly 90 seconds. This was to ensure rapid heating of the gel to synthesis temperature, the higher temperature not actually being reached. The main heating programme then took over after the first 90 seconds. This would govern the temperature and duration of heating as

well as the power to be used (typically 300 W). Once the microwave oven had started the heating, it was possible to pause the programme to enable sample removal at predetermined intervals. This was a quick process and the temperature of the remaining samples did not drop by more than 2 °C. The heating could then be restarted until all the samples had been removed.

Upon removal from the microwave or conventional ovens, samples were quenched with 20-50 ml of deionised water. They were then suction filtered and washed with more deionised water. The samples were transferred to a drying oven at ~50°C until dry. The powder was then ground and stored in airtight sample containers.

2.7.2 Ion Exchange and Occlusion Reactions

All the zeolites used in this section were synthesised in the laboratory, and their syntheses are also reported in chapters 4 & 5.

In a typical ion exchange experiment, an aqueous solution, typically 0.1 M, was made from the appropriate nitrate salt. The powdered zeolite was added to the solution and stirred for 24 hours. Some solutions required heating to aid the exchange process, and in some cases multiple exchanges were carried out to obtain the maximum level of ion exchange. The exchanged zeolite was then recovered from the solution via suction filtration.

When occlusion reactions were performed a quantity of the metal-exchanged zeolite was ground thoroughly with the corresponding metal nitrate. The resulting mixture was then transferred to an alumina boat for heating in a furnace.

In order for occlusion to occur, the samples were heated at 60°C/hr to a reaction temperature 40 – 50 °C higher than the melting point of the metal nitrate. Samples were kept at this elevated temperature for 8 hours before the furnace was cooled to room temperature. The cooling rate was usually 60°C/hr, but sometimes slower rates of 10°C/hr were employed as it had been indicated that slow rates are favourable[14].

After the sample was removed from the oven, a portion was kept, and the remainder was washed with deionised water and, following suction filtration, was dried in an oven at ~50°C.

Samples were stored in airtight sample containers, but in the case of the light-sensitive silver zeolites, aluminium foil was wrapped around the container to prevent sample degradation from exposure to light.

Chapter 3: Microwave Synthesis

3. Microwave Synthesis

3.1 Introduction

In 1941, at the University of Birmingham, Randall and Boot[1,2] developed the magnetron – a piece of equipment which produces a fixed frequency of microwaves. Its importance as a method of causing rapid heating was recognised and the basis of the present domestic microwave oven was born. Its use in the kitchen grew during the 1970s and 80s, but its employment has now spread to the chemistry laboratory.

The earliest report of heating zeolites in a microwave oven was in 1981 when Roussy and Chenot[3] dehydrated zeolite 13X. It was not until 1988 that Chu, Dwyer and Vartuli[4] were granted a patent for synthesising zeolites with microwave radiation. They claimed eighteen different zeolites could be produced including zeolites A, X and Y.

Since the patent, many articles have been published which relate the use of microwave heating in the synthesis of zeolites and related materials[5–15]. The majority of work focuses on formation of zeolite A[5–8], Y[9–12] and ZSM-5[9,12]. Regardless of the structure studied, all reports have come to the same conclusion: that zeolites can be crystallised in microwave ovens far more quickly than by conventional heating methods.

One of the biggest advantages with microwave technology, and an important factor in the reduction of heating times, is that the reaction medium can be at the required temperature in less than 3 minutes. This is because microwaves interact directly with the gel, in contrast to conventional routes where heating is via conduction and convection. With the elimination of the so-called 'thermal lag' (estimated to be up to 30 minutes[16]) the reaction can begin almost instantaneously. Claims have been made that microwave heating produces fewer impurities

at a given temperature when compared with zeolites formed in conventional ovens[12]. It was suggested that this is because the slow heating to synthesis temperature in standard ovens allows impurities to crystallise. As this period is virtually eliminated in microwave ovens, impurities do not have time to develop. A more detailed discussion of microwave heating is given in section 3.4: Microwave Heating.

3.2 Parameters Effecting Synthesis

Many factors have been found to affect the crystallisation rates of zeolites in microwave ovens. The impact of variables including reagents, pH, ageing and reaction vessels will be discussed in the subsequent sections.

3.2.1 Ageing

One parameter that can alter the heating duration required is whether or not a gel has been aged prior to use. Slangen *et al*[6] found that when a zeolite A gel was left for 24 hours, or had 10% by weight of aged gel added, the time taken for crystallisation to occur was reduced from 10 minutes to 1 minute. Seeding with zeolite crystals can also reduce the heating time necessary. This is thought to be because the seeds provide a surface on which crystallisation can occur. The formation of nuclei (defined as the smallest system which can support crystal growth) is thought to be the rate limiting step in zeolite crystallisation[16], and by negating the need for the gel to produce its own, the system can form products in a shorter time.

3.2.2 Reagents

When studying zeolite synthesis in a microwave oven, it has also been noticed that the reagents used in a gel can affect the time taken for crystallisation to occur. Arafat *et al*[9] reported that the synthesis of zeolite Y took 10 minutes in a microwave oven and de Araújo *et al*[10] found that their preparation took 18 minutes: both groups used fumed silica. However,

Katsuki *et al*[11] noted that zeolite Y synthesis took 2 hours from colloidal silica. This shows what a difference the source materials can make. The origin of the effect could be due to different gel pH or reagent solubilities, which affect the time the materials remain in solution. Another origin of the effect of silica source on crystallisation rates was proposed by Jansen[17]. Here Jansen discussed how the specific surface area of the silica source caused different nucleation and crystallisation rates for zeolite A. The larger the specific area of silica, the quicker the formation of a greater number of crystallites, however, their size was smaller when compared to those crystals formed from silica with a smaller specific area.

Studies have been carried out investigating how the silica source affects the progress of zeolite synthesis[18,19]. Mintova and Valtchev[18] looked at the reaction to form silicate-1 (MFI) using three different silica sources. After ageing for 30 hours, each of the gels were examined and found to have different sized precursor species. The time taken for silicate-1 to form varied between 10 hours and 15 hours with silica source. The final crystal size was also related to the size of the precursor species, and was therefore a consequence of silica source. It was proposed that as silica sources differ in their particle size, level of purity and ability to dissolve in alkaline solutions, so these factors can affect how nucleation and crystallisation proceed. The silica source not only affects the initial solution, but the silicate intermediates formed upon the dissolution of the reagents. This in turn has an impact on the rate of nucleation and therefore the crystallisation process.

The work of Li *et al*[19] also studied the effect of the silica source on the synthesis of TPA-silicate-1 (MFI). Three gels were used with the only difference being the silica-containing reagent. Again, particle sizes in the gels were different, and the time to synthesise products varied. Li and co-workers suggested that taking the traditional view, that supersaturation drives nucleation and growth, enables the observations to be explained by the fact that two

gels have an extra step to obtain the level of saturation required. There is a lower concentration of nuclei forming species in the amorphous silicas (Ludox TM and Ludox LS) compared to tetraethoxysilane. Therefore, the first step upon heating for the amorphous gels was to produce nuclei to participate in nucleation and crystal growth. This explained why the two Ludox gels take 120 hours to form TPA-silicate-1 compared to the 72 hours of the tetraethoxysilane gel.

Zeolite X (FAU) has also been the focus of a silica source study[20]. Whilst keeping all reaction parameters constant, the silica source was varied. Eleven different silica sources were investigated, varying by chemical composition and manufacturer. It was found that crystallisation rates varied with different silica sources, despite all other conditions being unaltered. The number of crystals formed and their sizes were also found to vary, but the origin of this effect could be explained by the heating period required for crystallisation – longer heating times cause fewer large crystals to form, whereas a short heating time yields many small crystals. The same observations were true of gels aged prior to heating. The percentage conversion to zeolite X produced from the different gels was also affected.

Analysis of the silica sources used showed vast differences in the level of impurities present[20]. Since all reaction parameters such as molar ratio of reagents, pH and heating conditions were identical between reactions, it was proposed that the quantities of impurities in the silica sources had the most significant effect on the nucleation and crystallisation steps of zeolite X syntheses.

3.2.3 Gel pH

Zeolites are crystallised from an alkaline gel, typically with a pH above 12. It is known that gel pH influences the solubility of the reagents, and the products formed[21]. The higher the

pH of the solution, the more soluble the starting materials, i.e. the more reactants are available in solution – this in turn enhances the rate of crystal formation[17]. However, it has also been seen that particular zeolites will only form in a given range of pH, and that this also affects the Si/Al ratio of the final product. For example, mordenite crystallises at a pH between 11.3 and 12.7, but at lower pHs ZSM-5 is formed[21]. In experiments performed by Donahoe and Liou[22] it was found that solution pH and Si/Al ratio of the product had a linear relationship. As the pH of the gel was lowered, more siliceous zeolites crystallised.

Research into the effect of the gel pH in $AlPO_4$-5 synthesis has also been published[23]. It was found that the initial gel pH influenced the average crystal size, the size distribution and the yield. Despite varying the pH of the starting gel between 4 and 7, the post-synthesis supernatant fluid always had a pH of 7.5. The lower the starting pH, the larger the crystals and the broader the size distribution became. The reason for an increased crystal size at low pH could in part be due to there being fewer reactants in the solution phase at any given time. This means there would be a lower probability of the species colliding and forming nuclei. With fewer nuclei present, there would not be as many crystals competing for reactants in order to develop, hence the crystals can grow larger. When gel pH was kept constant and the microwave heating time was increased it was found that the crystals became more elongated along the *c*-axis, whilst the *a* and *b* dimensions remained unaltered.

Barrer and Mainwaring[24] looked at factors which affect the synthesis of phillipsites and chabazites. When the concentration of alkali in the reaction mixture was kept constant, but the volume was altered, the yield of zeolite was reduced as more unreacted species remained in solution. However, with a higher pH, more species were dissolved into the solution phase, which increased the probability of collisions between the species. This caused an enhanced nucleation rate.

3.2.4 Reaction Vessels

Research into the effect of the geometry of the reaction vessels within the microwave oven was performed by Connor *et al*[25]. They compared the crystal growth rates and quality of silicalite (MFI) produced in two different vessels; all other reaction conditions remained the same between experiments. Each reaction container was cylindrical and contained 10 ml of gel. One container had a diameter of 33 mm and the other a diameter of 11 mm, with surface to volume ratios of 0.26 mm^{-1} and 0.38 mm^{-1} respectively. The results showed that the silicalite crystals produced in the 33 mm diameter reactor were larger, more uniform and in greater quantity than the crystals formed in the 11 mm diameter vessel. A plot of electric field distribution within the vessels showed that the 33 mm container had a higher density of "hot spots" – local areas which are hotter than surrounding regions. These hot spots are believed to cause increased crystal growth and nucleation, hence the greater yield for the 33 mm system.

Another way of explaining the phenomena observed by Connor *et al*[25] is related to the way microwaves interact with matter. As microwaves pass through a gel they lose energy, thus the quantity of gel present affects the reaction[26]. Microwaves have a penetration depth defined as "the depth into a material where the power falls to one half its value on the surface"[27]. This means that how effectively a gel is heated could depend upon the size and shape of the reaction vessel, as Connor found.

3.3 Features of Microwave Heating

A major feature of microwave synthesis is the smaller size of zeolite crystals produced when compared to those formed by the usual methods. This is most likely due to the accelerated rate of heating and gel dissolution, which means the gel is consumed quickly, forming more

nuclei from which crystals grow. As limited reagents are left after the nuclei formation period, they produce many, smaller crystals. The fact that the gel is heated for a shorter time also means that the crystals do not have as long to form.

The microwave frequency most commonly used is 2.45 GHz, and this is ideal for the interaction with water molecules and aqueous solutions. In their patent, Chu *et al*[4] are clear that the reaction system requires a "heat transfer agent sympathetic to microwave energy" i.e. a medium for the reaction which absorbs microwave energy and can transfer the heating effects to the reactants. The reaction vessel, therefore, must be transparent to, or absorb little of, the microwave energy.

It appears that microwave heating has many advantages over the conventional methods. Microwave samples are made faster, with low levels of impurities. It has been stated that due to the rapid crystallisation times, relatively unstable phases can be selectively formed and isolated[14]. There have also been claims[4] that the fact microwaves produce smaller crystals is an advantage with respect to their catalytic properties. By having smaller crystals, the catalytic activity is enhanced as this allows more rapid diffusion of reactants and products through the zeolitic crystals.

3.4 Microwave Heating

3.4.1 Theory

Microwaves are electromagnetic waves consisting of an oscillating magnetic field with a perpendicular oscillating electric field, and have wavelengths between 1 cm and 1 m, with frequencies ranging from 30 GHz down to 300 MHz, respectively.

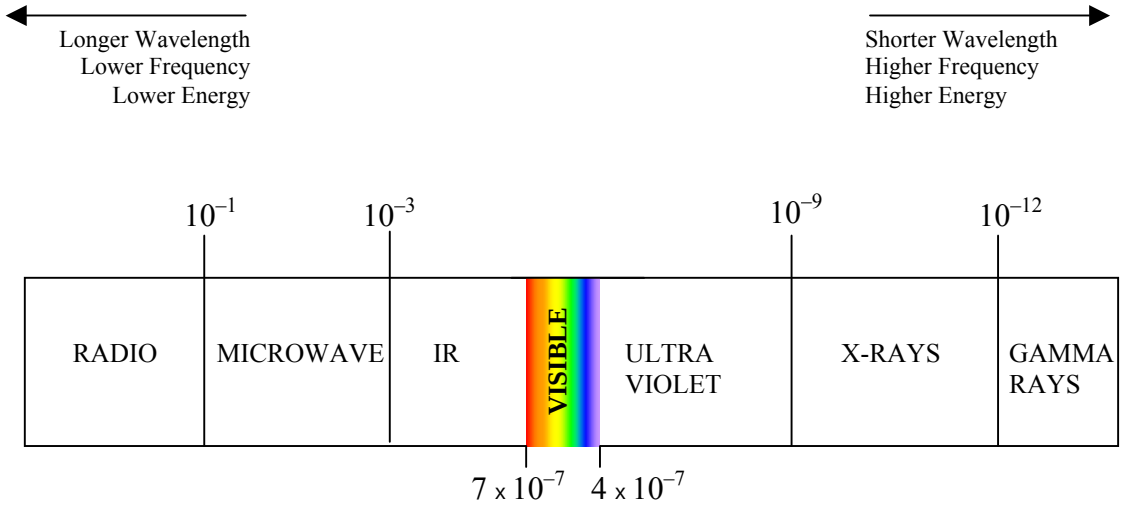

Approximate wavelengths indicated are in metres.

Figure 3.1: Representation of the electromagnetic spectrum (not to scale)

According to Rao *et al*[28] materials can be classified as belonging to one of three categories depending on their behaviour in a microwave field. The first class of materials contains bulk metals and alloys, and is termed "microwave reflectors". These materials are often used as microwave guides in the ovens. The second group are known as microwave transmitters, and are transparent to microwaves. Teflon and some types of glass are in this second group and are therefore eligible for use as cookware and reaction vessels in a microwave oven. In the final category, the microwave absorbers, are the many materials which can be used in microwave reactions because they interact with the microwave radiation.

Heating of these microwave absorbers is caused through the microwave dielectric heating

effect, which makes use of a solid or liquid's ability to convert the electromagnetic energy into heat[27]. When an electric field interacts with a solid or liquid sample, the charged particles or dipoles present attempt to align with the incident radiation. Due to the alternating nature of the radiation, the charged particles/dipoles are in constant motion. Once polarised in one direction, the material cannot quickly realign the polarisation in the opposite direction when the field alternates. At microwave frequency, the oscillation of the field takes a similar time to that for the dipoles to realign. This causes continual motion of the species as they attempt to align with the microwave field, which in turn results in heating[29].

The dipolar polarisation of a material depends on 2 terms: ε' and ε", which make up the dielectric constant, ε, according to:

$$\varepsilon = \varepsilon' + i\varepsilon'' \qquad \text{Equation 3.1}^{28}$$

ε', the relative permittivity, is the 'real' component, and represents the ability of molecules to be polarised by an electric field and ε", the dielectric loss is the imaginary component, which denotes the efficiency of the molecule at converting electromagnetic radiation to heat at a given frequency and temperature. *i* represents the imaginary value of $\sqrt{-1}$.

A material's ability to convert electromagnetic energy into heat can be represented by tan δ, the dielectric loss tangent:

$$\tan \delta = \varepsilon''/\varepsilon' \qquad \text{Equation 3.2}^{27,28}$$

The amount of energy converted varies with molecular properties[27], hence the starting materials used are important. This can also be important in introducing a degree of selectivity into reactions in a microwave oven[27]. No such issues are encountered conventionally as heating is caused by conduction and convection. Water and aqueous

solutions, as are commonly used in zeolite syntheses, will heat up at the microwave frequency commonly used (2.45 GHz).

Another important factor to be considered in the heating of materials in microwave ovens is the penetration depth, D_p, of the microwave radiation. Penetration depth is defined as "the depth into a material where the power falls to one half its value on the surface"[27]. The value D_p is expressed thus:

$$D_p \propto \lambda_0 \sqrt{(\varepsilon'/\varepsilon'')} \qquad \text{Equation 3.3}^{[26,27]}$$

where λ_0 is the wavelength of the microwave radiation.

The main disadvantage of conventional heating is the length of time required to bring the reactants up from room temperature to the reaction temperature. This period, referred to as "thermal lag", has been estimated to be as long as 30 minutes[16]. When microwave heating is employed it is possible to reach the desired temperature in less than 3 minutes. It is also possible to 'ramp to temperature', i.e. set the first few minutes of heating to a higher temperature than required in order to attain more rapid heating. After this period, synthesis is set to continue at the desired temperature.

It is claimed that microwave heating of gels causes rapid dissolution and that this leads to an enhancement of the reaction rate[15]. A consequence of the accelerated heating rate is that the gel is used faster and more nuclei result, thus smaller crystals form.

3.4.2 Equipment

It has been demonstrated[8,10] that microwave synthesis can be conducted with a modified commercial microwave oven. It is more satisfactory, however, to use specialist microwave

ovens, designed for chemical reactions.

The microwave oven used in this work was a CEM MARS 5000, which operates at 2.45 GHz and has a maximum power of 600 W. It was possible to program reactions by specifying such parameters as temperature, pressure, power and duration of microwave heating. It was also possible to use magnetic stirrers in the reaction vessels. The microwave has a thermocouple which supplies pressure and temperature feedback controls and is accurate to within ±1°C during the experiments. The thermocouple must be well shielded from the microwave field, and earthed in order to prevent sparking[27]. The microwave oven contained a dummy load of water sealed in a reaction vessel in the same manner as the zeolite gels. This dummy load is necessary when high powers, small loads or poorly adsorbing loads are in the microwave oven, as the water absorbs any excess energy[27].

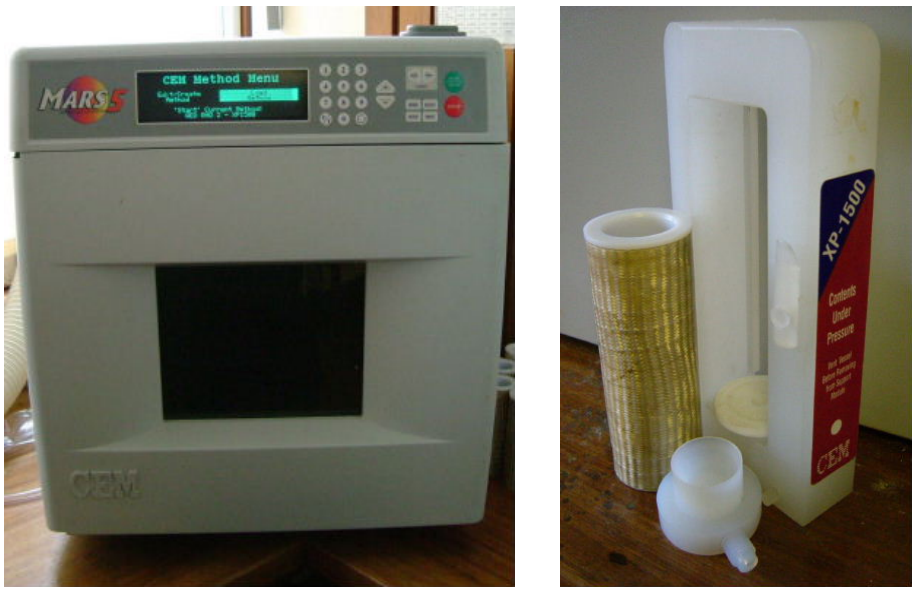

Figure 3.2: The CEM MARS 5000 (left) and a reaction vessel and cap with holder (right)

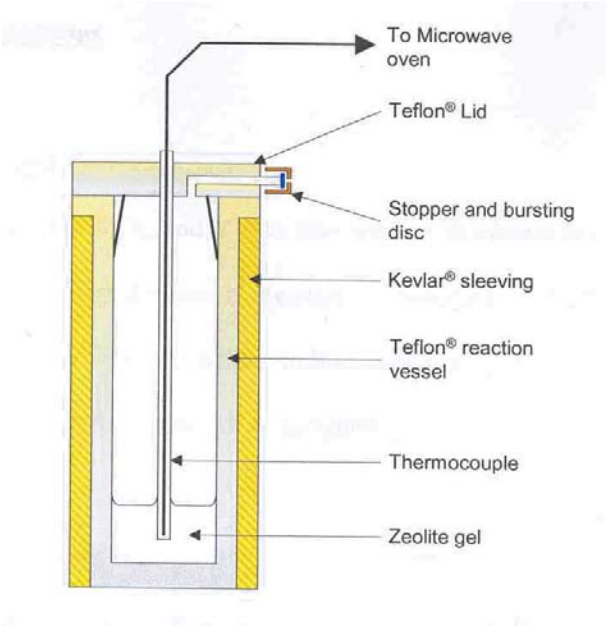

Figure 3.3: Cross section of a microwave reaction vessel, as set up for an experiment

The carousel into which the sample containers were inserted could accommodate up to 12 reaction vessels. These vessels (illustrated in Figure 3.3) were Teflon tubes within Kevlar sleeves. The caps were pre-stretched to ensure a tight fit and contained plastic rupture discs, designed to burst and release pressure in the event of pressure build-up in excess of 800 bar. The samples need to be on a carousel or turntable to ensure that the samples experience an average of the microwave field, as standing waves may form in the oven cavity and create hotspots and cool areas.

3.5 Microwave Reactions

3.5.1 Zeolites A, X and Y

The synthesis of zeolites A, X, and Y was attempted with microwave heating. The reagents used for each gel were varied to see if the starting materials used affected the synthesis time or product quality. Table 3.1 below indicates which gels were used for each zeolite preparation and the key to the letter codes assigned.

Each gel has been assigned a two-letter code. The first letter denotes the zeolite to be made, i.e. zeolite A, X or Y. The second letter represents the silica source, by initial, i.e. M = metasilicate, C = colloidal silica, F = fumed silica.

Table 3.1: Key to Gels used for each Zeolite

	Sodium Metasilicate	Colloidal Silica	Fumed Silica
Zeolite A	Gel AM	-	Gel AF
Zeolite X	Gel XM	Gel XC	Gel XF
Zeolite Y	Gel YM	Gel YC	Gel YF

The precise gel compositions used for each zeolite gel are given in the next section (3.6), but below is a list of the reagents and suppliers used in each gel.

Gel *M – 'Sodium Metasilicate'

Contained: Sodium metasilicate pentahydrate (Strem Chemicals)

Sodium aluminate (Strem Chemicals)

[Sodium hydroxide (BDH, AnalaR 99 % pellets) – for zeolite A only]

Deionised water

Gel *C – 'Colloidal Silica'

Contained: Colloidal silica (SiO_2: 30 wt. % with water, Dupont Ludox HS 30)

Sodium aluminate (Strem Chemicals)

Sodium hydroxide (BDH, AnalaR 99 % pellets)

Deionised water

Gel *F – 'Fumed Silica'

Contained: Fumed silica (Cab-o-Sil M5, BDH)

Sodium aluminate (Strem Chemicals)

Sodium hydroxide (BDH, AnalaR 99 % pellets)

Deionised water

3.5.2 Zeolite Rho

The synthesis of zeolite rho was also tried in a microwave oven. The gel used was different to those listed above. The proportions were sometimes altered, and seed crystals were added to some experiments.

The reagents used were: Sodium hydroxide (BDH, AnalaR 99 % pellets)

Caesium hydroxide (50 wt. % with water, Aldrich)

Alumina (Catapal B, Vista)

Colloidal silica (30 wt. % with water, Dupont Ludox HS 30)

Deionised water

[Seed crystals – some preparations only]

For the exact gel compositions used see section 3.6.4.

3.6 Gel Compositions

For the microwave experiments, as already stated, various gel preparations were used. These were used for zeolites A, X and Y. Below are the methods used to prepare each gel, along with details of the heating methods used for each gel. In all microwave experiments performed, a variety of temperatures were used. It was often the case that the temperature used in the microwave oven differed to that used conventionally. This is purely based on results from initial experiments, and the temperature which produced the best sample was used throughout further work. In some cases, another temperature was used so direct comparisons could be made to articles which reported similar work.

3.6.1 Zeolite A

Gel AM: 3.7 Na_2O: 1.6 SiO_2: 1 Al_2O_3: 106.4 H_2O

0.72 g of sodium hydroxide was dissolved in 80 ml of deionised water. This solution was split into two equal portions. To the first, 8.26 g of sodium aluminate was added and stirred until clear. To the second half of the sodium hydroxide solution 15.48 g sodium metasilicate pentahydrate was added. This was heated and stirred to aid dissolution. The two clear solutions were then recombined and the resulting white gel was shaken until homogeneous.

Gel AF, Literature[6]: 1.5 Na_2O: 1 SiO_2: 1 Al_2O_3: 96.4 H_2O

1.68 g of sodium hydroxide was dissolved in 72.19 ml of deionised water before the addition of 7.50 g sodium aluminate. Once the solution was colourless, 2.52 g of fumed silica was stirred in to form an even mixture.

Heating Regimes

Preliminary reactions were performed with each gel, using a procedure adapted from Slangen

et al[6] after they reported the synthesis of zeolite A was complete in 1 minute if an aged gel was used. In these initial experiments, aged and unaged portions of gel were heated at 100°C for 5 minutes after initial ramping to 120°C in 90 seconds. (Note: 120°C was never reached. During the "ramp" stage, which was used to enhance the attainment of reaction temperature, the gel usually reached 100°C). After examining these early results, the heating conditions were revised. Each reaction was performed with aged and unaged gels to establish the difference this practice made.

- Gel AF was subjected to a microwave heating program of heating to 120°C in 90 seconds, followed by holding at 100°C for 10 minute stages from 10 to 60 minutes.
- Gel AM, however, was heated in 5 minute intervals for periods between 5 and 30 minutes at the same temperatures as gel AF.
- For comparison, zeolite A was also produced in a conventional oven. The gel was heated with and without ageing at 99°C for 3.5 hours.

3.6.2 Zeolite X

Gel XM: 3.7 Na_2O: 2.7 SiO_2: 1 Al_2O_3: 128.8 H_2O

In the first experiment attempted (see "Preliminary Results on page 78) 12.72 g of sodium metasilicate pentahydrate was used in the gel, but due to zeolite A impurities in the product, this quantity was increased by 10% for all further reactions to 13.99 g.

13.99 g of sodium metasilicate pentahydrate was dissolved in 30 ml of deionised water with heating and stirring. In a separate container 4.32 g of sodium aluminate was added to 20 ml of deionised water. The two colourless solutions were mixed together and thoroughly shaken to form a white gel.

Gel XC, ratio 1: 5.7 Na_2O: 4.7 SiO_2: 1 Al_2O_3: 114.5 H_2O

8.65 g of sodium aluminate was dissolved in 31.61 ml of deionised water, before addition of 45.87 g of colloidal silica. 18.36 g of sodium hydroxide was dissolved in 31.61 ml of deionised water in a separate container, before being added to the first solution.

Gel XC, ratio 2: 5.4 Na_2O: 6.5 SiO_2: 1 Al_2O_3: 104.6 H_2O

25.06 ml of deionised water was measured out and 9.39 g of sodium aluminate was dissolved in the water, before the addition of 68.82 g of colloidal silica. In a separate container 25.06 ml of deionised water was used to dissolve 18.34 g of sodium hydroxide before being added to the first solution.

Gel XF: 5.7 Na_2O: 3.2 SiO_2: 1 Al_2O_3: 100 H_2O

21.22 g of sodium hydroxide was dissolved in 52.40 ml of deionised water. 10.00 g of sodium aluminate was added to this solution. A white gel was formed upon the addition of 7.94 g of fumed silica. In order to aid dissolution of the fumed silica an extra 5.50 ml of water was added to the gel.

Heating Regimes

Initially, samples prepared for microwave heating were used with and without ageing. After early experiments indicated ageing to be favourable, all samples to be microwave heated were aged for 24 hours. The gels were then heated in a microwave oven at either 80 or 90°C for up to 4 hours, with a sample removed every half hour.

Samples of zeolite X were also produced in a conventional oven. Ageing was used in some cases. The gels were heated at 80 and 90°C for 24 or 48 hours.

3.6.3 Zeolite Y

Gel YM: 12.4 Na_2O: 11.4 SiO_2: 1 Al_2O_3: 410 H_2O

In two separate beakers, solutions were made up from 21.96 g of sodium metasilicate pentahydrate dissolved in 32.61 ml deionised water with heating and stirring, and 1.62 g of sodium aluminate in 32.61 ml of deionised water. The two solutions were then mixed and shaken thoroughly.

Gel YC: 10 Na_2O: 20 SiO_2: 1 Al_2O_3: 408 H_2O

3.24 g of sodium aluminate was dissolved with 40 ml of deionised water to from a colourless solution. To this, 72.11 g of colloidal silica (SiO_2: 30 wt% with water, Dupont Ludox HS30) was added to form a white solid. A separate solution of 12.96 g of sodium hydroxide in 40 ml of deionised water was made and added to the first solution. This gel was shaken and used after ageing for 90 minutes.

Gel YF, Literature: 4Na_2O: 10 SiO_2: 1 Al_2O_3: 235 H_2O

This was adapted from Arafat *et al*[9] and used fumed silica. Firstly, the experiment was carried out in the ratio described in the literature.

5.39 g of sodium hydroxide was dissolved in 53.06 ml of deionised water. 4 g of sodium aluminate was then added to the solution. To this resulting solution, 13.49 g of fumed silica was added. As the gel was very dry from fumed silica, an extra 40 ml of deionised water was necessary to aid dissolution.

Gel YF, High Sodium: 10 Na_2O: 10 SiO_2: 1 Al_2O_3: 250 H_2O

63.89 ml of deionised water was used to dissolve 13.31 g of sodium hydroxide before adding 3.33 g of sodium aluminate. 11.11 g of fumed silica was weighed out and added to the solution. It was necessary to add an extra 20 ml water to dissolve the fumed silica.

Heating Regimes

For microwave heated gels, ageing was carried out for 24 hours.

- Gels YM and YC were heated at 100°C for 30 minute intervals up to 4 hours.
- Gel YF was heated for 15 minute periods between 15 and 60 minutes. This was due to reports in the literature[9-12] suggesting that zeolite Y would be yielded within an hour.
- Samples heated in conventional ovens were aged for 90 minutes before heating at both 90 and 100°C for 19 hours.

3.6.4 Zeolite Rho

The standard reaction and conditions used to synthesise zeolite rho was taken from research performed by Edmondson[30].

Gel Rho, standard: 0.8 Cs_2O: 6.3 Na_2O: 21.1 SiO_2: 1 Al_2O_3: 223.3 H_2O

18 g of sodium hydroxide (99% pellets, BDH) was dissolved in 25 ml of water, before the addition of 7.25 g of alumina (Catapal B, Vista). The resulting gel was warmed and stirred to aid dissolution. 18 g of caesium hydroxide (50 wt% with water, Aldrich) was added to the cloudy solution. 150 g of colloidal silica (SiO_2: 30 wt % with water, Dupont Ludox) was added last, and the thick white gel was shaken vigorously for 10 minutes to ensure complete mixing. This is essential for the formation of pure zeolite rho. The gel was aged for 24 hours.

Gel Rho, low Cs: 0.75 Cs_2O: 6.3 Na_2O: 21.1 SiO_2: 1 Al_2O_3: 220 H_2O

Due to problems with the microwave synthesis of the standard gel from above, a reduction in the level of caesium hydroxide was deemed necessary – the reasons for this are outlined in the

discussion later on.

18 g of sodium hydroxide (99% pellets, BDH) was dissolved in 25.12 ml of water. The solution was heated and stirred to aid the dissolution of 7.25 g of alumina (Catapal B, Vista). Once the alumina was dissolved, 16 g of caesium hydroxide (50 wt% with water, Aldrich) and 150 g of colloidal silica (30 wt% with water, Dupont Ludox) were added to forma white gel. The gel was shaken vigorously and left to age for 24 hours before heating.

Gel Rho, seeding

In this experiment, seeding was tried, in order to see if the synthesis of zeolite rho could be enhanced, as previous research has shown seeding to be effective in reducing synthesis time[6,16]. The gel prepared was exactly the same as the full caesium version ("*Rho standard*"). To this gel, approximately 100 g in weight, 1.00 g of zeolite rho was added, i.e. 1 wt.%. The crystals added were made in a conventional oven at 80°C in 5 days, using the method outlined in "*Rho standard*". As the nuclei, which lead to the final product, can start to form during the ageing process[6], seed crystals were added to the gel before it was left to age for 24 hours.

Heating Regimes

Firstly, all gels were aged for 24 hours at room temperature.

A detailed study of the synthesis of zeolite rho by Edmondson[30], found that the crystallisation time is still quite unpredictable and hence samples prepared in the conventional oven were heated for 5, 6 and 7 days at 80°C.

It should be noted that it was not practical to heat samples for more than 5 hours in the microwave oven.

- Initial experiments mirrored the conventional conditions. Gels heated in the microwave oven were held at 80°C for 1,2,3,4 and 5 hours. Gels were also heated at 100, 120 and 150°C following the results of the primary experiments.
- Any gels remaining after the 5 hours in the microwave oven were combined together into a preheated vessel and placed in a conventional oven and samples were taken daily.
- Gel “Rho, seeding” was only heated at 120°C due to previous results indicating this would be most favourable. The heating duration was 1-5 hours as for the other samples.

3.7 Results and Discussion

3.7.1 Zeolite A

3.7.1.1 Conventional Syntheses

Two different gels were used to prepare zeolite A, as outlined in the "Gel Compositions" section. To verify whether each gel, aged or not, yielded zeolite A under conventional heating, a sample was heated for 3.5 hours at 99°C. The product was collected by filtration before drying and subjecting to powder X-ray diffraction (XRD) analysis. These powder patterns were used to compare the microwave-heated samples against. The computer program CELL was used to verify that the peaks were correctly assigned and to determine the lattice parameter (see Table 3.2 on page 73).

The individual X-ray diffraction patterns are shown on the following page in Figure 3.4. Under conventional conditions, the reagents and ageing process did not appear to affect the outcome of the reaction, and all the gels formed pure zeolite A. It is believed that the variation in peak intensities seen in Figure 3.4 is due to the level of sample hydration.

3.7.1.2 Microwave Syntheses – Preliminary Results

Before the series of experiments into the effects of ageing and silica source were carried out, preliminary experiments were preformed to establish reasonable heating periods for each of the gels. Work undertaken by Slangen *et al*[6] demonstrated that after ageing a gel containing fumed silica for 20 hours, crystalline products were obtained after 5 minutes heating at 100°C in a microwave oven. Bearing this information in mind, 10 cm^3 of each gel prepared was heated for 5 minutes in a microwave oven at 100°C, after an initial ramping stage (to obtain the desired temperature more quickly) to 120°C in 90 seconds. Although the ramp temperature was set to 120°C, the gel generally only reached 100°C in the allotted time.

Figure 3.4: Zeolite A prepared from Gels AF and AM under Conventional Conditions at 99°C, 3.5 hrs

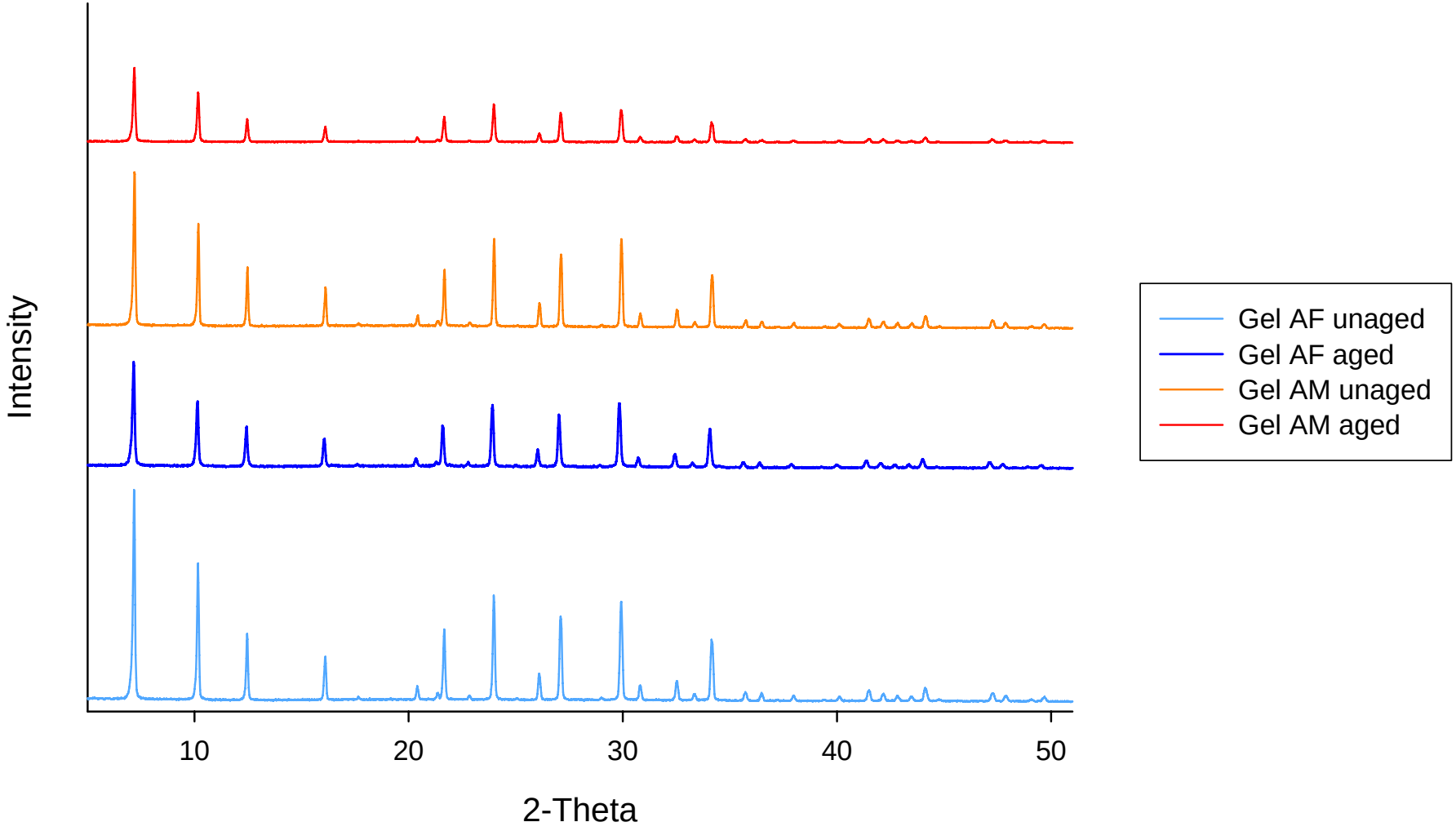

For aged gel AF, which used the fumed silica (as reported in Slangen's work[6]) the initial findings were disappointing. The powder XRD pattern showed no zeolite A peaks, as can be seen in the figure below.

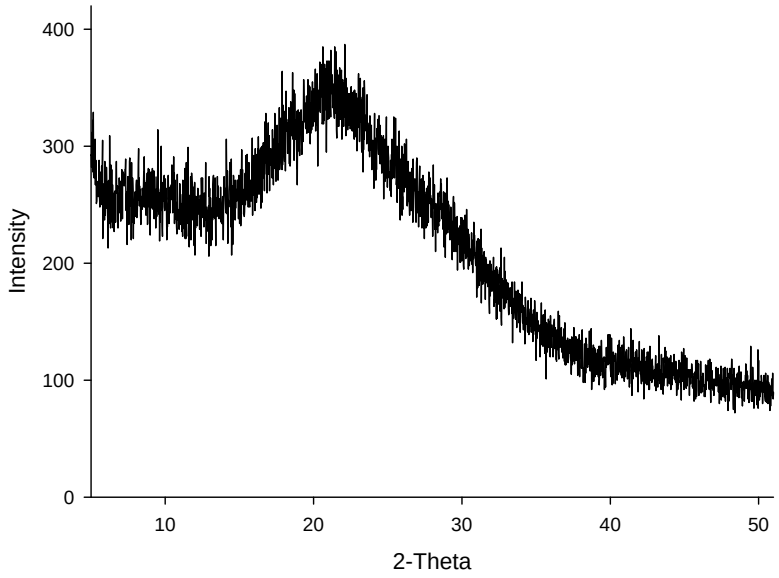

Figure 3.5: Aged Gel AF, heated in a microwave oven at 100°C for 5 minutes

The preliminary results for gel AM, which contained sodium metasilicate in place of fumed silica, showed far more promise than those from gel AF. After just five minutes of heating, the powder XRD pattern showed a large number of the zeolite A peaks to be present with a slightly amorphous background, as illustrated in Figure 3.6 below.

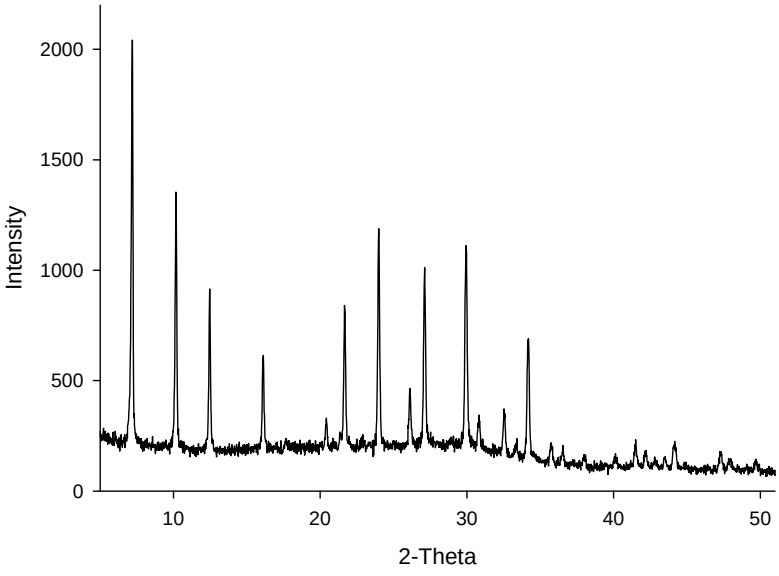

Figure 3.6: Aged Gel AM, heated in a microwave oven for 5 minutes at 100°C

These early experiments determined the heating durations to be used for each gel. It was clear that after 5 minutes, gel AF was far from producing crystalline zeolite A, and so a maximum time of one hour was used, with a sample being removed every 10 minutes.

For gel AM, however, which had yielded a zeolite A product, a maximum heating period of half an hour was used, and samples were removed every 5 minutes.

3.7.1.3 Microwave Syntheses – Full Experiments

Following the initial work, gel AF was heated at 100°C (after a "ramp" stage to 120°C in 90 seconds) and samples were removed, washed, filtered and dried at 10 minute intervals. This method was followed for aged and unaged gels. Stack plots of the powder X-ray diffraction patterns for gel AF are shown on the following page in Figures 3.7 and 3.8.

For the unaged gel AF (prepared from fumed silica), it took 60 minutes to produce a product which, through powder XRD, could be identified as zeolite A. However, this pattern was poorly formed as shown by the broad peaks and the relatively noisy background seen in Figure 3.9 on page 68. This suggests that crystallisation was incomplete.

When gel AF was heated in a microwave oven after ageing for 24 hours, the results were more impressive. After 20 minutes at 100°C, zeolite A was detected in the XRD pattern. When 30 minutes had passed, a good powder pattern was produced, as Figure 3.8 shows. This shows a clear improvement in the synthesis time when samples are aged prior to heating. This was expected, as previous workers found the ageing process to be advantageous in reducing the reaction time[6].

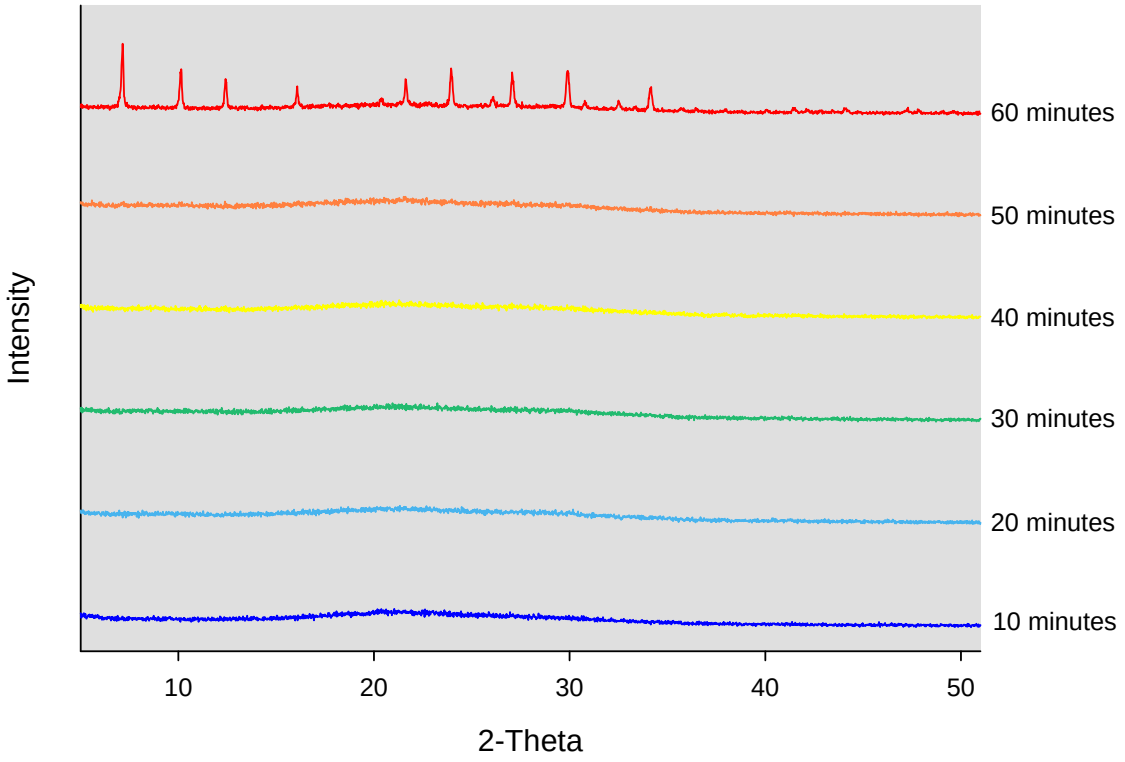

Figure 3.7: XRD patterns of Unaged Gel AF after Microwave Heating at 100°C

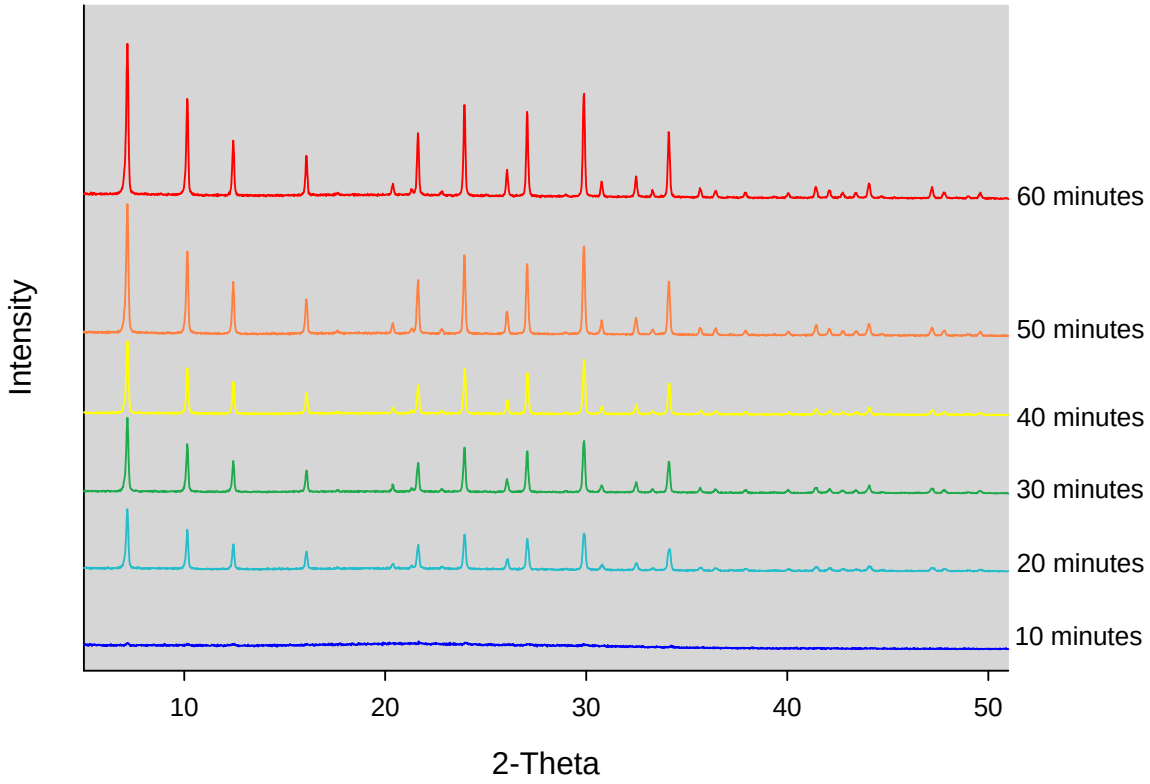

Figure 3.8: XRD patterns of Aged Gel AF after Microwave Heating at 100°C

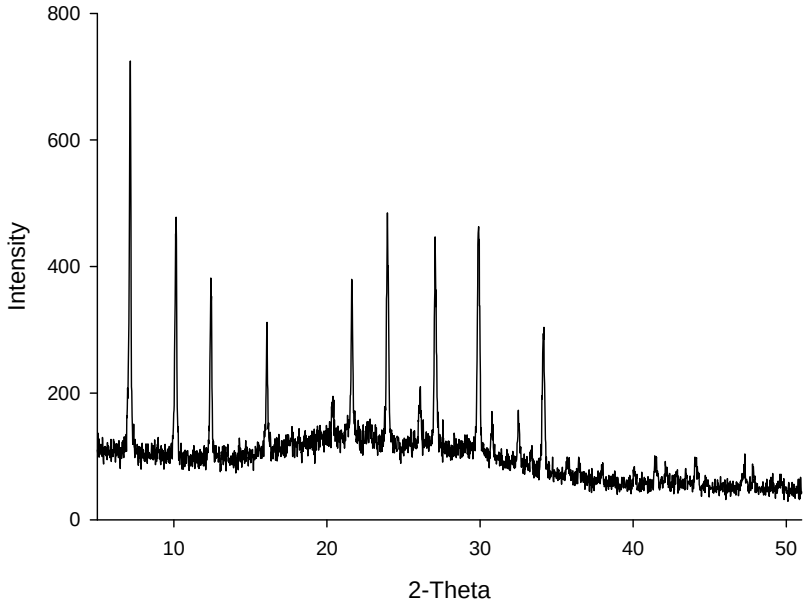

Figure 3.9: XRD pattern of Unaged Gel AF after Heating in a Microwave Oven for 60 minutes at 100°C

When the silica source was changed from fumed silica to sodium metasilicate, a further reduction in the synthesis time was observed. On the next page, stack plots of powder X-ray diffraction patterns for aged and unaged gel AM are shown. It is again clear that ageing was beneficial. This time, ageing lowered the time taken to yield zeolite A from 20 minutes to 10 minutes.

From longest to shortest synthesis time, the trend is:

Unaged Gel AF > Aged Gel AF ≈ Unaged Gel AM < Aged Gel AM

It would therefore appear that the silica source has significantly influenced the time taken to yield zeolite A. Ageing is also of great benefit to lowering the time necessary for heating the gel.

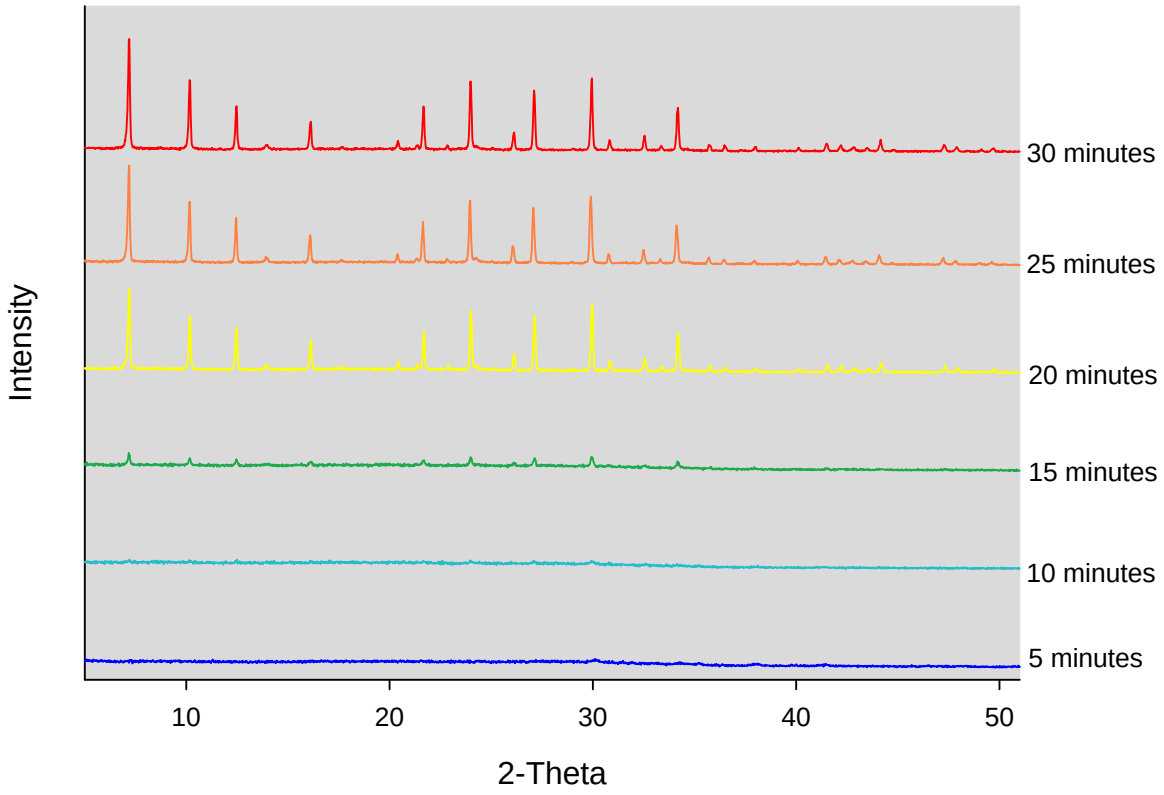

Figure 3.10: XRD patterns of Unaged Gel AM after Microwave Heating at 100°C

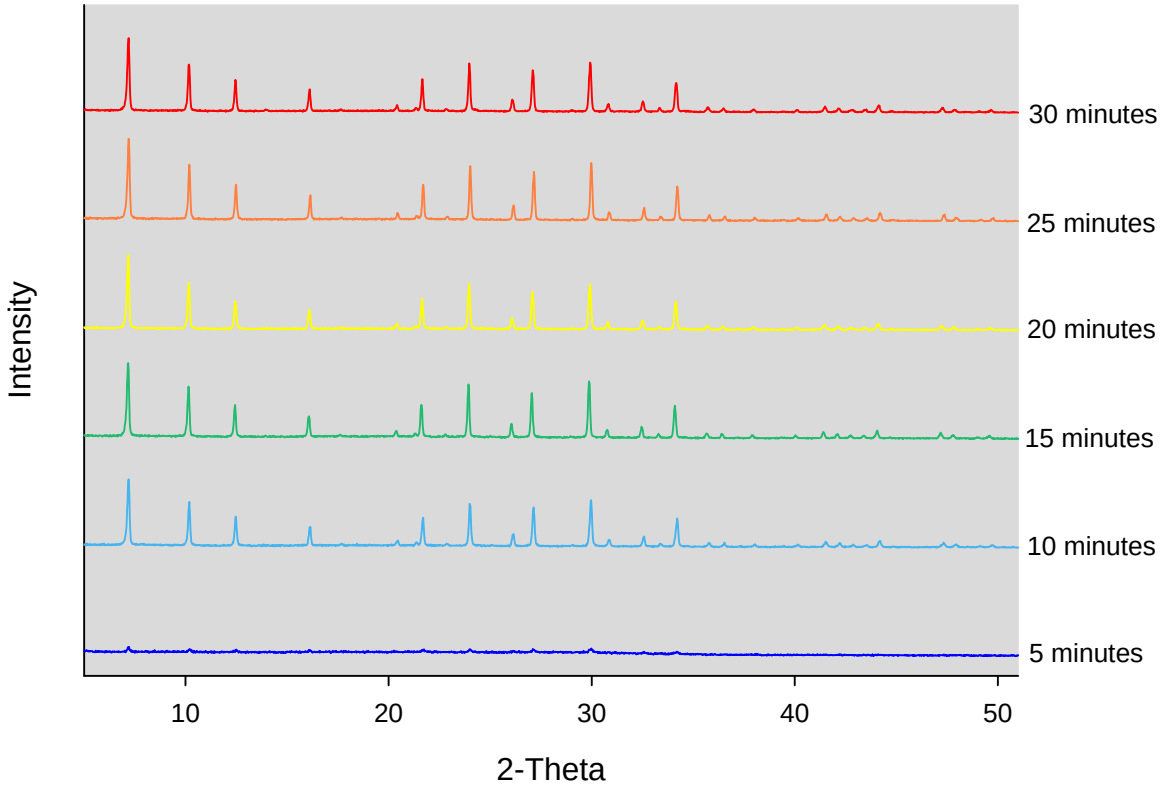

Figure 3.11: XRD patterns of Aged Gel AM after Microwave Heating at 100 °C

3.7.1.4 Comparison of Products with SEM

Some of the samples prepared were examined under a scanning electron microscope (SEM) to observe whether the different methods used in the synthesis of zeolite A had any effect on morphology or crystal size. It is acknowledged that zeolite crystals formed in a microwave oven tend to be smaller due to their more rapid formation, which limits growth time. A comparable set of samples was studied and their crystal sizes noted in Table 3.2 on page 73.

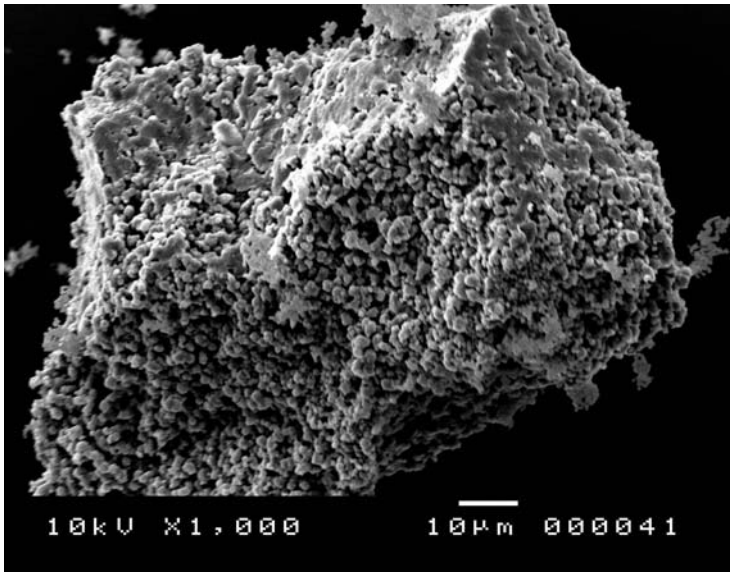

Figure 3.12: Zeolite A, prepared from aged Gel AF in a conventional oven (3.5 hrs at 99°C)

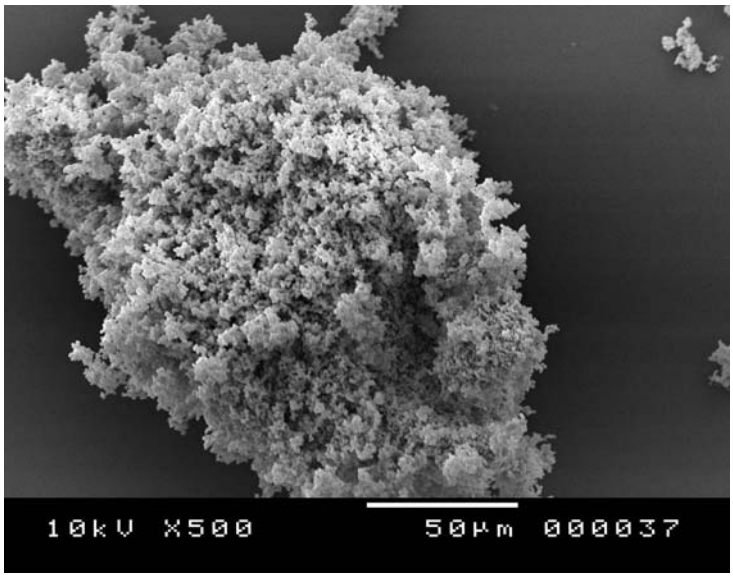

Figure 3.13: Zeolite A, prepared from aged Gel AM in a conventional oven (3.5 hrs at 99°C)

Figure 3.14: Zeolite A prepared in a microwave oven at 99°C in 30 minutes

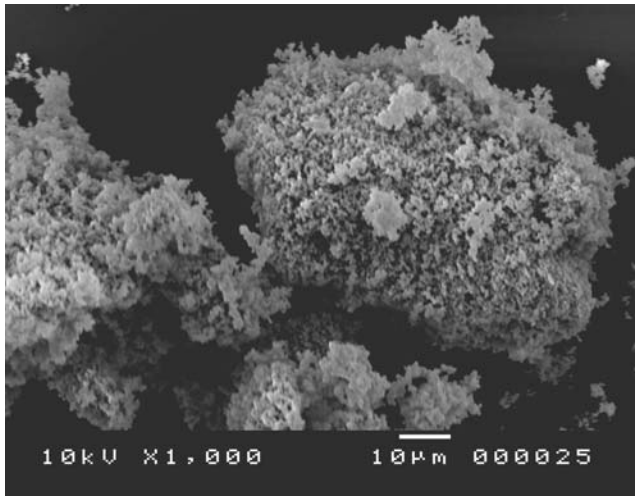

Figure 3.14a: Aged Gel AF

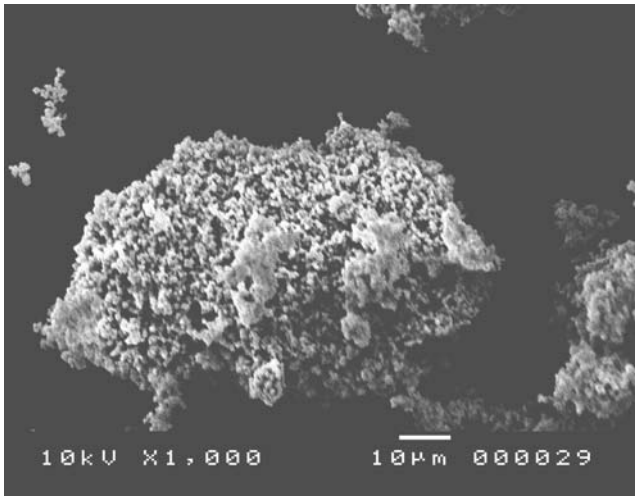

Figure 3.14c: Aged Gel AM

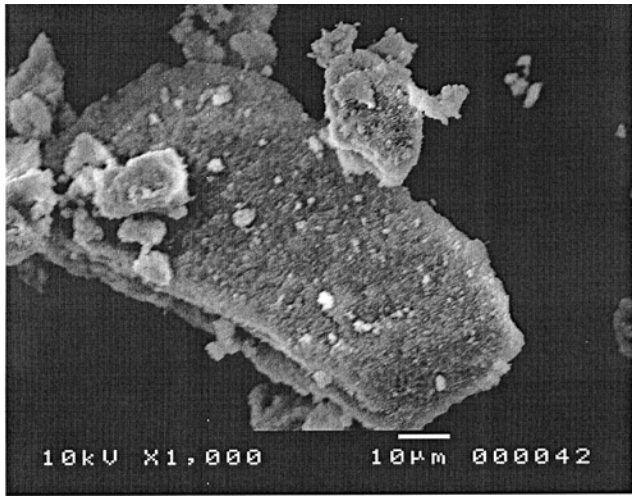

Figure 3.14b: Unaged Gel AF

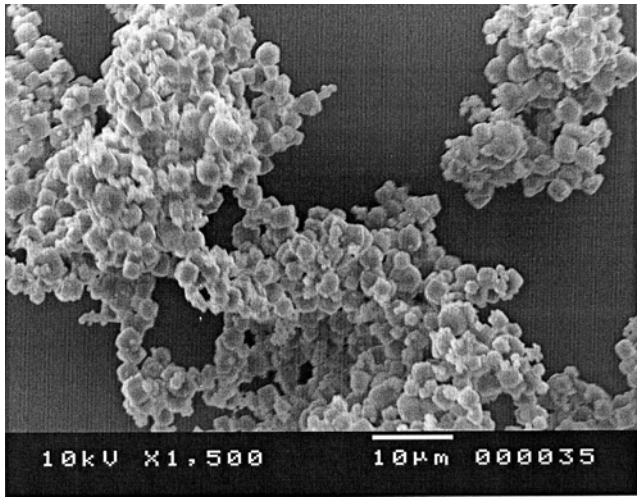

Figure 3.14d: Unaged Gel AM

Figure 3.15: Powder X-ray Diffraction Patterns of Zeolite A prepared in a Microwave Oven at 100°C in 30 minutes

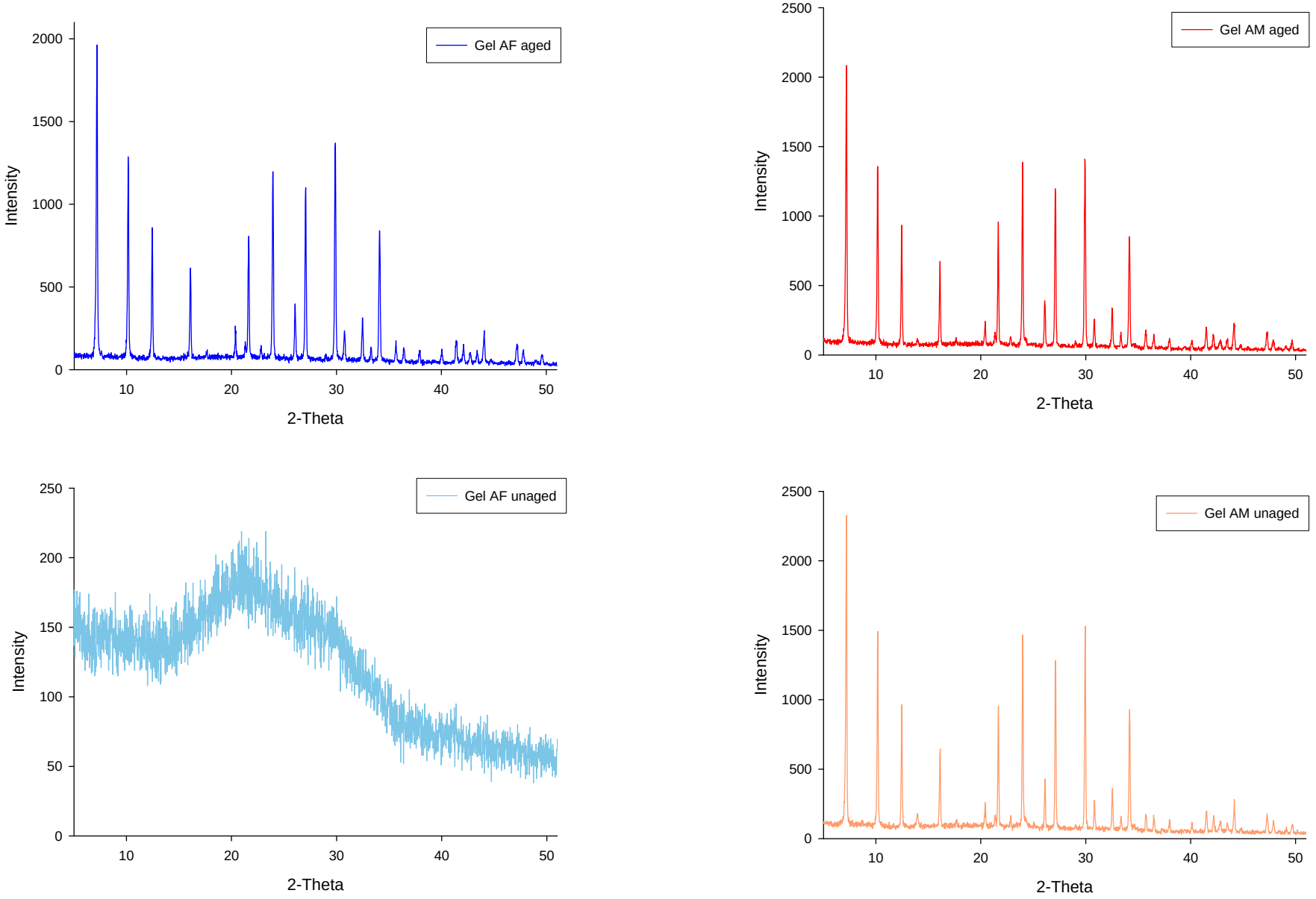

Table 3.2: Crystal Data Obtained from SEM and XRD Data

Gel	Aged?	Heating method & duration	Crystal size from SEM (μm)	Lattice parameter (Å)	ESD
AF	Yes	Conventional, 99 °C, 3.5 hrs	1.00 - 2.00	24.674	0.005
AF	No	Conventional, 99 °C, 3.5 hrs	–	24.602	0.003
AM	Yes	Conventional, 99 °C, 3.5 hrs	1.10	24.612	0.004
AM	No	Conventional, 99 °C, 3.5 hrs	–	24.613	0.003
AF	Yes	Microwave, 100 °C, 30 mins	0.50	24.646	0.004
AF	No	Microwave, 100 °C, 30 mins	–	N/A	N/A
AM	Yes	Microwave, 100 °C, 30 mins	0.60	24.604	0.004
AM	No	Microwave, 100 °C, 30 mins	0.50 - 2.50*	24.597	0.005

* Majority of crystals nearer 2.50 μm in size

The lattice parameters were determined using the computer program "CELL" which requires data from powder XRD patterns. The unit cell size is consistently ~ 24.6 Å, regardless of the method, so it can be concluded that the zeolite A formed is of a reproducible quality. The variation between the second decimal places is thought to be due to the level of hydration, which was affected by the length of the drying process of the zeolite crystals after filtration. On the whole, the zeolite A samples synthesised in a conventional oven have a larger crystal size, with the exception of unaged gel AM in a microwave oven.

Although ageing decreased the time required to form zeolite A, the quality of crystals produced was not necessarily improved. In fact, unaged gel AM showed the best formed crystals (see Figure 3.14d). This is due to the fact that the ageing period induces nuclei growth, and the more nuclei present, the smaller the final crystals. The unaged gel would not have had this period in which to form nuclei, hence the crystals will be larger as there are fewer nuclei competing for the reagents present.

Gel AF was less successful than gel AM in a microwave oven, although both gels were comparable when heated conventionally. This contrast is highlighted when Figures 3.14b and d are examined - 3.14b shows a piece of unreacted starting material from gel AF, whereas

3.14d shows a fully formed array of zeolite A crystals.

3.7.1.5 Discussion

The ageing of gels allows nuclei to form prior to heating in an oven. However, the slow heating to reaction temperature in a conventional oven also allows the formation of nuclei, so there was little difference between aged and unaged zeolite samples.

In the case of the microwave synthesis of zeolite A, it is clear that ageing the gel for 24 hours before heating reduces the time taken to synthesise the desired product, and from both gels used, it appears that the ageing process reduces the synthesis time by approximately half. It is also evident from the results displayed above, that the reagents used to synthesise zeolite A have an impact on not only the time taken to yield the zeolite product, but also the crystal morphology of that product. In this instance, the use of sodium metasilicate (in aged gel AM) instead of fumed silica (in aged gel AF) reduced the synthesis time from 30 to 15 minutes. The powder X-ray diffraction patterns and SEM photographs support this conclusion.

The shorter synthesis time when ageing is implemented is most likely due to the extra period in which nuclei can form[6]. Whilst it may be argued that the true synthesis time is the ageing period plus the heating time (for example, in the case of aged gel AM: 24 hours plus ¼ of an hour cf. unaged gel AM: 25 minutes), the total *heating* time required after ageing is less, and this on a large industrial scale would cut the cost of heating in half.

The effect the reagents have on the synthesis of zeolite A is quite dramatic. It is possible that these effects are due to the dissolution of the gel being altered by the chemicals present, which

would influence the pH of the gel and how many species could be dissolved into the solution phase to react. Literature work discussing the importance of gel pH and reagents in zeolite synthesis has shown that zeolites crystallise in a particular pH range[21] and the yield is also affected[23].

3.7.2 Zeolite X

3.7.2.1 Conventional Syntheses

Zeolite X was prepared from all three silica sources: sodium metasilicate pentahydrate in gel XM, colloidal silica in gel XC and fumed silica in gel XF. Precise quantities are listed in the section "Gel Compositions". Although zeolite X could be formed in 24 hours, the sample purity was enhanced if the heating period was extended to 48 hours. Conventional syntheses of zeolite X do not require ageing. However, for the purposes of direct comparison, gel XF was aged as the microwave sample required ageing.

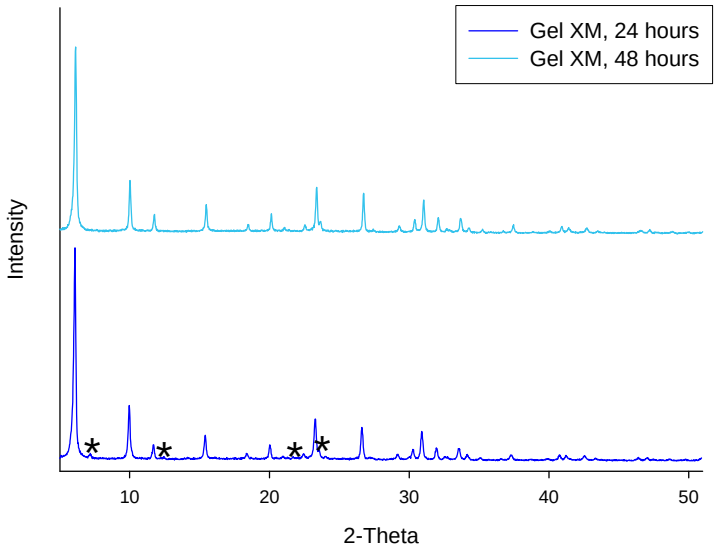

Figure 3.16: X-ray diffraction pattern of gel XM heated in a conventional oven at 80°C; * indicate zeolite A peaks

Zeolite X was firstly made from sodium metasilicate. According to the synthesis, zeolite X is formed at 80°C, although the higher temperature of 90°C was found to be advantageous in microwave syntheses of zeolite X, so all gels were heated at both temperatures in a conventional oven for direct comparisons to be drawn. The higher temperature in the conventionally heated gels appeared to be neither detrimental nor beneficial to the final product. Although there are a couple of differences between the patterns in Figure 3.17, these are most likely due to hydration levels of the products, caused by the drying process of

the recovered powders. These differences are reflected by the lattice parameters, which are 24.928 Å for the 80°C sample and 25.110 Å for the 90°C product.

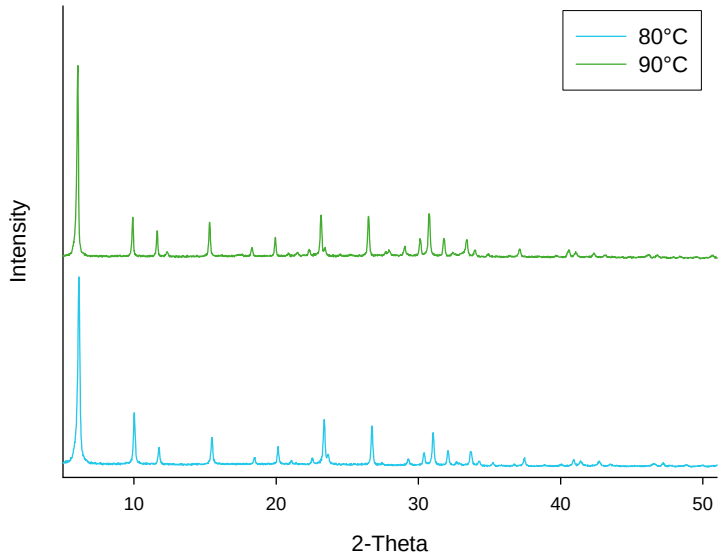

Figure 3.17: Comparison of zeolite X made from gel XM heated in a conventional oven for 48 hours

Results of heating the various gels conventionally indicate that gel XM yielded the best zeolite X product as can be seen in Figure 3.18 below.

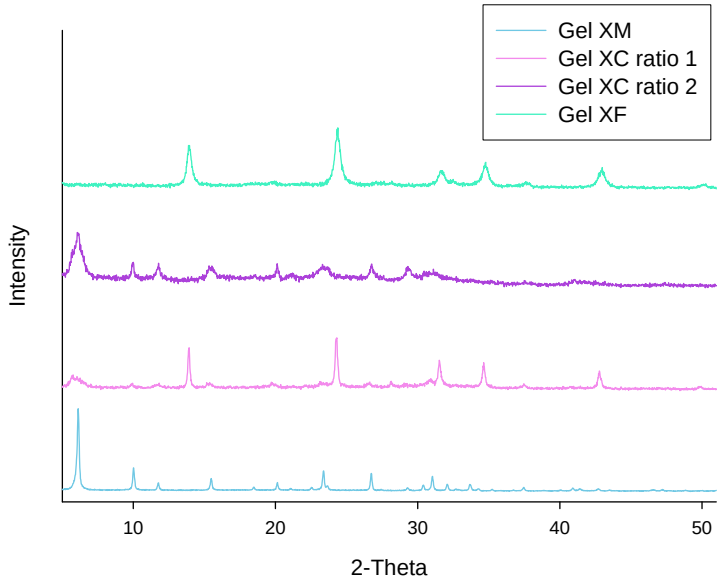

Figure 3.18: Comparison of zeolite X made from different gels in a conventional oven at 80°C in 48 hours

As illustrated in Figure 3.18, only gel XM yielded zeolite X. Gel XC (ratio 1) and gel XF both produced sodalite and gel XC (ratio 2) formed zeolite X, but the peaks are very broad and the background is so noisy as to obscure the peaks which appear at 2θ over 30°. The broad peaks are most likely a result of very small crystals. Indeed, peak width analysis using the Scherrer Equation (see section 2.1.4 on page 22) gives a crystal size estimate of just 26 nm (note that the zeolite X crystals formed by gel XM were over 0.3 μm in size). Although the gels used to make zeolite X varied in SiO_2/Al_2O_3 ratio, it was hoped that the excess silica used would help encourage zeolite X formation. However, it was gel XM, with the lowest Si/Al ratio, that formed the best zeolite X. Gel XC (ratio 2) formed some zeolite X and had the highest ratio of silicon to aluminium. Gels XC (ratio 1) and XF, of intermediate Si/Al levels, formed exclusively sodalite.

3.7.2.2 Microwave Syntheses - Preliminary Results

The first set of experiments performed used gel XM, which contained sodium metasilicate as the silica source. Work was carried out to compare the products obtained when the gel was heated in a microwave oven with and without ageing. It was clear that ageing the gel shortened the time taken to yield products.

As can be seen in Figure 3.19, ageing improved (albeit only slightly) the quality of product obtained. Increasing the amount of silica by 10% from 12.72 g to 13.99 g (see section 3.6 "Gel Compositions") altered the sample quality for the better. The impurity peaks are slightly diminished in intensity with respect to the zeolite X peaks when more silica was added to the initial gel. It was also hoped that lowering the temperature would decrease the incidence of zeolite A formation which is known to be produced at 100°C.

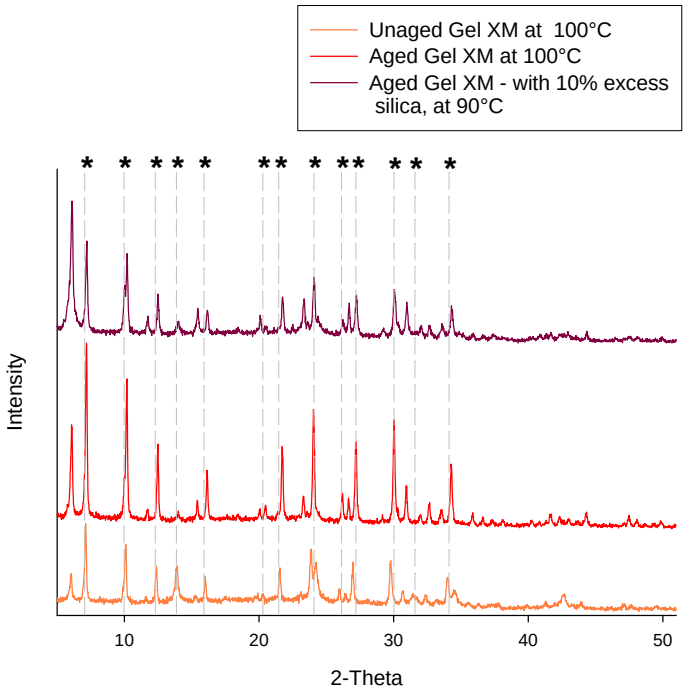

Figure 3.19: Zeolite X prepared from Gel XM in a microwave oven for 60 minutes

* indicate peaks due to impurities – in this instance predominantly zeolite A

3.7.2.3 Microwave Syntheses – Full Experiments

Further experiments were carried out with the reaction temperature in the microwave oven further lowered to 80°C (the same temperature used in conventional oven syntheses). As can be seen from Figure 3.20, the sample quality did not improve: the figure shows a comparison of products formed at 80°C in both conventional and microwave ovens. Prolonging the heating period in the microwave oven did not have any beneficial effects on crystallisation of the desired product.

The majority of peaks for the microwave oven prepared samples in Figure 3.20 can be indexed to zeolite A. A few peaks (indicated) can be identified as belonging to zeolite X and sodalite.

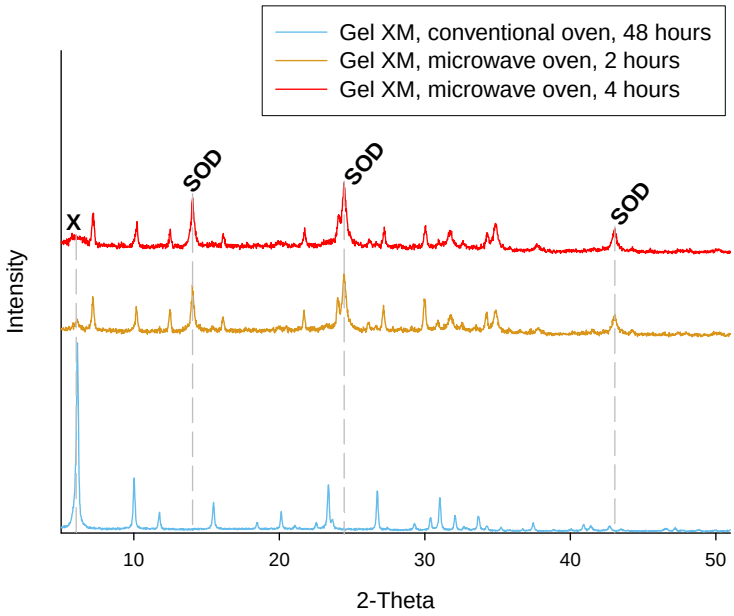

Figure 3.20: Comparison of products using powder XRD.

All samples were prepared at 80°C.

SOD denotes sodalite phase, X represents the major zeolite X peak (111).

When reagents were changed to colloidal silica (gel XC) two SiO_2/Al_2O_3 ratios were used. These ratios were increased relative to gel XM in an attempt to promote the slightly more siliceous zeolite X over zeolite A formation.

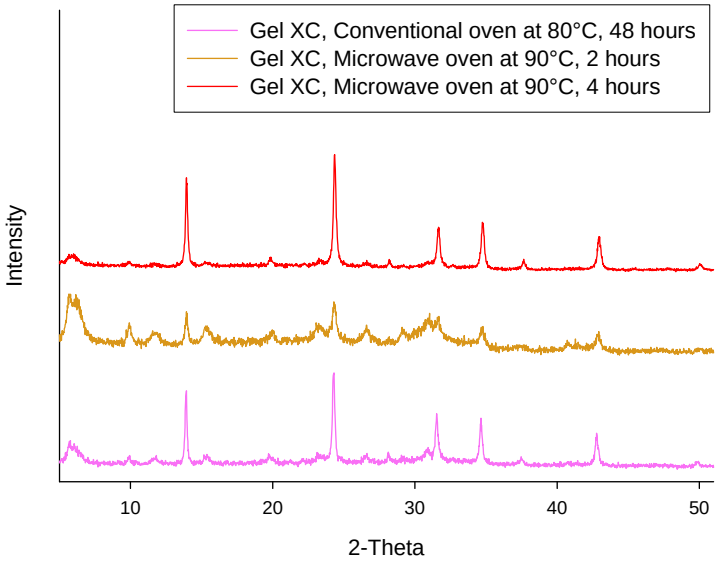

Figure 3.21: Powder XRD patterns for products formed by gel XC (ratio 1) via conventional and microwave heating methods

In the powder XRD patterns shown in Figure 3.21, it is clear that the product was predominantly sodalite. It is interesting to note that the microwave preparation seems to yield a better quality product of sodalite than the conventional heating method.

When the ratio of silicon to aluminium was increased slightly, there was a marginal improvement. Although the peaks in Figure 3.22 can be indexed to zeolite X, the peaks are broad and against a relatively high background. By examining the peak widths, an estimate of crystal size was obtained. The conventionally synthesised zeolite X had the largest crystals at 22 nm, and the two microwave produced samples had marginally smaller crystals of between 17 and 18 nm. There was no detectable improvement in sample quality or crystal size when the heating period was doubled from 2 to 4 hours.

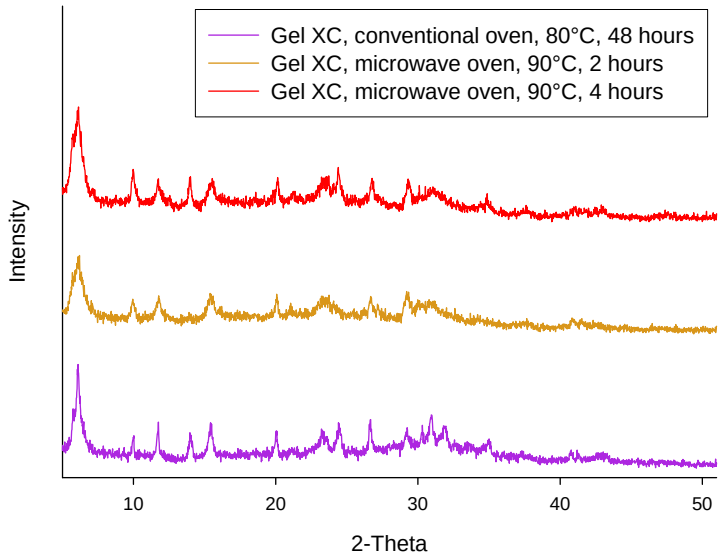

Figure 3.22: Powder XRD patterns of the product formed from gel XC (ratio 2) in conventional and microwave ovens

Finally, attempts were made to make zeolite X using fumed silica in gel XF. Figure 3.23 shows that the synthesis attempt again resulted in formation of sodalite. It was felt that due to the nature of the fumed silica, higher Si/Al ratios would not be used, as increasing amounts

of water would be necessary for dissolution into the gel phase.

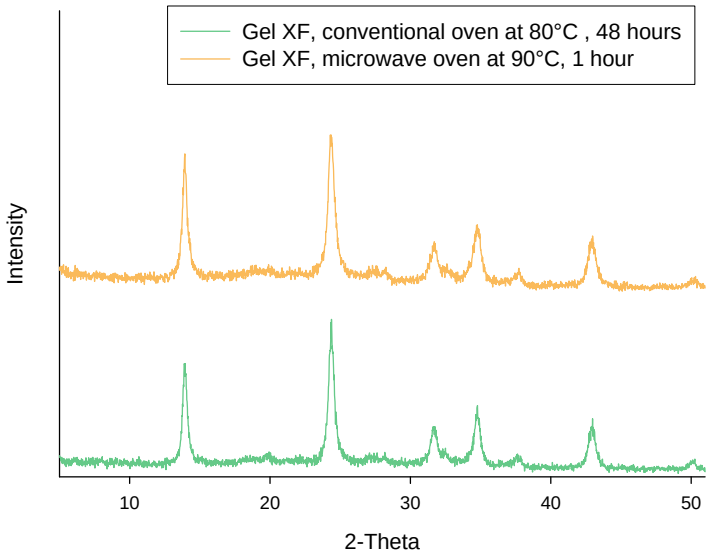

Figure 3.23: Powder XRD of gel XF products from conventional and microwave heating

3.7.2.4 Examination with SEM

Only gel XM heated in the conventional oven was successful in producing zeolite X. The micrograph below shows the size of the crystals formed in this way to be approximately 2 μm.

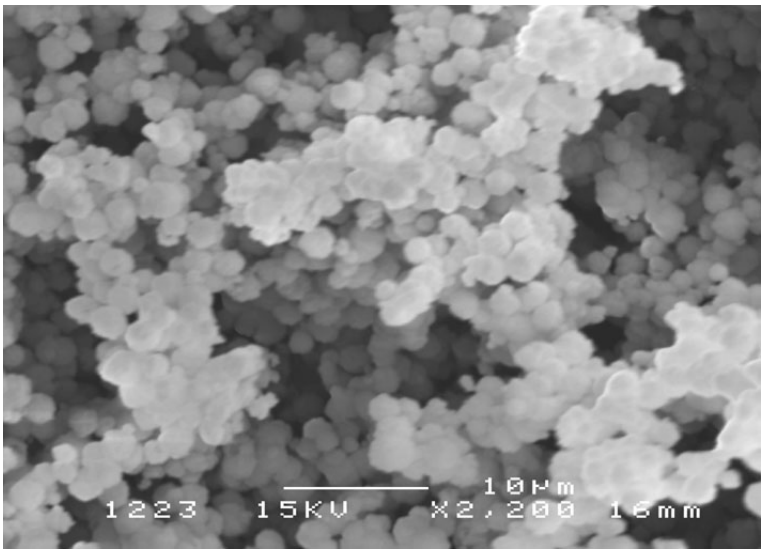

Figure 3.24: Zeolite X synthesised in a conventional oven at 80°C from gel XM

Some zeolite X, in the form of small crystals with sodalite impurities present, was formed from the gel containing colloidal silica, i.e. XC (ratio 2).

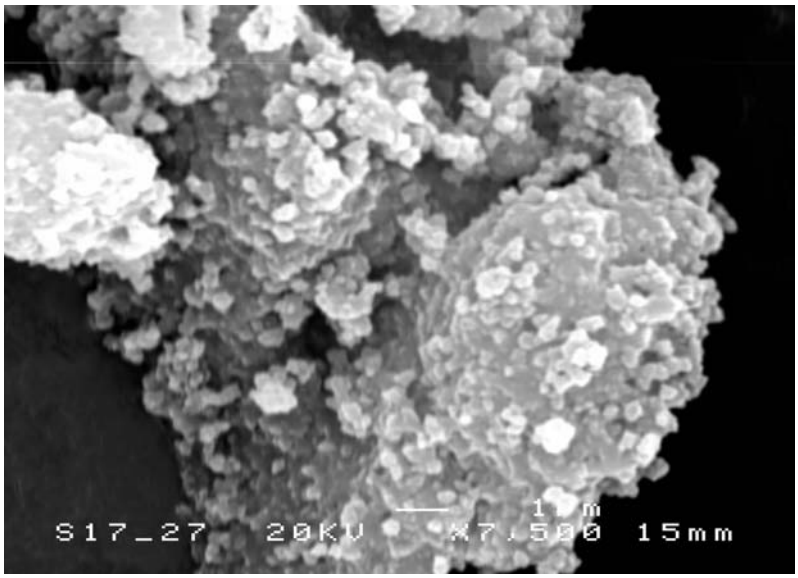

Figure 3.25: SEM image of sample produced from the conventional heating of gel XC (ratio 2) at 80°C, 48 hours

As can be seen in the above figure, the zeolite X crystals appear to be very small (~0.3 μm) and to be adhering to a piece of larger material. It is questionable whether the material was an unreacted reagent as there was no evidence of their presence in the powder X-ray diffraction pattern (see Figure 3.18).

From the powder X-ray diffraction patterns of other samples, it was deemed that the quality was insufficient to merit studying with the scanning electron microscope. The majority of products from the above set of experiments were mixed or partially amorphous and it was felt that no more useful information would be gained by further examination.

3.7.2.5 Discussion

Work examining the effect of silica source on the synthesis of zeolite X in a convection oven has already been reported[20]. It was found that the silica sources did indeed affect the level of impurities present, the particle dimensions and the time taken to yield zeolite X. It was hoped that the effects of silica sources in a microwave synthesis would be similarly successful and enable comparisons in this work. However, even though gel XM (which used sodium metasilicate) yielded pure zeolite X in 48 hours in a conventional oven at both 80 and 90°C, the same gel failed to produce results when heated in a microwave oven.

As zeolite A (which has a 1:1 silicon to aluminium ratio) is known to readily form in a microwave oven[5–8] (see also earlier work in this volume) it was decided that the Si/Al ratio of the zeolite gel should be increased in an effort to force production of the more siliceous zeolite X.

When zeolite A no longer formed as an impurity, sodalite was formed. Zeolite X was never synthesised alone and with a good level of crystallinity from either gel XF (fumed silica) or gel XC (colloidal silica).

No work has been published detailing synthesis of zeolite X in a microwave oven and it may be that the reasons for this are illustrated by the difficulties found in this work.

3.7.3 Zeolite Y

3.7.3.1 Conventional Syntheses

Zeolite Y was made in a conventional oven at 90°C in 19 hours. All three silica sources were used. In Figure 3.26 below are the powder X-ray diffraction patterns of all the samples produced in the conventional oven. It is interesting to note that gels YC, YM and YF (literature) formed good quality crystalline zeolite Y, whilst gel YF (which differed from the literature gel only by an increased level of sodium) produced a poor quality, partially amorphous sample of zeolite Y. The broad peaks for the latter sample indicated small zeolite Y crystals were formed. An estimation of crystal size was obtained from an SEM image (see Figure 3.32d) of the sample, and the crystals were found to be smaller than 0.2 μm. This was significantly smaller than the crystals produced by gel YC which were approximately 1 μm in size.

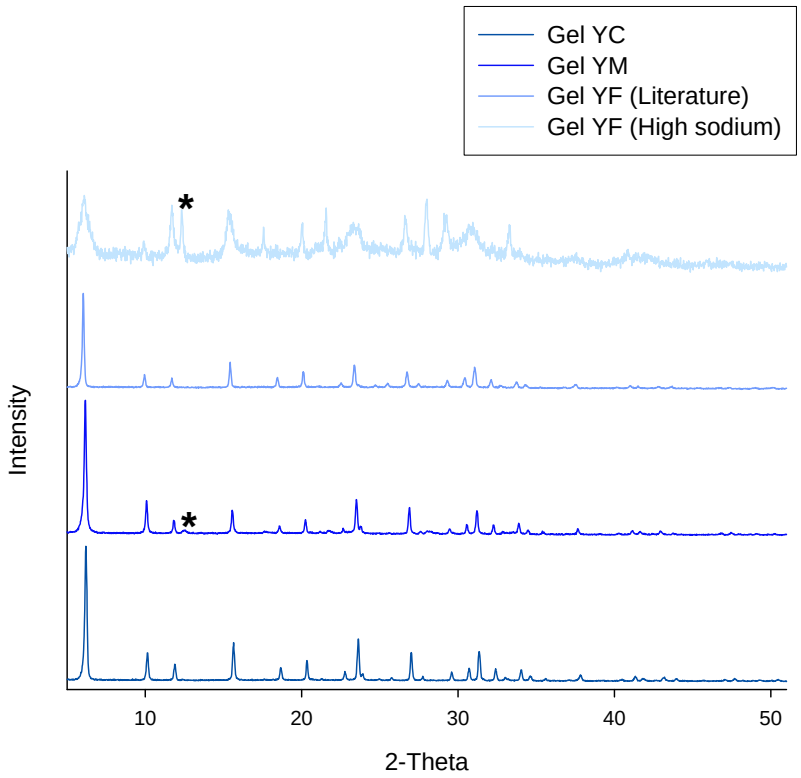

Figure 3.26: Powder XRD patterns of products formed in a conventional oven at 90°C in 19 hours.

* indicates zeolite A (222) impurity.

As microwave reactions were carried out at the higher temperature of 100°C, conventional syntheses were also carried out at this temperature to ensure that the elevated temperature alone was not responsible for any difference in sample quality. The powder XRD patterns of products formed from gel YC, in a conventional oven in 19 hours at different temperatures, are shown in Figure 3.27 below.

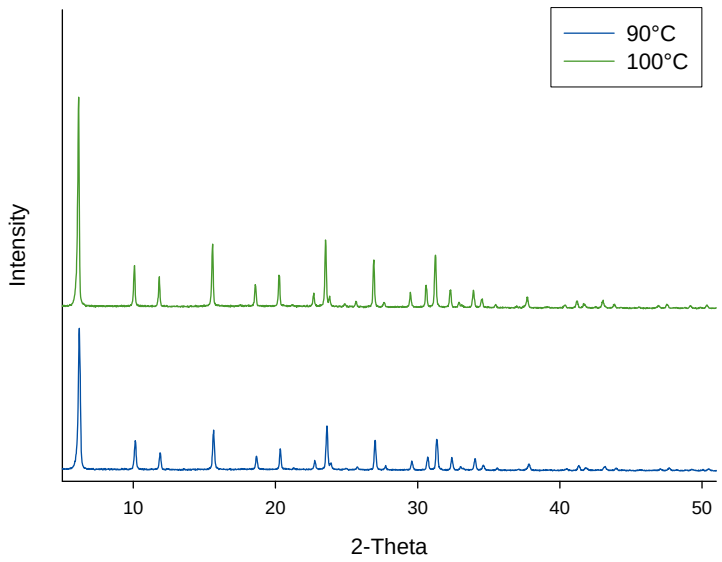

Figure 3.27: Powder XRD of products formed from gel YC in a conventional oven in 19 hours

As can be seen in the above figure, temperature does not affect the outcome of the reaction of gel YC.

3.7.3.2 Microwave Syntheses

As all previous work outlined in this volume and literature research[6,9] pointed to the benefits of ageing, all gels to be microwave heated were aged for 24 hours. Following on from the work of Arafat *et al*[1] which performed reactions in a microwave oven at 100°C, this temperature was used in this work.

When aged for 24 hours, heating of gel YC in a microwave oven was successful in that crystalline zeolite Y was formed. The powder X-ray diffraction patterns in Figure 3.28 show the evolution of the formation of zeolite Y.

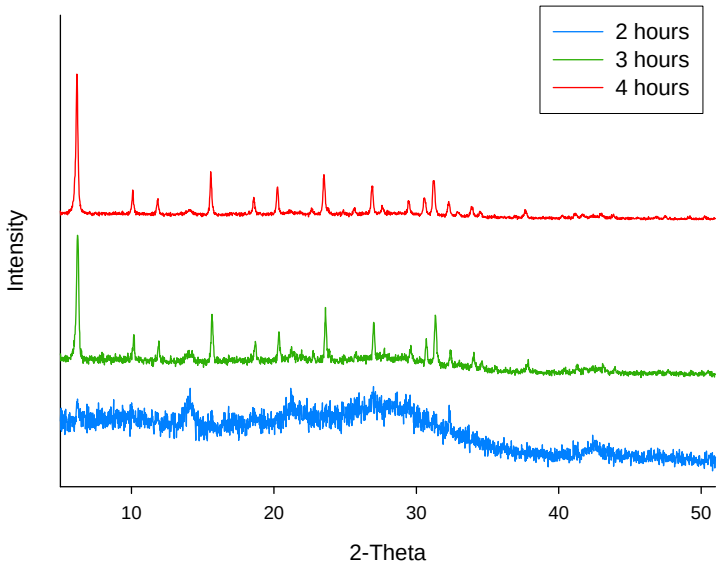

Figure 3.28: Powder XRD patterns of zeolite Y produced from gel YC in a microwave oven at 100°C

After two hours at 100°C, the product is largely amorphous. Leaving the gel to heat for three hours leads to the production of zeolite Y, the quality of which is slightly improved upon heating the gel for four hours. The zeolite Y peaks are narrow and well formed from early on as can be seen in the above figure.

Gel YM, which contained the sodium metasilicate, was also heated in a microwave oven under identical conditions. This time zeolite Y crystallised far quicker than seen with gel YC. In Figure 3.29 on the next page it can be seen that after just one hour of heating at 100°C there were already peaks attributable to zeolite Y present. Further heating at 100°C for two and three hours improved the quality of the sample, although after four hours, no further benefit was gained with respect to heating the gel for three hours.

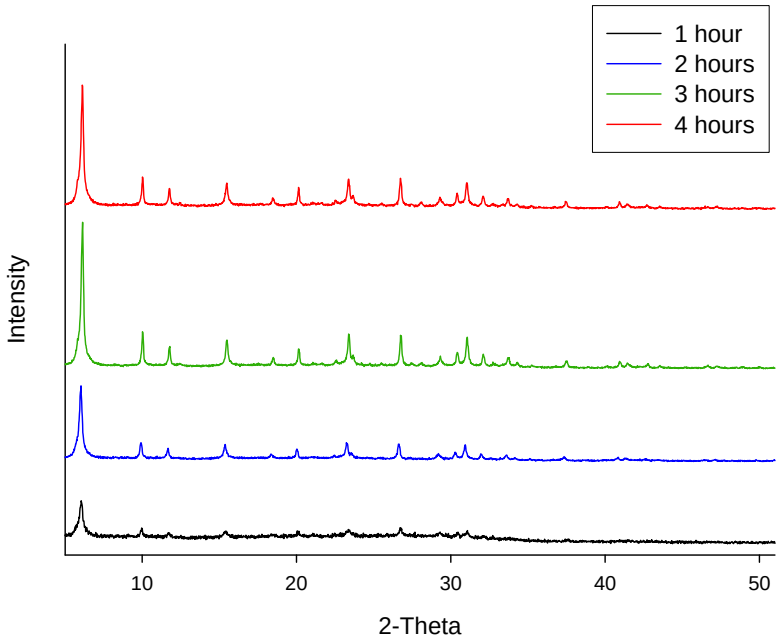

Figure 3.29: Powder XRD patterns of zeolite Y produced from gel YM in a microwave oven at 100°C

Arafat and co-workers[9] reported the synthesis of zeolite Y from fumed silica to be complete in just 10 minutes. Following on from this study, the first ratio used in this work was that suggested in the literature[9], and the duration of heating was lowered to 1 hour, with samples being removed at 15 minute intervals.

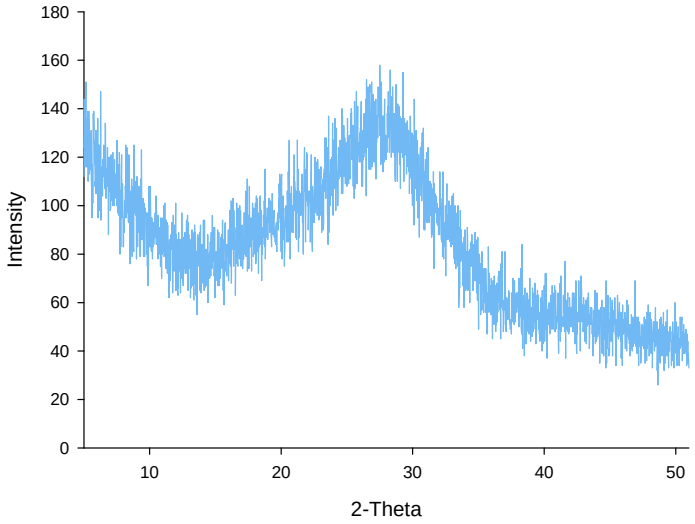

Figure 3.30: Result of heating gel YF (Literature) at 100°C in a microwave oven for 1 hour

Despite the claims made[9], the results obtained did not replicate those reported. All samples

(from 15, 30, 45 and 60 minutes) were amorphous and no trace of zeolite Y was found.

When gel YF was made with an increased level of sodium, the outcome of the synthesis was noticeably improved relative to gel YF (literature) (see the powder XRD pattern in Figure 3.31 below). Although the sample contained small crystals and was by no means totally crystalline zeolite Y, the potential is clearly there for the synthesis to be refined and a better quality sample produced. This could be due to the presence of more sodium hydroxide, which would lead to a higher pH. In more alkaline solutions, more reactants are available in solution and this leads to a faster rate of crystallisation[17].

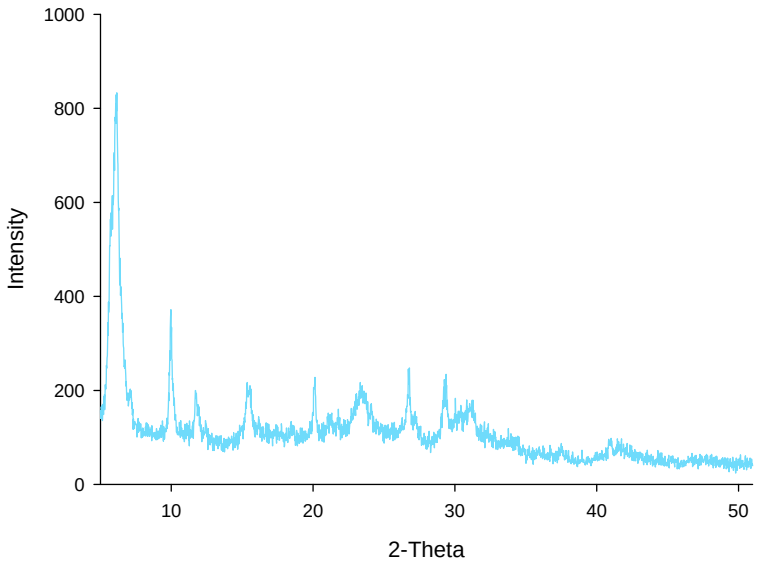

Figure 3.31: Powder XRD pattern of zeolite Y formed from gel YF in a microwave oven at 100°C for one hour

3.7.3.3 Comparison of Products using SEM

On the following page are four SEM pictures of the zeolite Y samples formed in the conventional oven. The photographs in Figure 3.32 a, b and c all show crystals of between 1 and 2 μm. However, Figure 3.32 d, which shows the product obtained from heating gel YF (high sodium), appears to show small crystals attached to a piece of unreacted starting material. This would account for the poor quality powder X-ray diffraction pattern shown in Figure 3.26.

Figure 3.32: SEM photographs of zeolite Y prepared in a conventional oven at 90°C in 19 hours

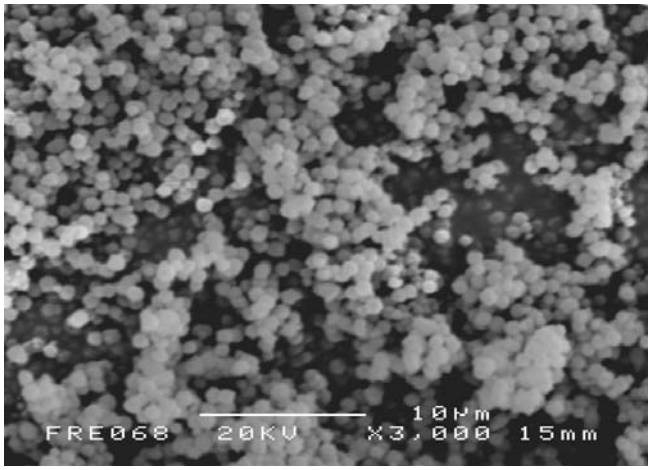

Figure 3.32a. Gel YC

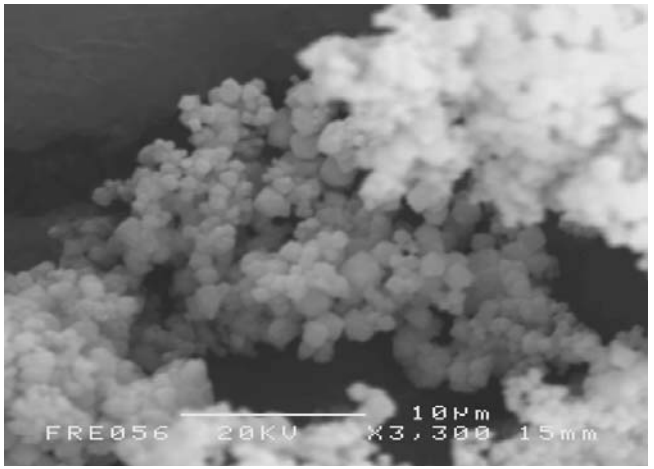

Figure 3.32c. Gel YF (literature)

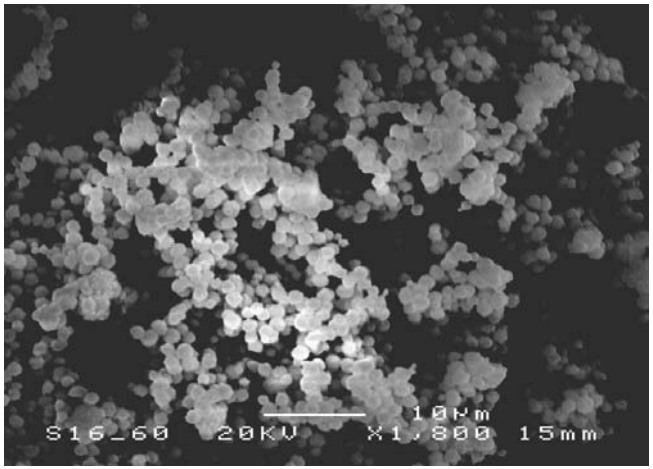

Figure 3.32b. Gel YM

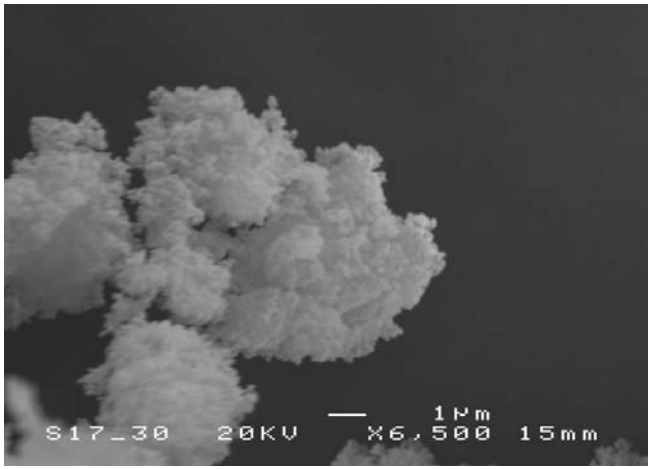

Figure 3.32d. Gel YF (high sodium)

Only gels YC and YM were successful in producing zeolite Y of good crystallinity in the microwave oven. Examination under the scanning electron microscope reveals that the crystals have the same morphology as those formed in the conventional oven. The crystal size is typically around 1 μm.

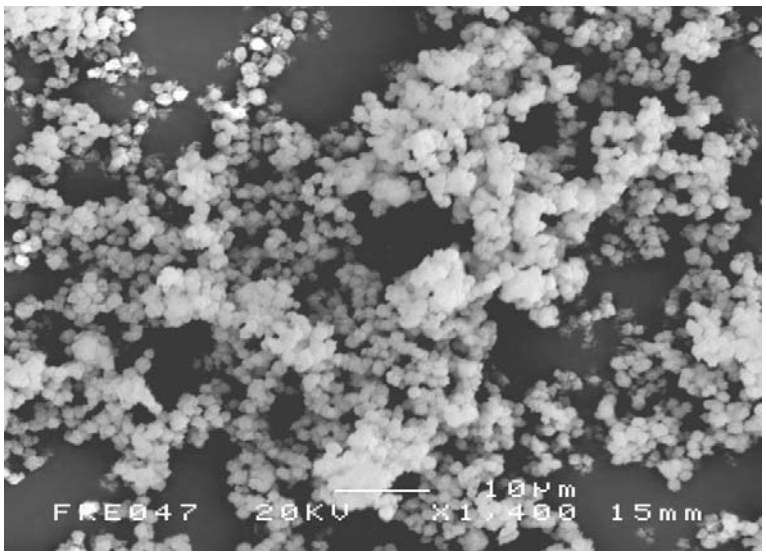

Figure 3.33: Zeolite Y synthesised from gel YM in a microwave oven at 100°C in 4 hours

3.7.3.4 Discussion

Whilst zeolite Y could be formed in a conventional oven at 90 and 100°C in 19 hours from all gels, the sample prepared from gel YF (high sodium) was poor and slightly amorphous. However, in the microwave oven, it was gel YF (high Na) which performed better than gel YF (literature). Although the zeolite Y sample showed incomplete crystallisation, some product was present, which was an improvement when compared to gel YF (literature). It is proposed that the increased sodium content, in the form of NaOH, increased the pH and brought more reactants into the solution phase, thus increasing contact between these species and enhancing the rate of crystallisation.

Gels which contained colloidal silica or sodium metasilicate were successful in synthesising zeolite Y in both conventional and microwave ovens. In terms of rate of crystallisation, gel YM was superior as good quality zeolite Y was formed in 3 hours, whereas gel YC took 4 hours to produce a sample of equivalent quality. It is believed that this is due to the difference in silica source purity[20] and pH influencing the rate of gel dissolution and nucleation, and hence crystallisation, of the products.

3.7.4 Zeolite Rho

3.7.4.1 Conventional Synthesis

Formation of zeolite rho in a conventional oven followed the method reported by Edmondson[30]. Samples were removed after heating at 80°C for 5 and 6 days to establish which heating period was most effective for synthesis of zeolite rho.

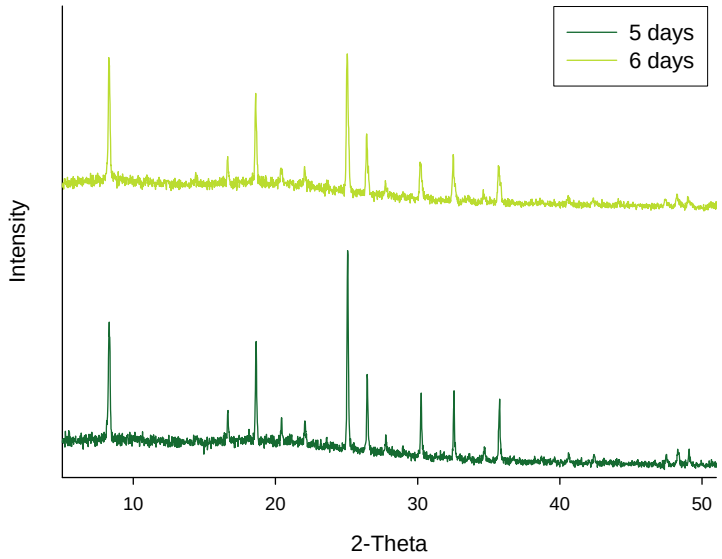

Figure 3.34: Comparison of zeolite rho samples produced in a conventional oven at 80°C

As can be seen from the powder X-ray diffraction patterns shown in the above figure, zeolite rho was satisfactorily crystallised in 5 days. No further benefit to sample quality was gained by heating the gel for a further 24 hours.

3.7.4.2 Microwave Reactions

Previous work in this thesis has shown that temperatures used in a microwave oven need to be slightly higher than those used in conventional synthesis techniques. When the zeolite rho gel was heated at 80°C for the maximum 5 hours, no product was formed. No microwave heating period over 5 hours was used for safety considerations.

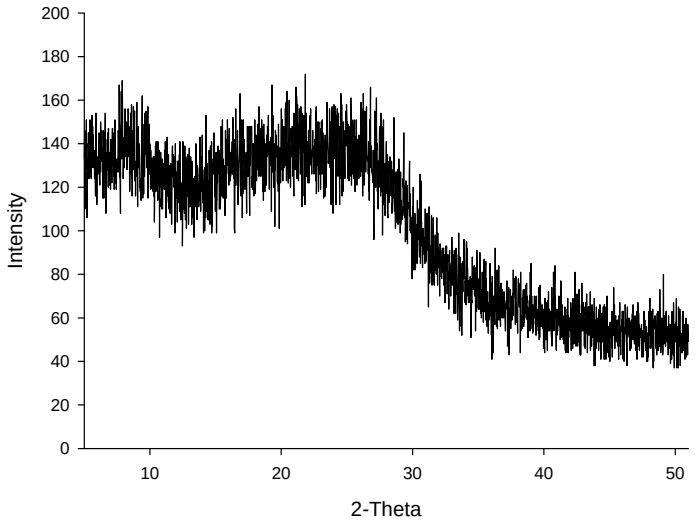

Figure 3.35: Result of heating zeolite rho gel at 80°C for 5 hours in a microwave oven

After the microwave heating program finished, any remaining gel was recombined into a preheated container which was then heated in a conventional oven at 80°C. Samples were removed after 5 and 6 days and powder X-ray diffraction patterns were obtained. It can be seen in Figure 3.36 below that the preheating in the microwave oven was not detrimental to the formation of zeolite rho, although whether this period in the microwave oven promoted crystallisation is unclear. It is certain that the gel was at the reaction temperature far quicker than would have been the case if it were heated solely in the conventional oven.

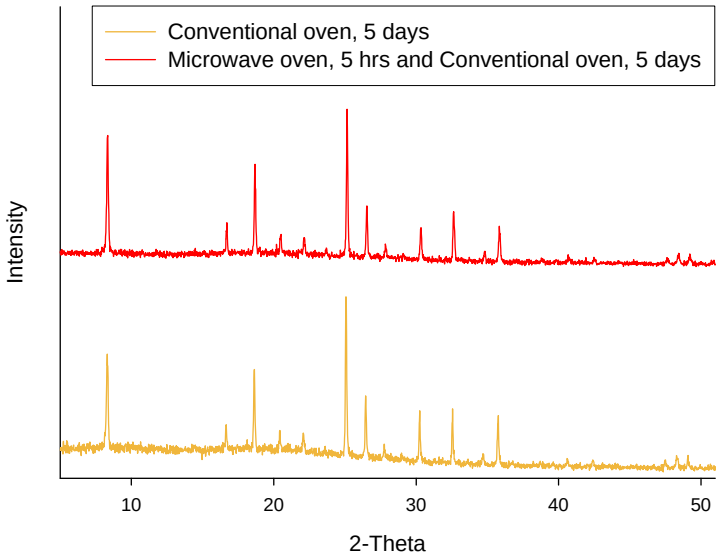

Figure 3.36: Comparison of samples of zeolite rho prepared at 80°C

This first set of experiments took place at 80°C and demonstrated that whilst the gel formed zeolite rho in a conventional oven with and without a preliminary microwave step, the synthesis was unsuccessful when microwave heating alone was used. It was reported by Zhao *et al*[12] that in the synthesis of zeolite NaY, a temperature increase of 15°C resulted in a reduction in crystallisation time by one half. Bearing this information in mind, syntheses were carried out in a microwave oven using the same zeolite rho gel as before, but at temperatures of 100, 120 and 150°C.

At 100°C no products formed in the microwave oven. Heating at both 120 and 150°C resulted in a distinct and separate piece of amorphous solid forming alongside a crystalline powder, however this was not the desired zeolite rho. The powder sample was collected separately from the amorphous solid, and the best example of this new powder phase was formed at 150°C in 5 hours. Figure 3.37 shows the formation of this sample over the 5 hours of microwave heating.

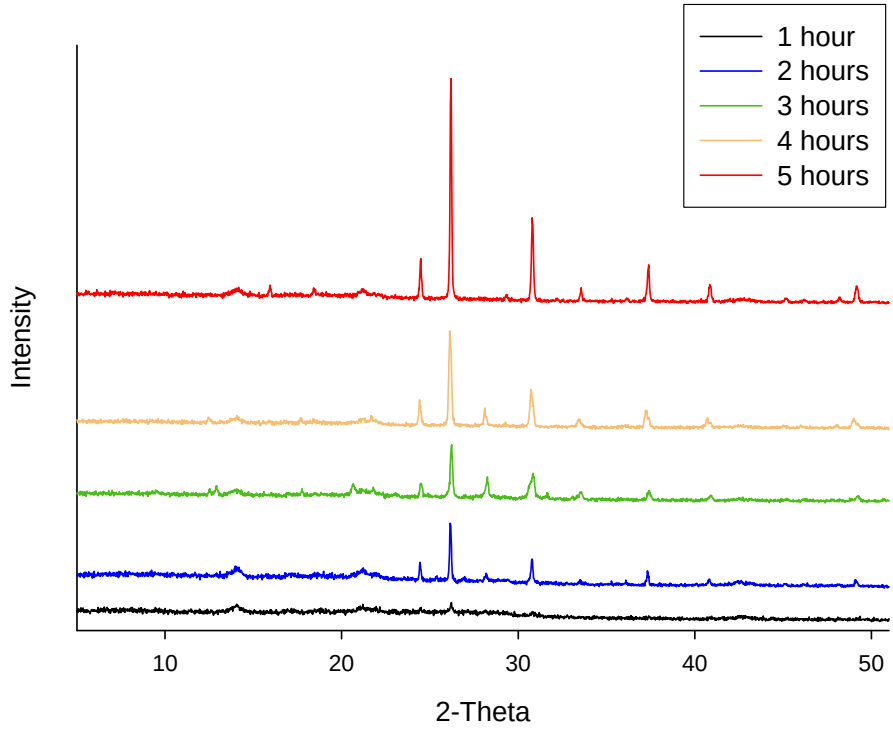

Figure 3.37: Powder X-ray diffraction patterns of products formed upon heating gel rho in a microwave oven at 150°C

Examination of the powder pattern led to the conclusion that the product was related to pollucite, a more dense phase known to occur in the presence of excess caesium in the gel[31]. The amorphous solid produced alongside the pollucite phase was assumed to be water glass, reported by Yanagisawa *et al*[32] to be formed in the synthesis of pollucite. Steps were taken to lower the level of caesium in order to determine whether zeolite rho would crystallise at these elevated temperatures if conditions were optimised. Further discussion about the pollucite phase takes place in section 3.7.4.3 "Identification of ANA-type phase" on page 97.

Given that the previous results showed that no products were formed at temperatures of 80 or 100°C, the reduced-caesium gel was heated at 120°C as this was the lowest temperature to yield a crystalline phase.

When the sample obtained after 5 hours of microwave heating was subjected to powder X-ray diffraction, the pattern showed the product to be completely amorphous. This outcome was unsurprising as the same gel failed to produce zeolite rho in a conventional oven. Therefore efforts to make zeolite rho from a reduced caesium gel were unsuccessful.

One further option remained to be investigated. It is known that the microwave heating process accelerates the formation of crystals, and when used in conjunction with ageing the rate of crystallisation is further increased. This is due to the presence of nuclei which are available for supporting crystal growth. It has already been stated that the formation of nuclei is now the bottleneck in microwave synthesis[16]. It is therefore possible that the 24 hours of ageing the zeolite rho gel is not sufficient for nuclei to form. In the final experiment, pre-made zeolite rho crystals were added to the gel as seeds. The elevated temperature of 120°C was again used for the reasons outlined earlier.

The results from microwave heating were again disappointing. All samples were shown to be amorphous. It is possible that during the ageing period the seed crystals dissolved in the alkaline gel, rather than acted as a surface for nuclei formation. The products formed in a conventional oven were also amorphous. This was surprising as the gel was exactly the same as used previously, but with 1% by weight of seed crystals.

The synthesis of zeolite rho in a microwave oven had not been reported at the time this work was carried out. Since the completion of the microwave experiments, however, Tompsett *et al*[33] have briefly commented on zeolite rho synthesis in their review paper of 2006. The authors refer to their own unpublished data, which involved heating the zeolite rho gel at 120°C for 2 hours. Their results concur with the present findings in this thesis, which are that products formed when zeolite rho gels were heated in microwave ovens were of poor crystallinity and not reproducible.

3.7.4.3 Identification of ANA-type phase

Pollucite, which has the analcime structure (ANA) and a formula of $CsAlSi_2O_6$, is known to form in zeolite rho syntheses which contain an excess of caesium[31]. When the powder XRD data obtained from the crystalline sample formed in 5 hours at 150°C in a microwave oven is compared with reported pollucite data[34] (see Table 3.3 on the following page for a comparison of these data) strong similarities can be seen.

	Pollucite Data				Analcime Data	
	XRD data (obtained)		XRD data (published)[34]		XRD data (published)[35]	
hkl	d	Intensity	d	Intensity	d	Intensity
211	5.558	9.4	5.580	9	5.605	61
220	-	-	4.840	<1	4.854	14
321	3.633	21	3.660	49	3.670	6
400	3.400	100	3.420	100	3.432	100
420	3.042	5	3.060	4	3.070	<1
332	2.901	39	2.914	45	2.927	51
422	-	-	-	-	2.803	6
431	2.668	8	2.684	4	-	-
521	2.482	4	2.499	9	2.693	15
440	2.405	18	2.419	29	2.507	12
611,532	2.207	10	2.220	18	2.227	6
620	-	-	-	-	2.171	1
631	2.005	4	2.018	7	2.024	1
444	1.963	3	1.975	4	1.982	<1
541	-	-	-	-	2.119	1
640	1.886	4	1.897	<1	1.904	15
721,552	1.851	9	1.862	16	1.868	2
a (Å)	13.602		13.677		13.567	

Table 3.3: Comparison of powder X-ray diffraction data (obtained and published) for pollucite and analcime.

Intensities quoted are relative intensities.

However, results from inductively coupled plasma atomic emission spectroscopy (ICP-AES) analysis indicate a negligible quantity of caesium to be present in the sample, whilst sodium levels are high. It now seems unlikely that the sample is pure pollucite. There are two possible identifications for the product formed in the microwave oven. The first is that the sample is analcime, the formula of which is $Na_x[Al_xSi_{48-x}O_{96}]:16H_2O$ where x is between 15 and 17.

Whilst the powder XRD data, particularly the peak intensities, do not agree so closely with analcime data (see Table 3.3) as with the pollucite data, this can be explained. It was reported that a solid mixture of pollucite and analcime is indistinguishable from pollucite by

X-ray diffraction[32,37]. Therefore, a mixture of analcime (in the majority) and a trace level of pollucite could have formed in the microwave oven. This trace amount of pollucite both accounts for the caesium in the ICP analysis and the appearance of the powder X-ray diffraction pattern. Due to caesium being a heavy atom, it is a stronger scatterer of X-rays than any of the other elements known to be present in the sample (sodium, silicon, aluminium or oxygen). Even a small quantity of caesium in a sample can influence the appearance of an XRD pattern.

The second possibility is that the powder is one product (not a mixture of analcime and pollucite) with a formula somewhere in between the extremes of all caesium and all sodium. It was noted that washing pollucite samples with water could remove some of the caesium present, and it should instead be washed with acetone[36]. Samples in this work were washed with deionised water, and this may account for some caesium loss.

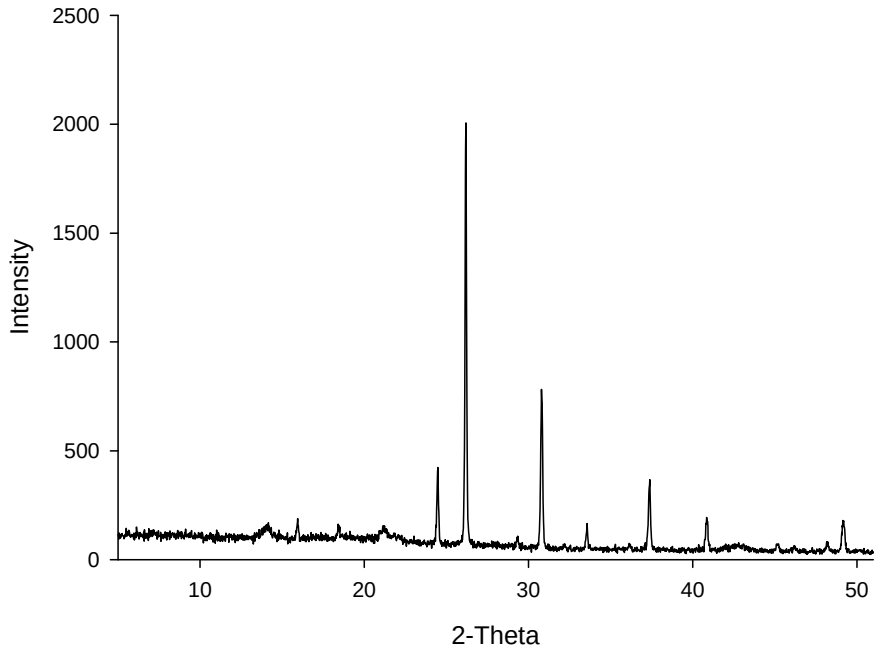

Figure 3.38: Powder X-ray diffraction pattern of analcime/pollucite-type material formed in a microwave oven at 150°C in 5 hours

As a route to synthesising analcime, the microwave heating technique is not new, although the other work published has used fly ash[38] or alumatrane and silatrane (which are $Al(OH)_3$ and SiO_2 respectively, in organic solvents)[39]. In the former case, analcime formation took 30 minutes at 225°C and in the latter instance, 8 hours at a temperature of 130°C was necessary.

The SEM micrograph below shows the crystals to be spherical and approximately 2-3 μm in diameter.

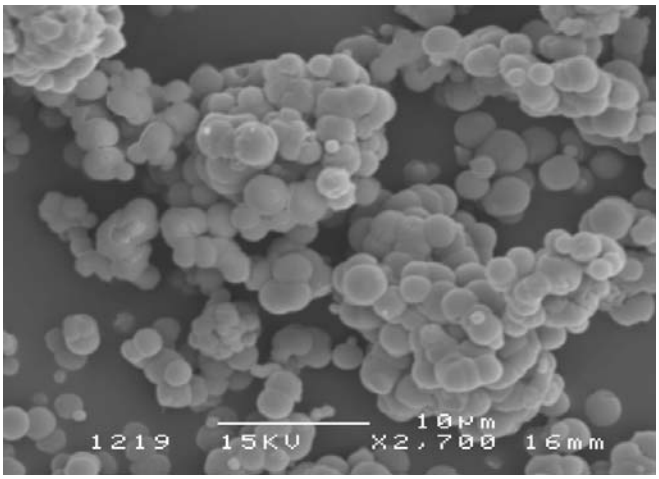

Figure 3.39: SEM image of pollucite-type material

3.7.4.4 Discussion

Overall, the work with zeolite rho has not been as successful as was hoped. However, in the course of this work, a mixed sample containing analcime and pollucite was produced. The failure to produce zeolite rho in a microwave oven can probably be explained as a problem forming the nuclei crucial to further crystal development. As mentioned earlier, the presence of nuclei are necessary to initiate crystal growth, and it is considered that this step of nuclei formation is now the bottleneck in zeolite synthesis[16]. The microwave heating merely helps the gel rapidly attain reaction temperature so that crystallisation can occur, and speeds gel dissolution which is necessary to feed and form nuclei. As zeolite rho has a long synthesis

period in a conventional oven, it could well be the case that much of this time is taken in the formation of the nuclei. Therefore, when the gel is heated in a microwave oven, even after ageing, the rapid heating to reaction temperature has only saved the 30-40 minutes estimated to be the heat-up time in conventional ovens. This does nothing to impact on the lengthy (possibly days) required to form nuclei.

3.8 Conclusions

Throughout this section, the emphasis has been on forming zeolites in a microwave oven in a shorter time than they could otherwise be made in a conventional hydrothermal oven. As far as zeolites A and Y are concerned the research has been a success. Both zeolites were formed in a fraction of the time usually required. The best result for zeolite A was found when the aged gel contained sodium metasilicate and was heated at 100°C for 10 minutes. For zeolite Y, crystallisation from the sodium metasilicate gel was complete in 3 hours at 100°C.

For zeolite X, no microwave syntheses produced a pure crystalline sample. Products were usually predominantly zeolite A or sodalite, with zeolite X being formed as a minority impurity. Efforts were made to alter silicon to aluminium ratios to favour the more siliceous zeolite X, and other reagents were used. However, these alterations made no improvement to the quality of product.

In the case of zeolite rho, the gel failed to yield a sample in the microwave oven, although a phase with the analcime structure did form alongside water glass. Despite a variety of temperatures and seeding of the initial gel, zeolite rho did not form when gels were microwave heated. Indeed, any changes to the gel failed in a conventional oven, demonstrating the precision required for zeolite rho synthesis. Given the length of time necessary for zeolite rho crystallisation in a conventional oven (5–7 days is usual) it is not surprising that a mere 5 hours in a microwave oven was insufficient for zeolite rho production.

Where conventional syntheses are already short (under 48 hours) it was seen that zeolitic products could be obtained from the same gel when heated in a microwave oven. In all

cases, ageing lowered the heating time necessary in microwave syntheses. This is due to the formation of nuclei in the ageing period, which then grow rapidly once heat is applied to aid gel dissolution and migration of species to nucleation sites. In the case of zeolite rho it is believed that the gel takes of the order of days to form even the preliminary nuclei necessary to sustain crystal growth, therefore, even when aged and heated in a microwave oven there are no nuclei present to develop. Although the gel reaches reaction temperature within 2 minutes in a microwave oven, instead of 30–40 minutes for a conventional oven, it is unlikely that this time saving on a typically 5–7 day synthesis has made any impact on the nucleation and crystallisation periods.

Examination of samples under the scanning election microscope showed that there were differences in crystal sizes between the conventionally and microwave prepared samples. Due to the rapid crystallisation period in the microwave oven, it was not surprising that the crystals were smaller than those formed in a conventional oven. Crystal morphologies appear to be unaffected by the heating method.

In conclusion, microwave heating of zeolite gels can be a useful and rapid synthesis technique. Reagents are crucial to a successful reaction in a microwave oven as their pH and purity affect reaction outcomes, and when the timeframe is shortened, these effects can be magnified. Ageing was also found to be significant in further reducing reaction times.

Chapter 4: Occlusion Reactions with Silver Nitrate

4.1 Introduction

4.1.1 Ion Exchange

Overall, zeolites have a negative framework due to the presence of AlO_4 tetrahedra. This negative charge is countered by non-framework cations, typically from group 1 of the periodic table. The majority of such cations are available for exchange, depending on reaction conditions, the structure of the zeolite and the location of the cations.

The cation exchange capacity (CEC) of a zeolite is in theory determined by the number of Al^{3+} present in the zeolite framework, as the cations balance the negative framework charge caused by the AlO_4 tetrahedra. Therefore, the more Al^{3+} present in the structure, the higher the CEC of the zeolite[1]. In practice, however, ion exchange depends on factors such as the dimensions, shape and orientation of channels and cavities within the zeolite. High alumina zeolites contain many sites which can accommodate cations – more in fact than is required for neutrality. Some sites are more favourable to particular cations than others due to accessibility, location and proximity to other cations. The interconnecting channels of some zeolites are sometimes of different dimensions, so whilst an ion may be able to penetrate one system, it may be unable to migrate further. It is not necessary for the incoming ion to occupy the same site as the leaving ion[1].

The majority of ion exchange reactions are carried out using aqueous solutions. A salt is typically dissolved and stirred with the zeolite for several hours. The solution can be heated to aid the ion exchange. The extent of the exchange may depend not only on the temperature, but the concentration of the solution. When the ions in the zeolite have a different charge to ions in the solution, the concentration of the aqueous medium is very significant[1]. As the solution becomes more dilute, the zeolite becomes more selective for the more highly charged

ion[1].

In aqueous media, the size not only of the cation, but of the hydrated cation needs to be considered, especially for divalent cations and the small, highly charged lithium ion. Selectivity series have been drawn up for various zeolites, and it should be noted that an ion will not exchange if there is already a preferred ion within the zeolite (i.e. higher up the series). Although both zeolite X and Y have the same structure (FAU) they have different silicon to aluminium ratios which means that their selectivity series are very different[2].

Zeolite X: Na > K > Rb > Cs > Li

Zeolite Y: Cs > Rb > K > Na > Li

Zeolite X, with its lower silicon to aluminium ratio, favours univalent cations in order of decreasing size. However, zeolite Y, which is more siliceous than zeolite X, favours the cations in order of increasing size. Lithium is small and highly charged and therefore is heavily hydrated and this not only increases the effective size of the ion, but shields the framework charge, and hence Li appears at the bottom of both series.

An alternative method for introducing the cations to the zeolite structure is solid state ion exchange (SSIE). In this technique, a salt with a relatively low melting point is heated with the zeolite. SSIE can be advantageous where the salt solution would be acidic and degrade the zeolite structure, and can also provide a high level of exchange in one step. For small, highly charged ions such as lithium, a significant hydration sphere is present in aqueous solutions which hinders the diffusion of the ions through the zeolite, and for circumstances such as this, SSIE is also a preferred method.

Ion exchange reactions are almost exclusively reversible, and an equilibrium is set up. Factors such as temperature and solution concentration can influence where the equilibrium lies. Pabalan *et al*[1] reported that the concentration of the solution is only of significance with respect to exchange when the charges of the ingoing and outgoing cations are different. Of course, if the solution is too acidic, the zeolite framework can be destroyed through the leaching of aluminium.

The equilibrium of a reversible aqueous ion exchange can be written with the general formula shown below[2,3]. All ion exchanges should be reversible, and an equilibrium established.

$$bA^{a+}_{(s)} + aB^{b+}_{(z)} \rightleftharpoons bA^{a+}_{(z)} + aB^{b+}_{(s)}$$

Equation E4.1: Equilibrium of an ion exchange reaction

A represents one ion, of charge *a*

B represents the other ion, of charge *b*

(s) denotes the ion in solution whilst *(z)* is used for the ion within the zeolite

An isotherm may be drawn to display the equilibrium concentrations of ions in the solution and zeolite, at a given temperature. From the profile of the equilibrium curve, it can be deduced whether or not the zeolite has a preference for the ions in solution. Specific details of ion exchange equilibria and kinetics are given by Colella in *Mineralium Deposita*[3].

Some of the commercial uses of zeolites rely on their ion exchange properties. Some typical examples of zeolites as ion exchangers include water softeners, where they take up calcium and magnesium ions, and the clean-up of nuclear waste in which ^{137}Cs, ^{90}Sr and ^{90}Y need to be removed, primarily by clinoptilolite. For these purposes, the zeolite must be stable at

elevated temperatures and in radioactive environments. A major advantage of zeolites is their selectivity for particular ions, which is often determined by the size of the channels and framework charge. More information on zeolites as ion exchangers can be found in section 1.2.2 of the introduction earlier in this volume.

4.1.2 Occlusion

Ionic salts may be introduced into the pores of many zeolites. The process commonly involves heating a salt above its melting point in the presence of a zeolite, so that it can diffuse into the zeolite structure, replacing the intrapore zeolitic water. Nitrate salts are commonly used because their melting points are in a suitable temperature range for reaction with zeolites[4]. The level of occlusion depends upon many factors, particularly the size of atoms compared to the pore size of the zeolite.

Research carried out by Park *et al*[5] examined the affect of silicon to aluminium ratio and pore dimensions in relation to the occlusion of ammonium nitrate. The amount of silicon present affected the occlusion capacity of the zeolite, in that the greater the level of silicon, the higher the capacity for the salt. The explanation given for this observation was that zeolites with a low level of silicon have more aluminium in the framework and this requires a greater number of cations to compensate for the charge. With the increased number of cations, there is less void space available to accommodate species or for them to migrate through the framework. This means that the Si:Al affects the amount of salt that a zeolite may contain.

However, it was found that a good size match between the salt and zeolite pores was also important, and influenced the stability of the occluded sample to washing and thermal treatment[5]. The occluded salts can be removed, but with a degree of difficulty. Park *et al*[5]

further defined two other categories of "occlusion", one where the salt ions were slightly larger than the zeolite pores and became tightly trapped and could not be removed under ambient conditions, and the other where the pore was large in comparison to the salt, and the salt could be freely dispersed in and out of the zeolite[5].

There are many proposed uses for occluded zeolites, and one of the main areas is as agricultural slow release fertilisers[6,7]. As has already been stated, occluded salts can be removed from the zeolite with extensive washing. Hence, the occluded fertiliser is gradually released when the zeolite is subjected to watering or rain, and this prevents a sudden release of the chemicals into the environment.

When salts are contained within a zeolite, their properties appear to be different from when they are outside the zeolite in the bulk state. It has been suggested that harmful salts can be contained within a zeolite and handled safely: an example of this is the potentially explosive perchlorates[4].

Zeolites that contain occluded salts have also attracted great interest for their properties, in particular the growth of silver nanowires from zeolites occluded with silver nitrate[8]. When placed in an electron beam, wires were found to grow from the silver occluded within the zeolite.

4.1.3 Zeolites Containing Silver Species

There has been much interest in zeolites containing silver clusters. One of the earlier papers investigated the occlusion of silver nitrate in zeolite A[9]. In this work, Barrer and Meier discussed the presence of non-framework peaks in the powder X-ray diffraction pattern of the occluded product. The extra lines were attributed to the formation of a superlattice,

originating in the ordering of the occluded silver nitrate species within the zeolite.

The work of Barrer and Meier[9] reports the use of a vast excess of silver nitrate in the occlusion reaction. One focus of this present work was to establish whether such an excess was necessary in order to effect occlusion and the formation of superlattice by silver nitrate. It has previously been reported that for the occlusion of lithium chloride in low silica zeolite X (FAU) the reaction progressed at a greater rate in the presence of excess salt[10].

Superlattices have been seen when silver iodide was occluded in zeolite A[11–13]. Some interpretations of the structure were made from the X-ray diffraction patterns. Due to the presence of the superlattice peaks at low values of 2-theta, it was deduced that the ordering of the AgI was long range. There were no distortions of the peaks (for example, peak splitting) so it was assumed that cubic symmetry was maintained. Due to the size of the silver iodide units (which are believed to diffuse as a whole), it was thought that all the occluded ions were in the α-cages as they would not be able to pass through the 6-ring into the β-cages. From the point of view of volume, α-cages can accommodate 10 AgI units, but in order to maintain reasonable bond distances, the reality is that a maximum of 4 AgI units can be contained within one α-cage[12]. It was suggested that the average structure of the $(AgI)_4$ clusters in the α-cage was such that the silver ions were in a cubic arrangement, with the associated iodide ions in a tetrahedral formation. A space group of $F4\bar{3}c$ was proposed for the superlattice-containing zeolite A[12].

There have been previous attempts to elucidate the structure of zeolite A containing silver nitrate[14]. Investigations using the $Pm\bar{3}m$ space group were carried out and Fourier maps were calculated in order to determine the positions of cations within the framework. However, in the case of structure refinement for zeolite A which contained silver nitrate, the

process "did not proceed in a satisfactory manner". Petranović *et al*[14] uncovered a "high degree of disorder of Ag cations" and claimed that further work on this structure was in progress. No further developments or reports of this work have been published.

Other papers have focused on the formation and structures of silver clusters within zeolite cavities[15–17]. These silver-exchanged zeolites undergo colour changes when dehydrated. In zeolite A, it is thought that the origin of the colour change is a result of the stabilisation of the hexasilver cluster in the dehydrated form[16]. The cluster, which is in a sodalite cage, is co-ordinated to nearby silver atoms which are in the 6-rings. The cluster appears to have no charge due to the Ag-Ag bond lengths being close to those in silver metal[16]. This means that the cluster has effectively been reduced upon dehydration of the host zeolite.

4.1.3.1 Uses

The applications of silver zeolites are briefly discussed by Pavlovskaya *et al*[15]. Hydrated silver-exchanged zeolites, being light sensitive, could be used to photocatalyse the decomposition of water if used in membrane electrodes. The dehydrated silver-exchanged zeolites are a brick-red colour[15], and, due to the fading of this colour upon re-hydration (through orange and yellow), can be used as moisture sensors.

Silver zeolites have also been shown to be useful in catalysis of organic reactions such as silver mordenite in the epoxidation of ethylene[15,16] and silver faujasites in the regio-stereroselective formation of a glycosyl linkage in sialosaccharides[18].

As mentioned earlier, it has been reported that the silver nitrate occluded within zeolite A can form silver nanowires when exposed to an electron beam[8]. The production of nanowires is

potentially very significant for nanotechnology applications.

The silver-exchanged zeolites also have reversible redox properties which can be used in electrode surfaces. The advantages of using zeolites in electrodes are that they provide stability under reactive and corrosive conditions and they are selective with regard to which molecules are absorbed[16].

4.2 Reactions

4.2.1 Zeolite A Synthesis

The zeolite A used in the reactions outlined in this section was prepared with 0.723 g sodium hydroxide (BDH, AnalaR 99 % pellets) which was dissolved in 80 ml of deionised water. This solution was divided into two portions. To the first portion 8.258 g of sodium aluminate (Strem Chemicals) was added and dissolved. To the second measure, 15.48 g of sodium metasilicate pentahydrate was dissolved with heating and stirring. The two solutions were then recombined and immediately heated at 99°C in a conventional oven. The zeolite powder was recovered by filtration and was washed and dried at ~ 50°C.

4.2.2 Silver Ion Exchange

A 250 ml, 0.1 M solution of silver nitrate was prepared by dissolving 4.25 g of $AgNO_3$ (99+%, Aldrich) in deionised water. 4 g of sodium zeolite A was added to the solution, and the mixture was stirred at room temperature for 24 hours. As silver nitrate is light sensitive the flask was wrapped in aluminium foil to prevent light affecting the reaction.

After stirring for 24 hours, the solution was filtered, washed and dried at 60°C. The resulting powder was stored in a sample container covered with aluminium foil so that light could not alter the product.

4.2.3 Occlusion Reactions

Occlusion experiments were carried out, initially following the method set out by Barrer and Meier[9].

The majority of samples were prepared from silver-exchanged zeolite A, but in some cases unexchanged sodium zeolite A was used. The appropriate quantities of zeolite A and silver nitrate were ground together and placed in an alumina reaction vessel before heating in a furnace. The ratio of silver nitrate to zeolite was varied between sub-stoichiometric levels and 10 times excess. It should be noted that according to Barrer and Meier[9], 9 $AgNO_3$ units were accommodated per α-cage (equivalent to 72 per 24 Å unit cell), so stoichiometry in this instance refers to 9 $AgNO_3$ per α-cage.

Typical heating programs involved heating samples to 260°C at a rate of 60°C/hour, then maintaining this temperature (which is above the 212°C melting point of silver nitrate) for a minimum of 8 hours. Samples were then cooled down to room temperature at a rate of 60°C/hour, although sometimes this was altered to a slower rate of 10°C/hour.

A two step occlusion reaction was also used: the first step being to melt the nitrate salt at full occlusion temperature (260°C) with zeolite A, and the second step was to hold the reactants just below the melting point of the silver nitrate (at 200°C) for a period between 4 and 120 hours. This, in conjunction with the slow cooling was intended to allow the migration of the silver nitrate ions to the appropriate locations to form a regular, organised superstructure. Tables 4.1 and 4.2, on the following page, detail the compositions and heating regimes used in the occlusion reactions carried out.

All samples produced were split into two portions – the first was stored as made, and the second was washed with deionised water.

Table 4.1: Occlusion reactions carried out with silver-exchanged zeolite A.

	Mass $AgNO_3$ (g)	$AgNO_3$ per 24Å unit cell	Temperature (°C) & Duration (hrs) of occlusion	Cooling Rate (°C/hr)
1 step occlusion	5	759	230, 8	60
	5	759	260, 8	10
	5	759	260, 8	60
	5	759	260, 8	60
	5	759	260, 16	10
	4	607	260, 8	60
	3	455	260, 8	60
	2	304	260, 8	60
	1	152	260, 8	60
	1	152	260, 8	60
	0.78	118	230, 8	60
	0.78	118	260, 8	60
	0.7	106	260, 8	60
	0.6	91	260, 8	60
	0.5	76	260, 8	60
	0.4	61	260, 8	60
	0.3	46	260, 8	60
	0.25	38	260, 48	60
	0.2	30	260, 8	60
	0.12	19	260, 48	60
	0	0 extra	260, 8	60

	Mass $AgNO_3$ (g)	$AgNO_3$ per 24Å unit cell	Temperature (°C) & Duration (hrs) of occlusion	Cooling Rate (°C/hr)
2 step occlusion	5	759	260, 8 & 200, 4	10
	5	759	260, 1 & 200, 48	10
	5	759	260, 1 & 200, 120	10
	3	455	260, 1 & 200, 48	10
	3	455	260, 8 & 200, 48	10
	2	304	260, 8 & 200, 48	10

Notes
1. Mass of $AgNO_3$ is per 1g Ag- zeolite A
2. Heat up rate was 60 °C for all samples

Table 4.2: Occlusion reactions carried out with unexchanged sodium zeolite A.

	Mass $AgNO_3$ (g)	$AgNO_3$ per 24Å unit cell	Temperature (°C) & Duration (hrs) of occlusion	Cooling Rate (°C/hr)
NaA occlusion	5	516	260, 8	60
	4	413	260, 8	60
	3	309	260, 8	60

Notes
1. Mass of $AgNO_3$ is per 1g Na- zeolite A
2. Heat up rate was 60 °C for all samples

4.2.4 Reactions with Dehydrated Zeolite A

It was proposed that the zeolitic water could be contributing to the distribution of silver nitrate within the pores, so a series of occlusion experiments were carried out using dehydrated Ag zeolite A.

Zeolite A synthesis and the ion exchange reactions were carried out as detailed in sections 4.2.1 and 4.2.2. The silver-exchanged zeolite A was then dehydrated for 12 hours at 425°C using a pressure of 1×10^{-5} mbar. The resulting yellow powder was then ground with the 0.56 g (equivalent to 72 ions per 24 Å unit cell or 9 ions per α-cage) of silver nitrate in a glove box to eliminate the possibility of water absorption from the atmosphere. The sample was then sealed in a glass tube before being heated in a furnace in the same manner described in section 4.2.3. In order for comparisons to be made, as-synthesised zeolite A was dehydrated and subjected to powder XRD.

4.2.5 XRD Pattern Simulations

Unsuccessful attempts were made to explain the differences seen in powder XRD patterns before and after the ion-exchange process, through Rietveld analysis of the data using GSAS. Good fits were not achieved owing to disorder in the cation positions and the relatively poor quality of the data, in the limited 2-theta data range over which the original XRD patterns were recorded.

Due to the problems encountered with Rietveld refinement, an alternative approach was tried. Simulations of powder X-ray diffraction patterns for the ion-exchanged zeolites were instead carried out using the computer program Poudrix[19], in order to confirm that ion exchange had occurred.

It is necessary to enter atom co-ordinates into Poudrix, and these were obtained from the Inorganic Crystal Structure Database supplied by EPSRC's Chemical Database Service at Daresbury. Other data required includes the lattice parameters, a space group and, in order to predict an XRD pattern an X-ray source and wavelength must also be included. Poudrix generates an expected XRD pattern based on the information entered. This generated pattern can then be compared with the laboratory data.

As the only changes between each Poudrix simulation are the cations and their co-ordinates, this gives some insight into how peak intensities are altered in the real X-ray diffraction patterns, and helps prove that significant ion exchange took place. It can therefore be seen that Poudrix is a useful tool in predicting the expected X-ray diffraction pattern.

4.3 Silver Occlusion Results

4.3.1 Preliminary Experiments

Before occlusion reactions were performed it was necessary to synthesise zeolite A. This was prepared according to the experimental section on page 113 in good yield. The powder X-ray diffraction pattern (see Figure 4.1 below) showed that there were no impurities present, and after indexing using the $Pm\bar{3}m$ space group with the program CELL, the lattice parameter was found to be 12.295 Å (esd = 0.003). The 12 Å, $Pm\bar{3}m$, cell is used for future structure discussions in preference to the 24 Å, $Fm\bar{3}c$ cell. The lattice parameter value (if doubled to 24.589 Å) agrees well with the published data value of 24.61 Å[20].

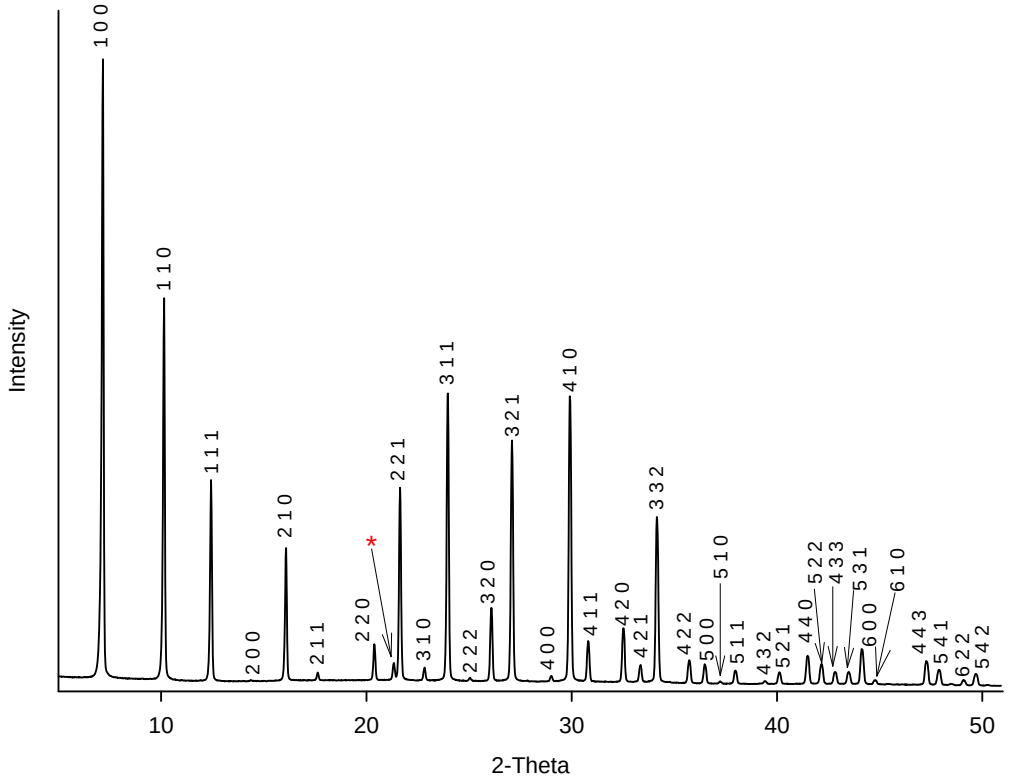

Figure 4.1: Powder XRD of zeolite A formed in a conventional oven at 99°C for 3.5 hours.

* marks the only peak arising from Si/Al ordering in the 24 Å cell (the 531 peak).

The sample of as-synthesised sodium zeolite A was then ion-exchanged with 0.1 M silver nitrate. The silver-exchanged product was recovered by suction filtration and after drying was examined using powder X-ray diffraction. It was clear that silver ions had indeed replaced sodium ions from the alterations in relative peak intensities. In particular note how the 220 and 222 peaks diminished in size and the 400 increased (see Figure 4.2).

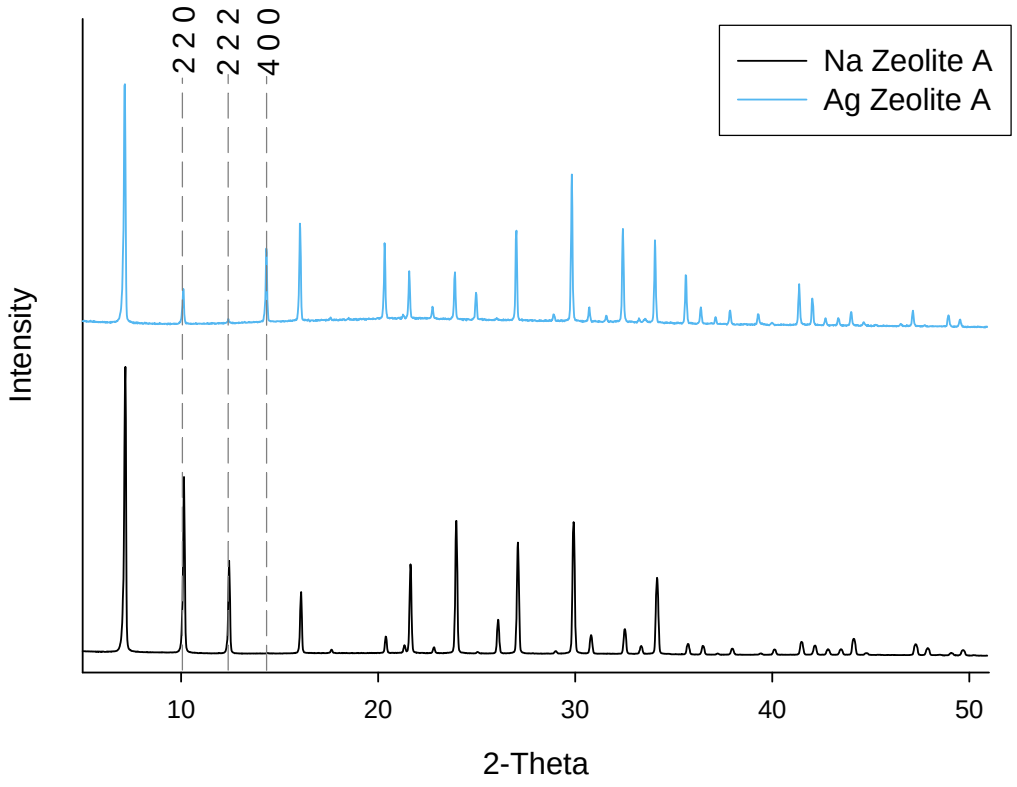

Figure 4.2: Comparison of sodium and silver-exchanged forms of zeolite A

Upon ion exchange to the silver form of zeolite A, there was an increase in the lattice parameter to 24.652 Å (esd = 0.003).

The powder XRD pattern generated by Poudrix for hydrated sodium zeolite A uses atom co-ordinates taken from the paper by Barrer and Meier[21] and is shown in Figure 4.3.

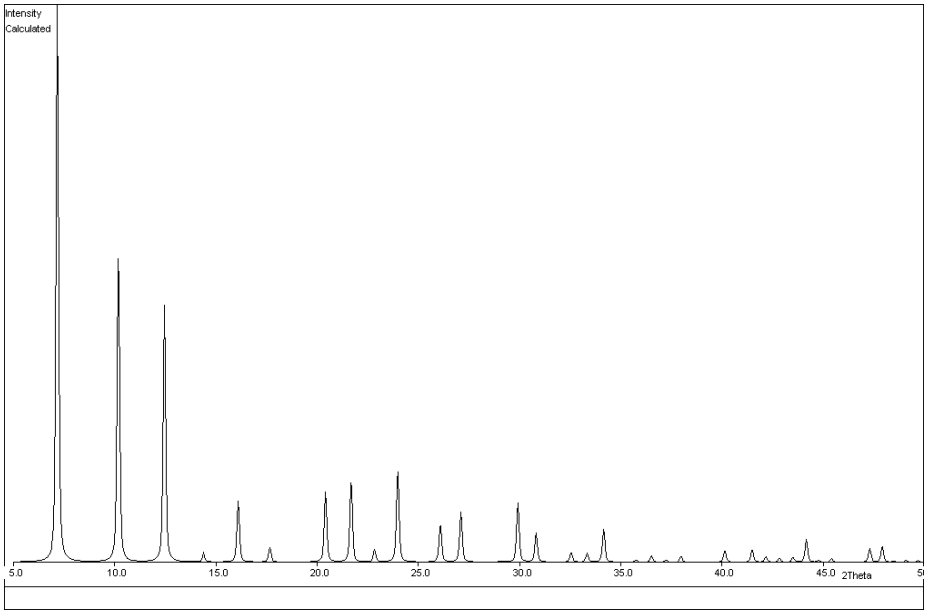

Figure 4.3: Simulated powder XRD pattern for sodium zeolite A

On comparison of the simulated pattern with the powder X-ray diffraction pattern from the laboratory prepared sample of sodium zeolite A (in Figure 4.1), it can be seen that there are similarities in the peak positions and relative intensities in the two patterns.

When the cation data entered into Poudrix was altered from sodium to silver ions (and hence also the atom co-ordinates are changed) the calculated pattern was markedly different. The data used for the hydrated silver-exchanged zeolite A was taken from the paper of Kim and Seff[22]. The simulated powder XRD pattern generated by Poudrix can be seen in Figure 4.4.

Again, the simulated and real XRD patterns are broadly similar, although both are quite different from their Na-A counterparts. Note, for example, the dominant first peak at ~7° two theta and the greatly reduced size of the neighbouring peak at ~10° two theta.

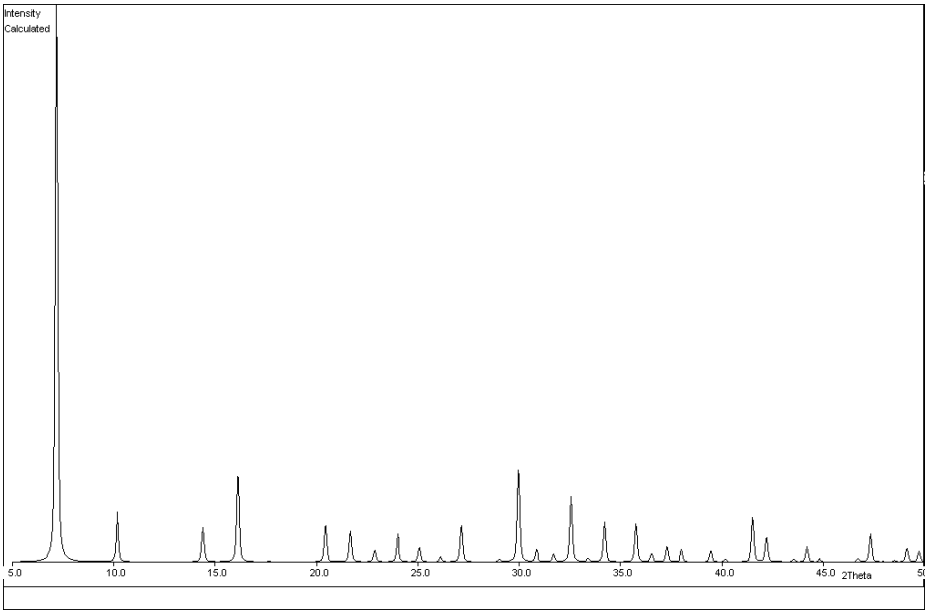

Figure 4.4: Simulated powder XRD pattern for silver-exchanged zeolite A

Initial occlusion experiments followed work performed by Barrer and Meier[9]. This involved grinding silver-exchanged zeolite A with silver nitrate, and heating in a furnace at 260°C for 8 hours with heating and cooling rates of 60°C/hour (see Experimental section). The first experiment carried out was the reaction between 5 g of silver nitrate and 1 g of silver-exchanged zeolite A. A portion of this sample was stored without washing, and the remainder was washed with deionised water and dried at ~60°C. Both samples were subjected to powder X-ray diffraction to determine whether the occlusion had been successful (as can be judged from the zeolite A peak intensities) and to establish if a superlattice due to ordering of silver nitrate in the zeolite A framework had been formed (this can be determined by the presence of extra, non-framework peaks).

In the unwashed sample, mainly silver nitrate was identifiable in the powder X-ray diffraction pattern, with very few zeolite A peaks discernible (see Figure 4.5). This was expected as 5 g of silver nitrate was a large excess in terms of the number of ions per unit cell which can be

accommodated in zeolite A. 5 g is equivalent to 759 silver ions per 24 Å unit cell. It is believed that each of the eight α-cages in the unit cell can contain 9 silver nitrate units[9], this gives a total of 72 per 24 Å unit cell.

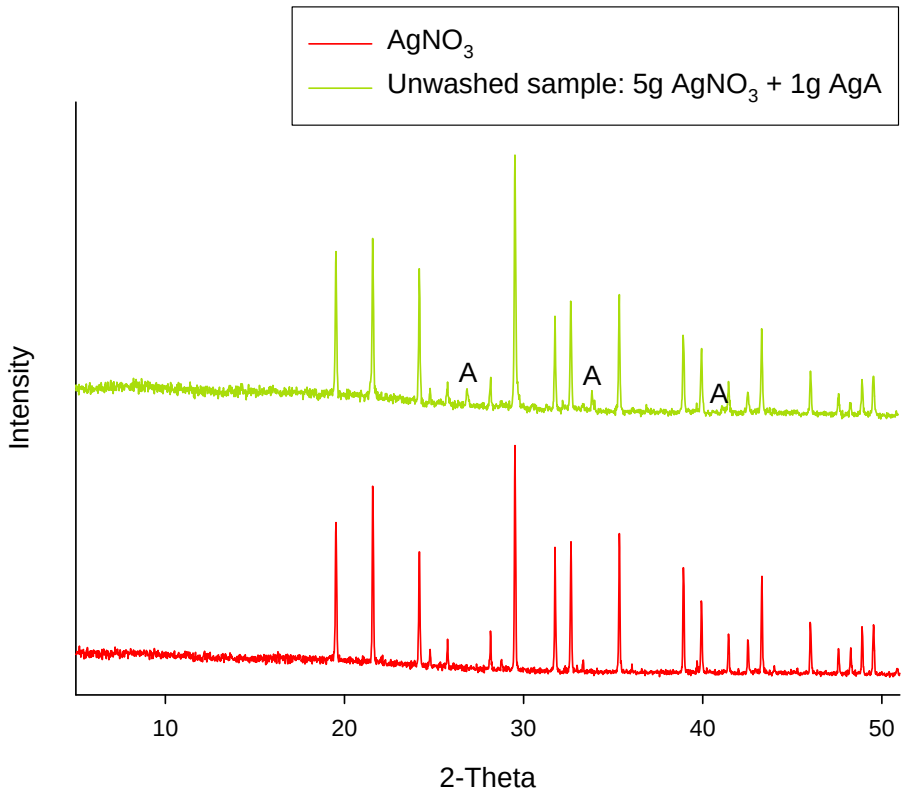

Figure 4.5: Comparison of unwashed sample with pure silver nitrate. Peaks marked with "A" indicate peaks due to zeolite A.

All the samples which were unwashed after their reaction with excess silver nitrate, when subjected to X-ray diffraction, showed in their patterns only peaks corresponding to silver nitrate. This is due to the fact that the majority of the sample was composed of silver nitrate. It is also true that any excess salt, which contained heavy silver atoms that are more dominant X-ray scatterers, may adhere to the zeolite surface and therefore contribute most to the powder XRD pattern.

Silver nitrate peaks no longer dominated the powder XRD pattern when the sample, which formed following a reaction with 5 g of silver nitrate, was washed, as can be seen in Figure 4.6 below. Peak intensities were affected by the occlusion of silver nitrate. Of great interest are the extra, relatively broad, peaks which cannot be indexed to silver nitrate or zeolite A. It is thought that these peaks arise from ordering of silver nitrate within the zeolite structure, i.e. a superlattice.

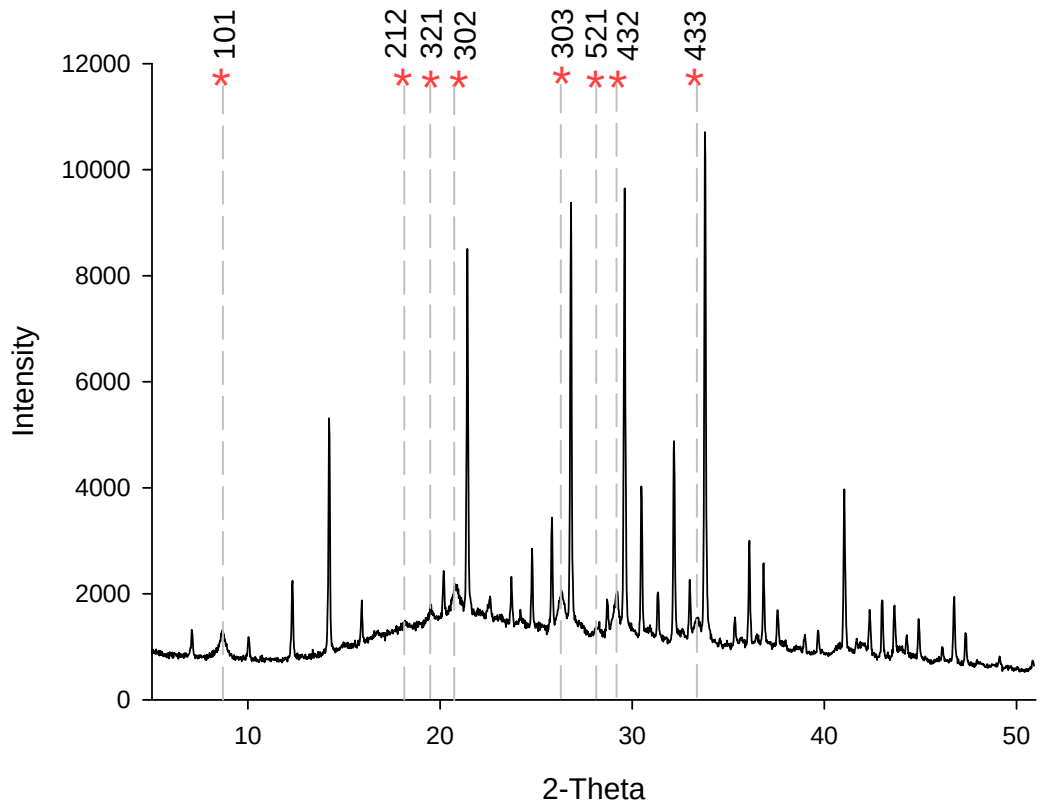

Figure 4.6: Powder XRD pattern of sample formed from reaction of zeolite A with 5 g $AgNO_3$ at 260°C for 8 hours, after washing

* denotes superlattice peaks indexed using a tetragonal unit cell with a = 17.576 Å, c = 12.428 Å

A discussion and interpretation of the superlattice follows in "Section 4.4.4 – Superlattice Structure Interpretation". The focus of the present chapter is on the conditions which cause the superlattice to form.

Barrer and Meier's original experiment[9] was then adapted to examine whether a superlattice would be observed when conditions were altered. The factors investigated included the quantities of silver nitrate used in the occlusion reaction, as the present 5 g is far above stoichiometric levels. Work examining the use of unexchanged zeolite A was performed, and the use of other temperatures was also studied, along with the cooling rate and the use of multiple heating steps.

4.3.2 Mass of Silver Nitrate Experiments

Systematic experiments were performed where the quantity of silver nitrate present in occlusion reactions was reduced from 5 g down to sub-stoichiometric levels. Table 4.3 on the following page details the experiments performed and indicates whether a superlattice was seen in the powder XRD pattern of the sample.

From the data in Table 4.3 it can be seen that the superlattice was only found in washed samples when an excess of silver nitrate was used. Some peaks attributable to the presence of a superlattice were present when occlusion reactions were performed with a ratio of 106 ions per 24 Å unit cell, however, it was not until this quantity was increased to 455 ions that the full array of superlattice peaks were observed. It is possible that when washing the sample, water enters the zeolite framework and destroys the superlattice, and this could explain why superlattices are only seen when large quantities of silver nitrate are used. When greater amounts of silver nitrate are reacted, some superlattice domains within the crystals persist while those nearer the surface may be washed away, and the remaining domains are seen in powder XRD patterns. However, for lesser quantities of silver nitrate, not enough superlattice remains after washing for any peaks to be observed in the powder XRD patterns.

Table 4.3: Data from experiments where mass of $AgNO_3$ was varied.

Mass of $AgNO_3$ (g)[a]	Nominal $AgNO_3$ units per 24 Å unit cell	Washed?	Superlattice Peaks?
5	759	No	$AgNO_3$ pattern
5	759	Yes	Yes
4	607	No	$AgNO_3$ pattern
4	607	Yes	Yes
3	455	No	$AgNO_3$ pattern
3	455	Yes	Yes
2	304	No	$AgNO_3$ pattern
2	304	Yes	Some present
1	152	No	$AgNO_3$ pattern
1	152	Yes	Some present
0.78	118	No	$AgNO_3$ pattern
0.78	118	Yes	Some present
0.7	106	No	No
0.7	106	Yes	Some present
0.6	91	No	No
0.6	91	Yes	No
0.5	76	No	No
0.5	76	Yes	No
0.4	61	No	No
0.4	61	Yes	No
0.34	52	No	No
0.34	52	Yes	No
0.3	46	No	No
0.3	46	Yes	No
0.25	38	No	No
0.25	38	Yes	No
0.2	30	No	No
0.2	30	Yes	No
0.13	19	No	No
0.13	19	Yes	No
0	0[b]	No	No
0	0[b]	Yes	No

Notes:

a). Mass given is per gram of silver-exchanged zeolite A.

For all experiments listed, the heating and cooling rates were both 60°C/hour and the reaction was performed at 260°C for 8 hours.

b). The reaction with 0 g $AgNO_3$ involved heating silver-exchanged zeolite A alone.

For unwashed samples, even at stoichiometric levels, the superlattice was not seen. When

the mass of silver nitrate was low this was due to insufficient ions to form a superlattice being present, and when the mass was increased, silver nitrate peaks dominated the powder XRD pattern.

4.3.3 Unexchanged Zeolite A Experiments

As-synthesised sodium zeolite A was used for a series of occlusion reactions to study whether the silver exchange was necessary for superlattice formation to be observed. The masses of silver nitrate used were the same as those used in previous reactions using silver-exchanged zeolite A. However, this would not give the same number of ions per 24 Å unit cell, as the mass of silver zeolite A is 1.46 times greater than sodium zeolite A (assuming a 100 % ion exchange).

After the molten salt has entered the zeolite, the first stage of the occlusion reaction probably involves an ion exchange with the molten silver nitrate, although it is possible that the sodium present in the zeolite reacts with the silver nitrate to yield sodium nitrate which remains within the cavity. Whilst there is no evidence of sodium nitrate in the powder XRD patterns, this does not mean that none is present. Since silver ions scatter X-rays much more heavily than sodium, they may simply have over-shadowed traces of $NaNO_3$.

The same superlattice peaks were observed when unexchanged zeolite A was reacted with silver nitrate as when the same reaction was performed with silver-exchanged zeolite A (see Figure 4.7 on the following page).

The quantity of silver nitrate reacted with sodium zeolite A was gradually reduced until there was no further evidence of superlattice peaks. Table 4.4 details the reactions performed.

Table 4.4: Reactions performed with sodium zeolite A and silver nitrate

Mass of $AgNO_3$ (g)	Nominal $AgNO_3$ units per 24 Å unit cell	Washed	Superlattice Peaks?
5.00	516	No	$AgNO_3$ pattern
5.00	516	Yes	Yes
4.00	413	No	$AgNO_3$ pattern
4.00	413	Yes	None
3.00	309	No	$AgNO_3$ pattern
3.00	309	Yes	None

As no superlattice peaks were evident in the powder X-ray diffraction patterns for occlusion levels of 413 and 309 ions per 24 Å unit cell, experiments ceased. The lack of a superlattice could be due to some of the occluded silver nitrate being used in a molten phase ion exchange, which would reduce the number of silver ions per unit cell by 96. However, the silver nitrate is still in vast excess to the number of ions per unit cell which could be accommodated, even after molten salt ion exchanges.

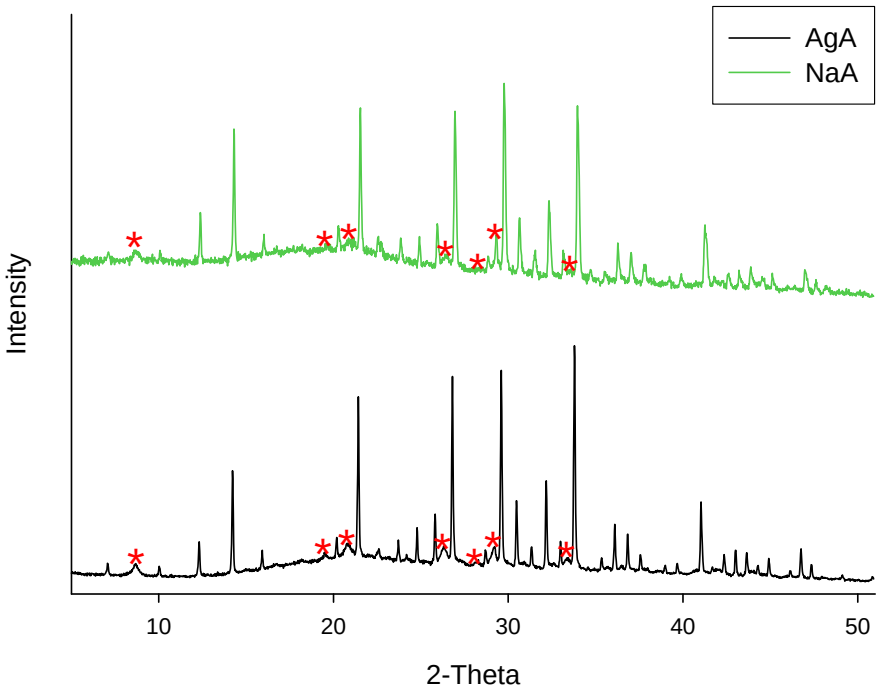

Figure 4.7: Powder XRD patterns of sodium and silver zeolite A following occlusion reaction with 5 g $AgNO_3$ (equivalent to 516 and 759 ions per 24 Å unit cell respectively) at 260°C

* denotes the superlattice peaks

Possibly as a result of sodium in the zeolite A starting material, superlattices were not seen for samples reacted with less than 5 g silver nitrate. However, in the presence of a significant excess of silver nitrate, superlattices were seen to form just as readily in unexchanged zeolite A as in silver-exchanged zeolite A. Again, an excess of silver nitrate was essential in obtaining any superlattice peaks in the powder XRD pattern.

4.3.4 Temperature, Cooling Rates and Multiple Heating Steps

Reactions have been carried out at 260°C following the work of Barrer and Meier[9], and this temperature exceeds the melting point of silver nitrate at 212°C. The temperature used in occlusion was lowered to 230°C, still above the melting point, to see whether the silver nitrate would still enter the zeolite and form a superlattice.

The reaction carried out at this lower temperature was between silver-exchanged zeolite A and 5 g $AgNO_3$. The sample was washed and dried to ensure excess silver nitrate was removed. The powder XRD pattern of this sample is shown in Figure 4.8. The lattice parameter for the sample formed at 230°C was similar to that of the sample formed at 260°C. Weight losses of water and nitrate from the TGA data show that a comparable level of occlusion was achieved at the lower temperature.

It can therefore be concluded that the reduction of reaction temperature was not detrimental to the formation of a superlattice (indicated by the peaks marked with * in the figure over the page). The slightly narrower superlattice peaks imply that the lower temperature was beneficial with respect to superlattice ordering.

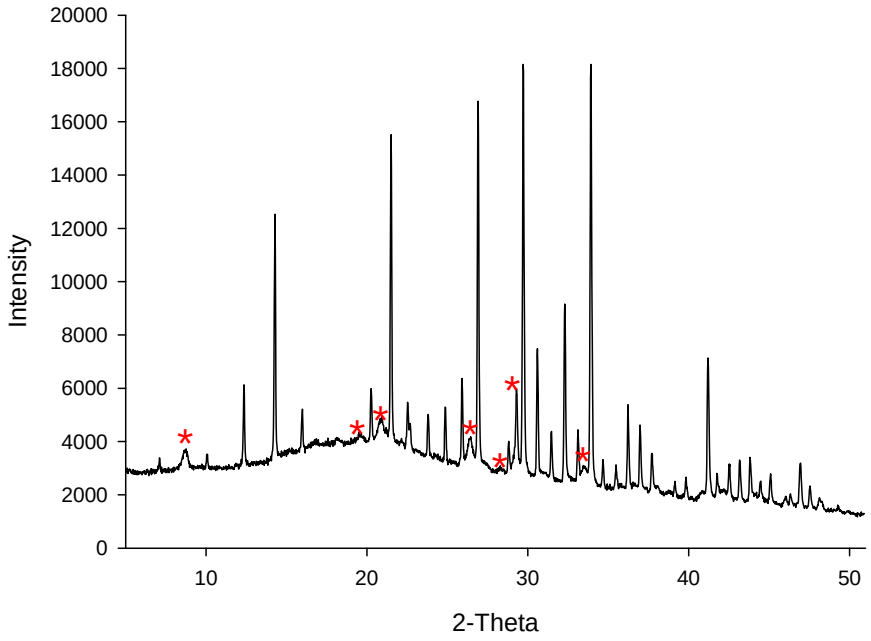

Figure 4.8: Powder XRD pattern of silver zeolite A occluded with 5 g $AgNO_3$ at 230°C.

Barrer and Meier[9] state that samples were gradually cooled from reaction to room temperature over a period of "at least 6 hours". All experiments conducted in the previous sections were cooled over a similar time frame. Some occlusion reactions were also performed using the furnace cooling program "step", which effectively cuts all heat and allows the sample to cool as fast as the furnace loses heat. In these cases the superlattice was not seen.

Examination of the superlattice peaks in the powder X-ray diffraction patterns reveals that these peaks are always quite broad relative to the zeolite A peaks. This would indicate ordering of the occluded silver nitrate on a scale shorter than the size of the zeolite crystallites. In a series of experiments, the duration of heating at the occlusion temperature of 260°C was varied and the cooling rate was also adjusted to see whether a longer occlusion reaction would encourage a more ordered occlusion of the silver nitrate ions. The use of two-stage reactions was also investigated to ascertain whether holding the sample just below the melting point of silver nitrate after the main occlusion step would cause a more regular

superstructure to form.

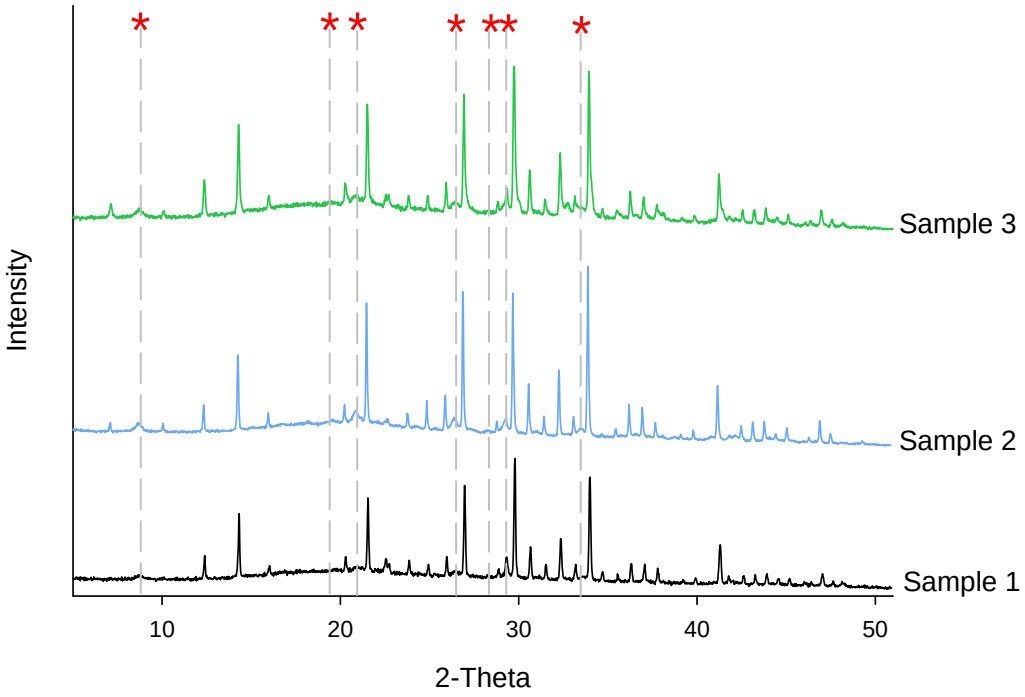

Figure 4.9: Comparison of superlattice formed from the reaction of 3 g of silver nitrate with 1 g of silver-exchanged zeolite A under different reaction conditions.

Figure 4.9 above shows a comparison of three samples formed from identical reactions between 3 g of silver nitrate and 1 g of silver-exchanged zeolite A, but performed under different conditions. Sample 1 was heated to 260°C and was held at this temperature for 8 hours before cooling at a rate of 60°C/hour. Sample 2 was also heated at 260°C for 8 hours, but was then cooled to 200°C and held at this temperature for 48 hours – the cooling rates for transitions from 260°C to 200°C and from 200°C to room temperature were both 10°C/hour. For sample 3, there were many stages and the occlusion period was increased as slow cooling and annealing steps are reported to lead to sharper superlattice peaks in the case of occlusion by dehydrated zeolite A[23]. The mixture of silver nitrate and silver-exchanged zeolite A was held at 260°C for 4 days, before cooling to 100°C over a 12 hour time frame (equivalent to 13°C/hour). There was no holding step before cooling from 100°C to 80°C over 2 days.

The sample was then cooled, again without a holding step, to room temperature taking 12 hours (equivalent to 4.5°C/hour).

Examination of the powder X-ray diffraction patterns shown in Figure 4.9 reveals that slower cooling rates do marginally improve the quality of the superlattice peaks, although the peaks are still not of a similar width to the zeolite peaks. This shows that the superlattice is still not ordered throughout the entire zeolite crystallite, but would indicate that there is improved ordering of the silver nitrate within the zeolite brought about by the longer cooling period. However, the single step occlusion with a cooling rate of 60°C/hour is still adequate for superlattice formation.

4.3.5 Occlusion with Dehydrated Zeolite A

Some experiments were performed in the absence of water to see whether the zeolitic water was contributing to the occlusion reaction. The powder XRD patterns of dehydrated as-synthesised zeolite A, dehydrated silver-exchanged zeolite A and dehydrated zeolite A occluded with 0.56 g silver nitrate are shown in Figure 4.10.

As can be seen in Figure 4.10, there are superlattice peaks for the dehydrated sample of zeolite A which contains 0.56 g of occluded silver nitrate. This is equivalent to 72 ions per 24 Å unit cell (or 9 ions per α-cage) a level at which there were no superlattice peaks in hydrated samples. A comparison of the superlattice peaks seen for dehydrated and hydrated samples is shown in Figure 4.11.

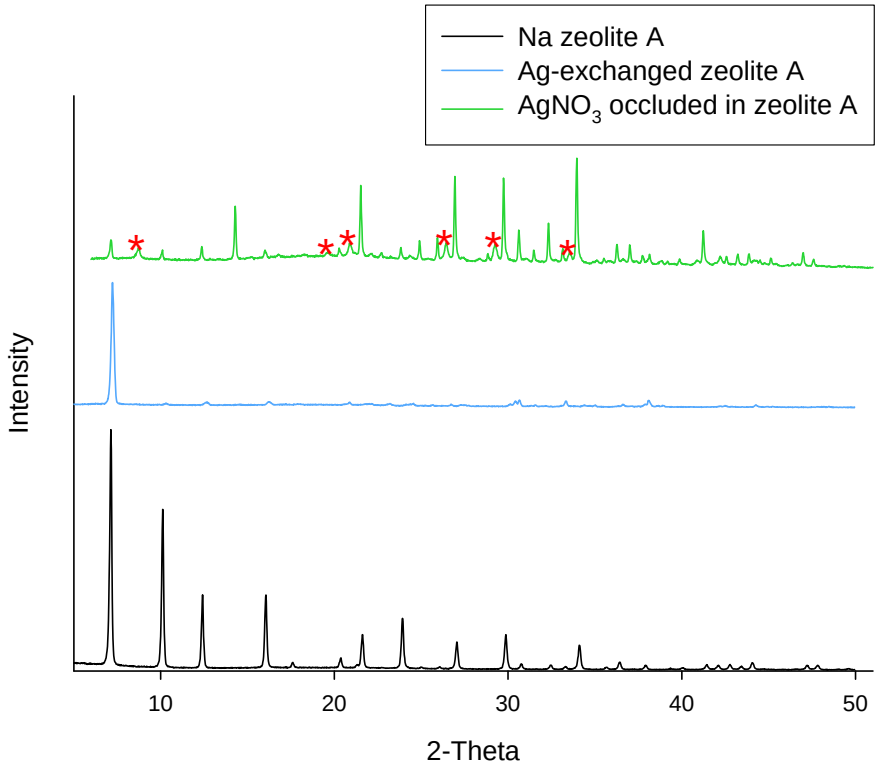

Figure 4.10: Powder XRD patterns of dehydrated zeolite A following reactions with $AgNO_3$.

* indicates superlattice peaks.

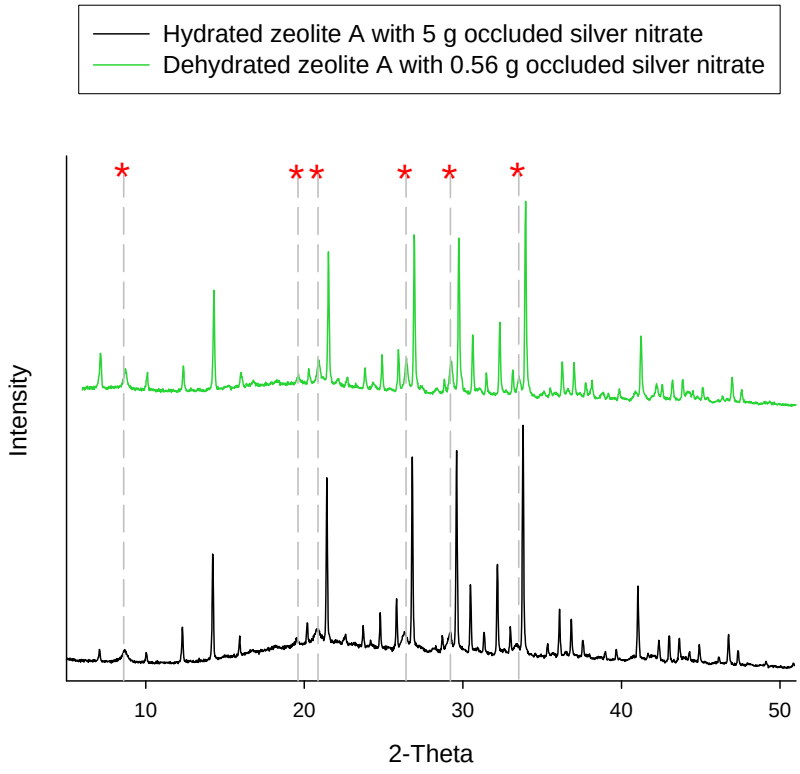

Figure 4.11: Comparison of superlattice peaks seen in dehydrated and hydrated samples

* indicates superlattice peaks

The superlattice peaks of the dehydrated sample appear taller and narrower than those seen for the hydrated sample, despite the dehydrated sample containing one tenth the mass of silver nitrate used in the hydrated sample. It appears that the presence of water in the zeolite structure is detrimental to the formation of a superlattice; indeed it may even destroy any superlattice present upon washing. Even when unwashed, the moisture re-absorbed from the air destroys the superlattice at low loadings in hydrated samples. This would explain why superlattices are observed with far lower quantities of silver nitrate in dehydrated samples than in the equivalent hydrated samples.

4.4 Silver Occlusion Discussion

When powder X-ray diffraction patterns are compared, peaks are shifted towards higher d-spacings (lower two theta) for occluded samples. This indicates that with increasing amounts of silver nitrate, there is an increase in lattice parameters.

The trend in lattice parameters is best displayed in the form of a graph, and Figures 4.12 and 4.13 on the following page illustrate the data (the raw data can be found in the Appendices).

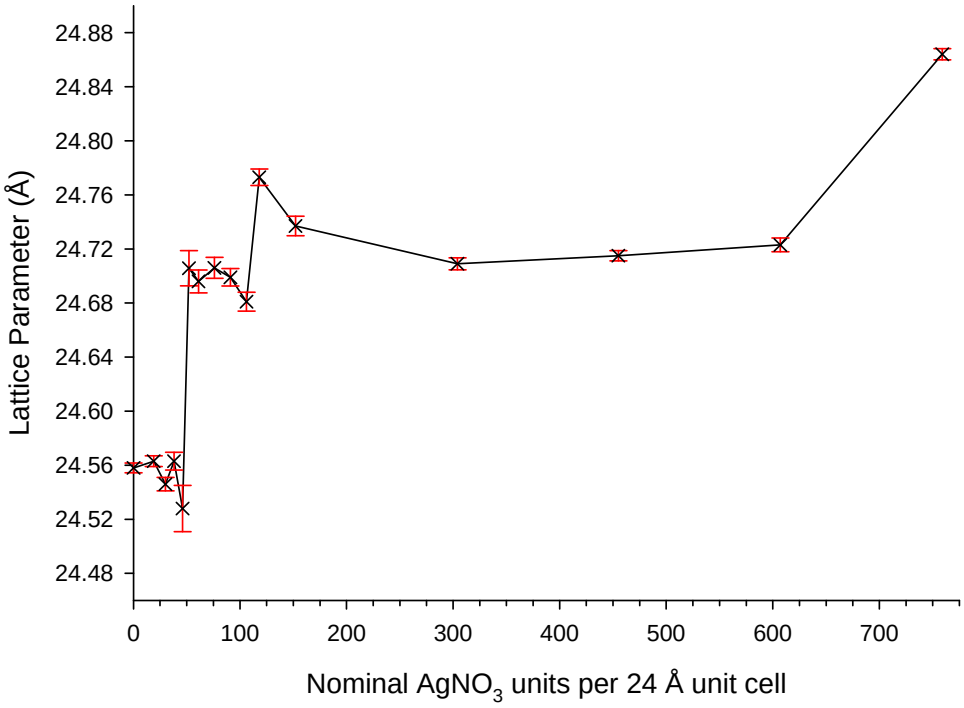

Figure 4.12: Trend in lattice parameter with varying amount of $AgNO_3$ per 24 Å unit cell for washed samples

The trend in lattice parameters with respect to increasing levels of occlusion appears to fluctuate initially, especially for washed samples (this could be influenced by the level of washing and the length of drying process following this washing, i.e. the level of hydration affects the lattice parameter). However, there would appear to be two distinct lattice sizes,

and the overall shape of the plot in Figure 4.12 is very similar to that in Figure 4.13.

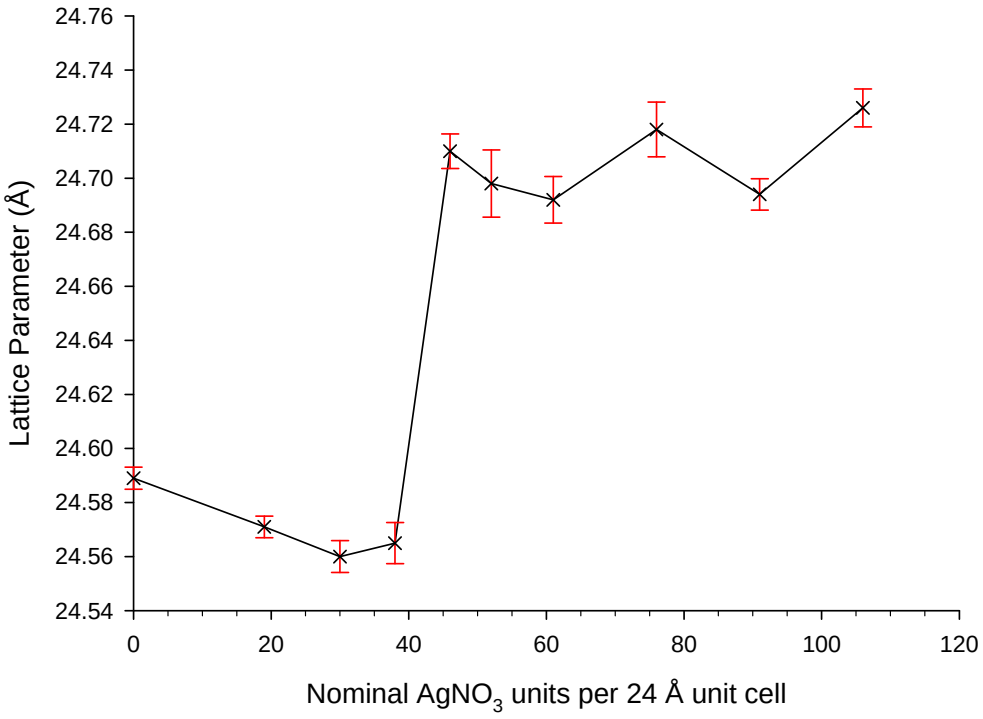

Figure 4.13: Trend in lattice parameter with varying amount of $AgNO_3$ per 24 Å unit cell for unwashed samples

Initially the lattice parameter for washed and unwashed samples is fairly constant at around 24.55 – 24.57 Å. Then, as the loading level increases from 38 to 46 ions per unit cell, there is a marked jump in the lattice parameter to approximately 24.72 Å. This step occurs below stoichiometric levels of occlusion (which would be 72 ions per 24 Å unit cell) and so this increase in cell size cannot be traced to the complete filling of the zeolite framework.

Thermogravimetric analysis (TGA) was performed to identify whether the quantity of silver nitrate within the zeolite was significantly altered when the occlusion reaction was carried out with differing masses of silver nitrate. It was anticipated that one of two trends would be

observed: either the percentage of weight lost would be approximately the same indicating that the same amount of $AgNO_3$ entered the zeolite framework, regardless of starting mass present and that excesses were washed away; or secondly, a steady decrease in percentage weight loss as the quantity of $AgNO_3$ reacted decreased, showing that the more reactant, the greater the amount occluded.

All TGA plots from occluded samples showed two steps. The first weight loss in the temperature range 50 – 200°C was attributed to the loss of water. The second drop in mass took place at 280 – 400°C and was assigned to the decomposition of the NO_3^- ion.

Graphs have been plotted from the TGA data to compare the trends of weight loss (see Appendices for the complete data table and weight loss plots). The data from unwashed samples (see Figure 4.14 on the next page) mainly charts those products whose powder XRD patterns were not dominated by silver nitrate peaks, with the exception of the last two data points. The steady increase in loss due to the nitrate ion was to be expected as there was no washing and the samples were reacted with ever increasing amounts of silver nitrate.

There is a clear crossover point between water and nitrate being in the majority within the zeolite, and this occurs for the same number ions per unit cell as seen for the jump in lattice parameter. As the quantity of silver nitrate increases, so there is less room inside the zeolitic cavities available to accommodate water. As these samples were unwashed, it was known that the water present within the zeolite was not from the washing process. As moisture would be driven out of the zeolite at the occlusion reaction temperature of 260°C, water most likely re-entered the zeolite from the air during cooling. The amount of water within the unwashed zeolite samples was not subject to the same variations which were observed for washed samples.

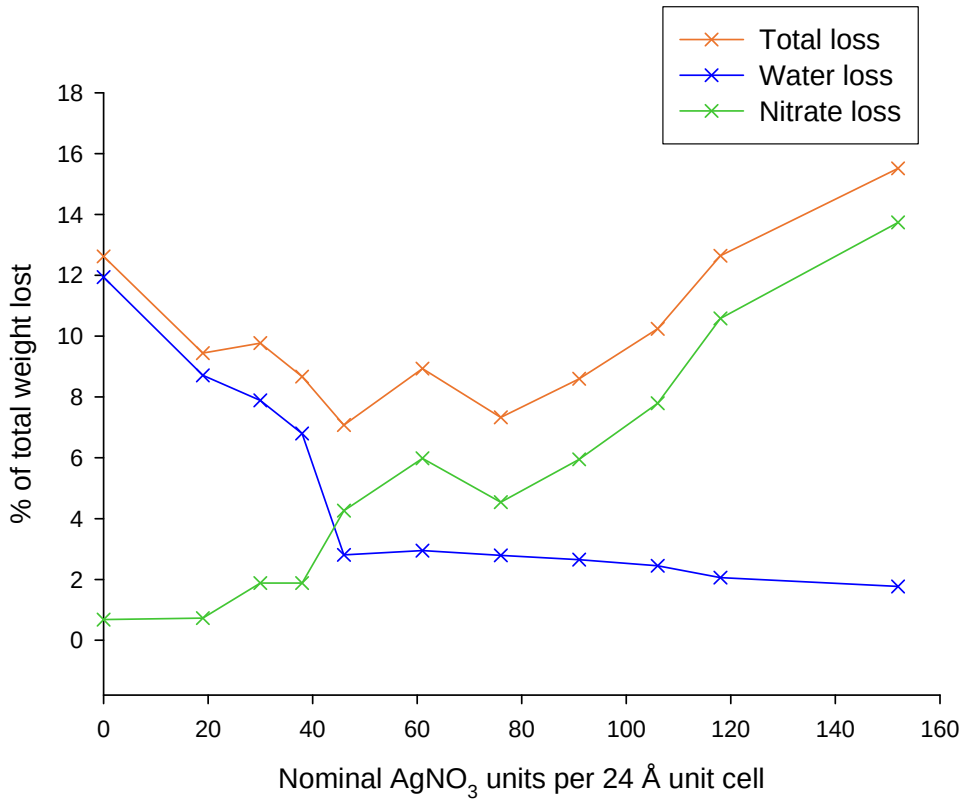

Figure 4.14: Percentage of total weight lost from unwashed silver occluded zeolite A

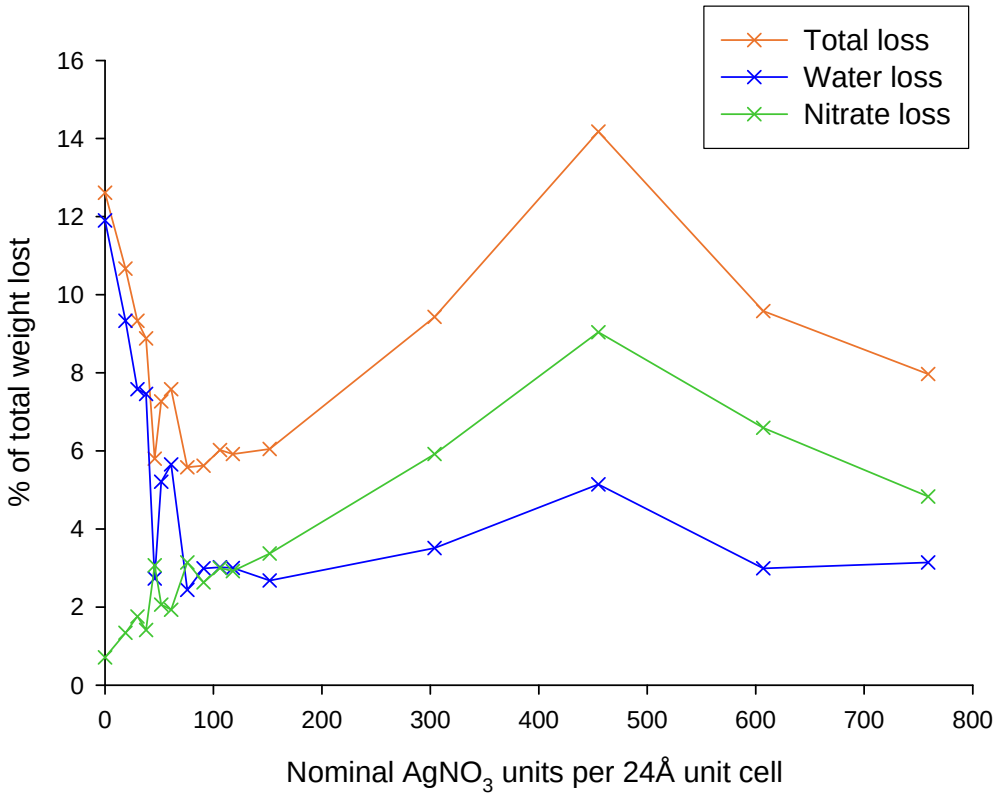

Figure 4.15: Percentage of total weight lost from washed silver occluded zeolite A

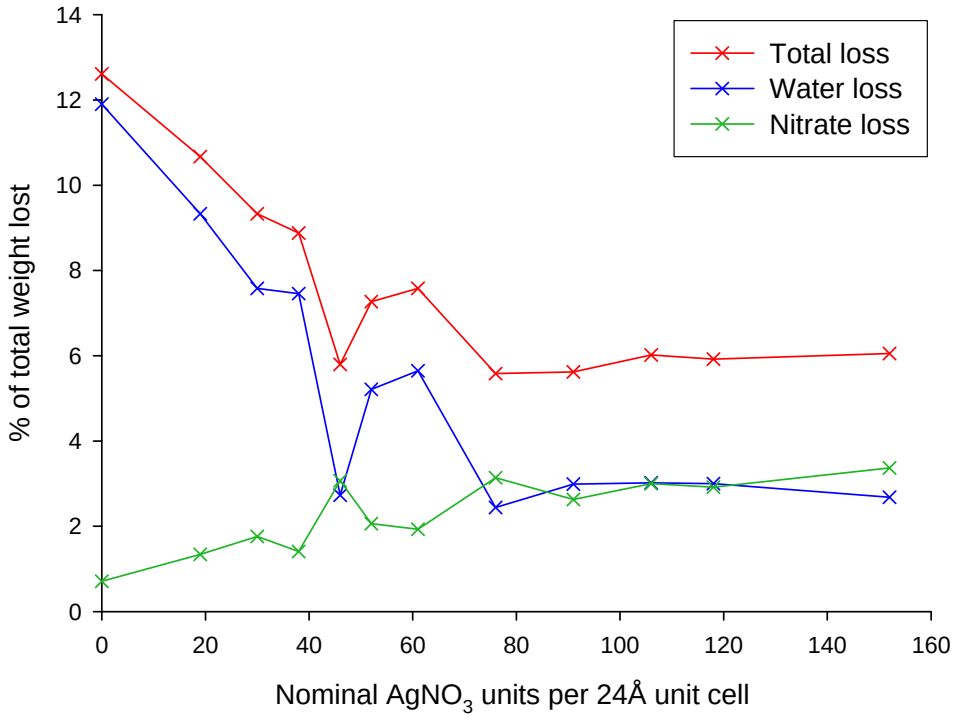

Figure 4.16: Expansion of Figure 4.15 showing percentage of total weight lost from washed silver occluded zeolite A at low occlusion levels

In the case of washed samples (see Figure 4.15 on the previous page and Figure 4.16 above), trends are less obvious. This could in part be due to the washing process, particularly at low levels of occluded silver nitrate. It is entirely possible that in removing excess silver nitrate which was adhered to the surface of the zeolite, some of the occluded silver nitrate near the surface of the zeolite crystals was removed.

The TGA plots for both washed and unwashed samples appear to show two distinct trends for water loss. These are best seen in Figures 4.14 and 4.16. With fewer than 38 ions per 24 Å unit cell, the water loss decreases quite steeply with increasing levels of silver nitrate ions being occluded. At occlusion levels of 46 ions per 24 Å per unit cell and over, the water loss has plateaued out to a minimum. This pattern is less obvious in the washed samples, but this is most likely due to variations in washing.

This steep change coincides with the increase in lattice parameter noted for the washed and unwashed samples. Therefore, the transition from 38 to 46 ions per unit cell appears to cause an expulsion of water as nitrate levels increase and this causes the lattice to expand. This expansion could be a result of repulsions between the negatively charged nitrate ions being in proximity, without the screening effect of water molecules.

One possible origin of the increased cell size and the coincidental drop of water content is the supersaturation of silver nitrate within the zeolite pores. It should be noted that the water in these samples was most likely lost during the occlusion process, but for washed samples water was reabsorbed during washing and for the unwashed samples, moisture from the atmosphere could be enough to penetrate the zeolite. At 38 ions per 24 Å unit cell and below, the silver nitrate is effectively in "solution" with the water within the zeolite but above this occlusion level, the silver nitrate could "solidify" blocking the pores to reabsorption of water.

On the following pages are two figures (4.17 and 4.18) which show the weight gain seen upon cooling of samples during thermogravimetric analysis. Both washed and unwashed samples regained weight upon cooling in the TGA. This increase in weight has been attributed to absorption of water from the air. The graphs are most striking and show that when low levels of silver nitrate are present, the absorption of water is high. As the quantity of occluded silver nitrate increases, the amount of absorbed water decreases and reaches zero. The loading level at which no moisture is absorbed varies according to whether or not the sample was washed. Washed samples stopped reabsorbing water at a lower occlusion level than the unwashed samples (34 or 48 ions per 24 Å unit cell compared to 106 ions, see section 4.4.1 where the approximate occlusion level is calculated). Unfortunately, given the difficulty in the estimation of actual loading levels from TGA data, it is hard to be certain at this stage that the difference is significant. Further investigations are required.

A possible reason for the cessation of water absorption is that the silver (which is not lost during the heating for thermogravimetric analysis) blocks the zeolite pores. At low occlusion levels there is not sufficient silver to cause obstruction to the water molecules, and significant amounts of water can re-enter the zeolite.

During the washing process, some silver nitrate will be lost from the sample, meaning that for an equivalent occlusion level, there will be fewer remaining silver atoms for the washed sample than the unwashed sample. This means that at a particular occlusion level, the unwashed sample will have more pores blocked by silver ions than the washed product, and thus will be unable to re-absorb as much water.

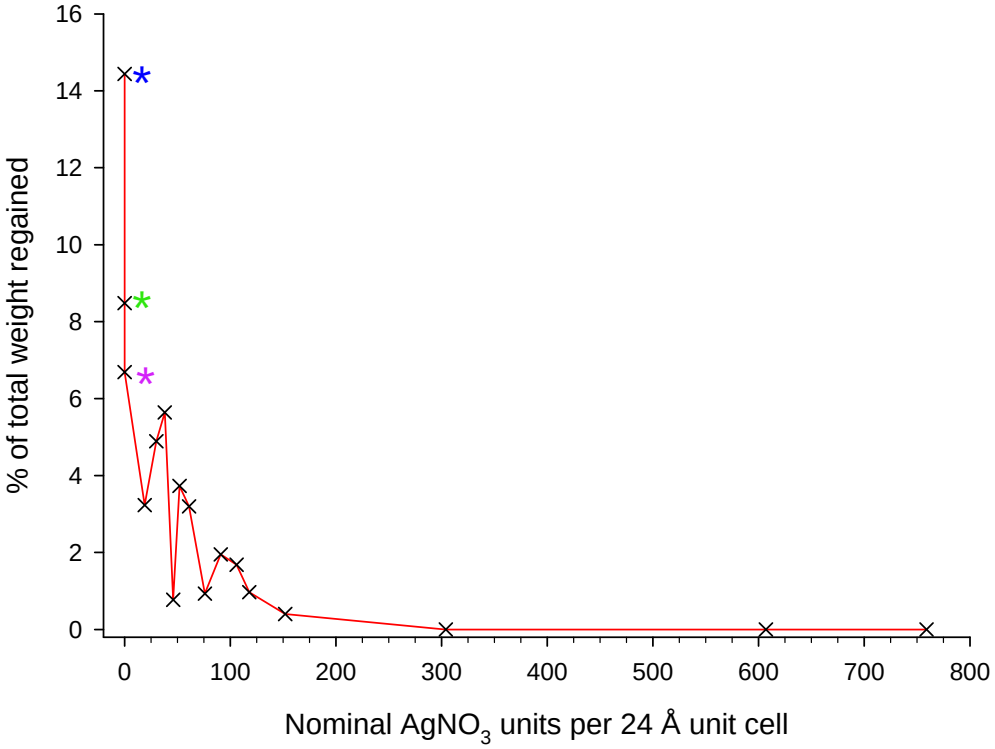

Figure 4.17: Weight gain for washed samples of zeolite A occluded with silver nitrate. * represents as-synthesised sodium zeolite A. * represents silver-exchanged zeolite A. * represents silver-exchanged zeolite A heated under occlusion reaction conditions without $AgNO_3$.

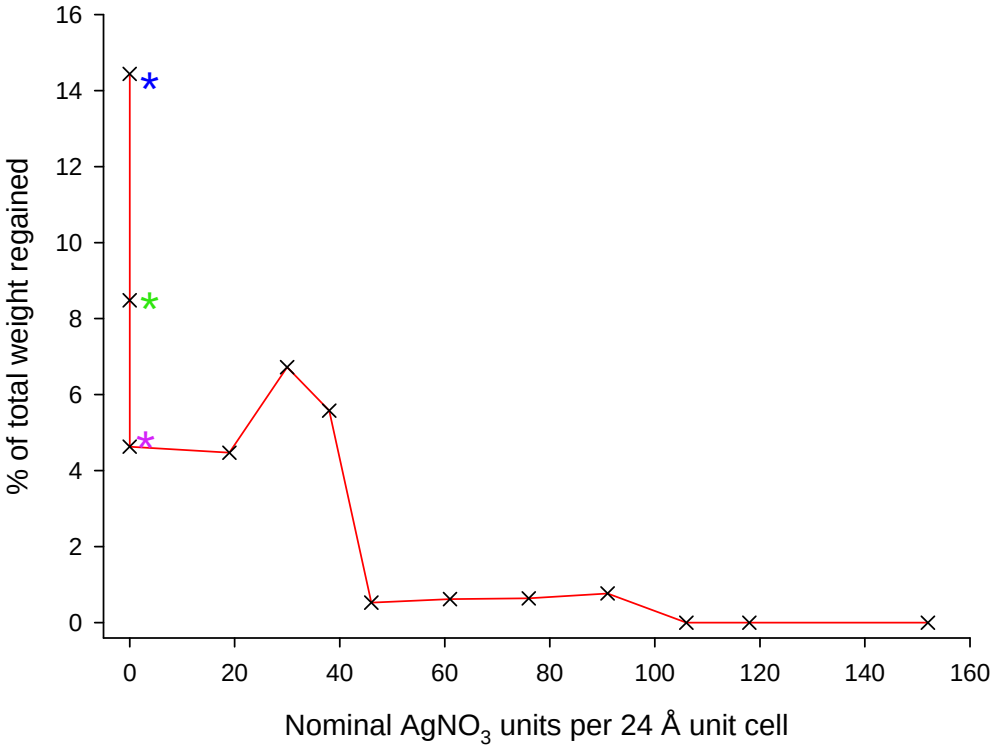

Figure 4.18: Weight gain for unwashed samples of zeolite A occluded with silver nitrate

* represents as-synthesised sodium zeolite A. * represents silver-exchanged zeolite A.

* represents silver-exchanged zeolite A heated under occlusion reaction conditions without $AgNO_3$.

4.4.1 TGA as a Means of Estimating the Level of Occlusion

The data obtained from thermogravimetric analysis can be used to estimate the number of $AgNO_3$ units occluded per unit cell. The raw data used in the calculations, as well as the TGA plots themselves, can be found in Appendices 2 and 3, respectively. By calculating the quantity of nitrogen and oxygen lost during the heating, it can be estimated how much silver nitrate has been occluded in the zeolite. The identity of the silver nitrate decomposition products has a bearing on the calculation to determine the actual quantity of $AgNO_3$ occluded. Note that the gaseous products lost are irrelevant, other than in terms of mass lost from the sample. Therefore, two reactions have been considered:

$$AgNO_3 \xrightarrow{heat} Ag + \text{“}N + 3O\text{”}$$

$$AgNO_3 \xrightarrow{heat} Ag_2O + \text{“}N + 2O\text{”}$$

The first of the two reactions is most likely to occur, since it is known that silver nitrate decomposes into silver metal with the loss of nitrogen oxides. However, since the exact contents of the zeolite have not been identified, it is possible that the second equation is valid.

In order to verify the method used, the calculations were run for the unwashed samples which were subjected to thermogravimetric analysis. Since no washing took place it was expected that the calculated values would approximately tally with the amount reacted with the zeolite. Figure 4.19 shows the relationship between calculated and expected occlusion levels.

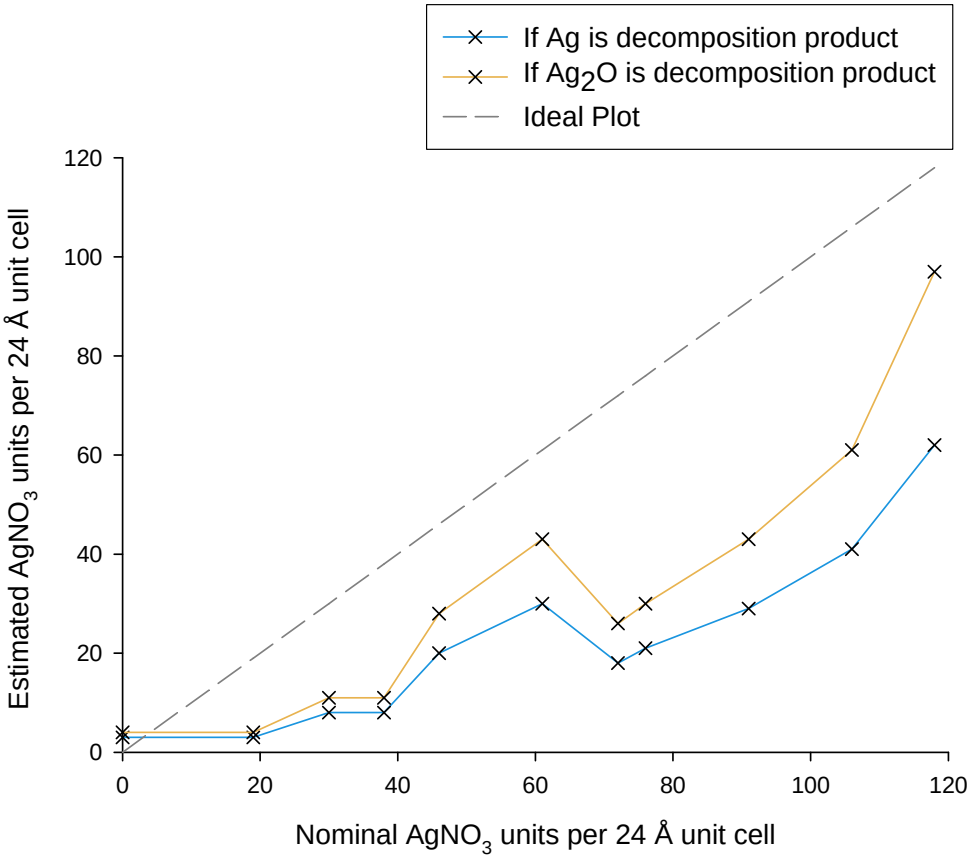

Figure 4.19: Number of ions per 24 Å unit cell of zeolite A for unwashed samples estimated from TGA data

It is clear from the data presented in Figure 4.19 that the calculations based on the TGA experiments are underestimating the true occlusion level of samples an average of 33%. The origin of the errors is possibly an incorrect assumption of the product remaining in the zeolite following heating in the TGA machine.

In light of this, the data presented for washed samples have been revised to reflect the inaccuracy.

Figure 4.20 shows a plot for each of the proposed reactions as a function of the amount of $AgNO_3$ used in the occlusion reaction.

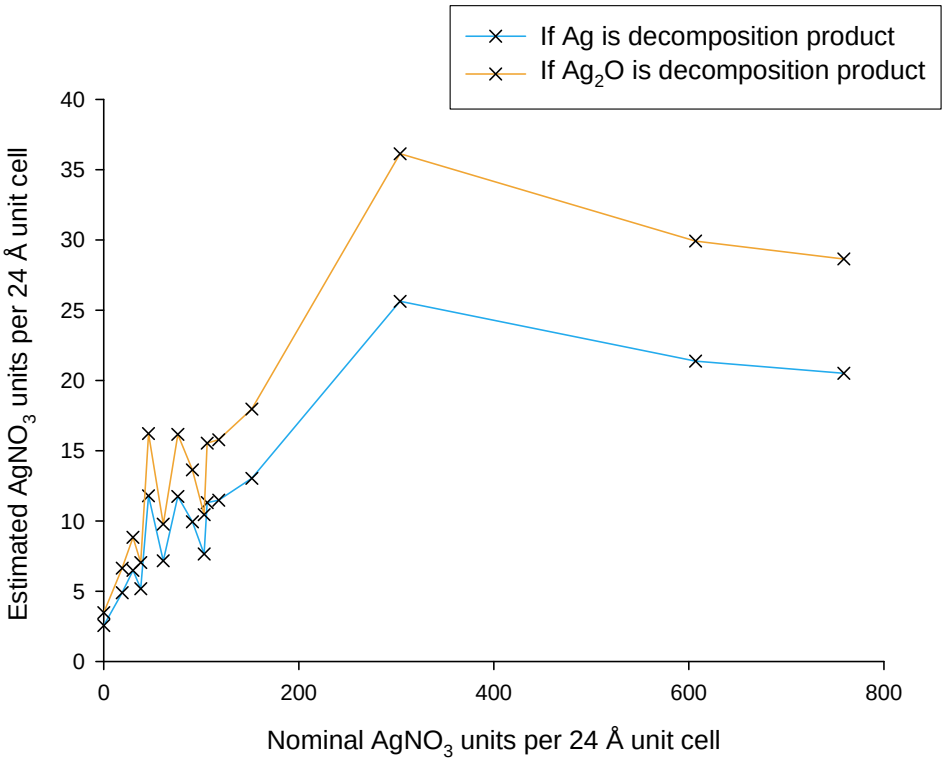

Figure 4.20: Number of ions per 24 Å unit cell of zeolite A after washing estimated from TGA data

As it is known that these values are probably lower than actual levels, it is necessary to revise these to reflect the average error of 33%. The data in Figure 4.21 has been adjusted to take

account of the error. It should be noted, however, that the degree of the discrepancy in Figure 4.19 varies considerably from case to case and is in some cases much greater than 33%. It follows that these estimates may not be entirely reliable.

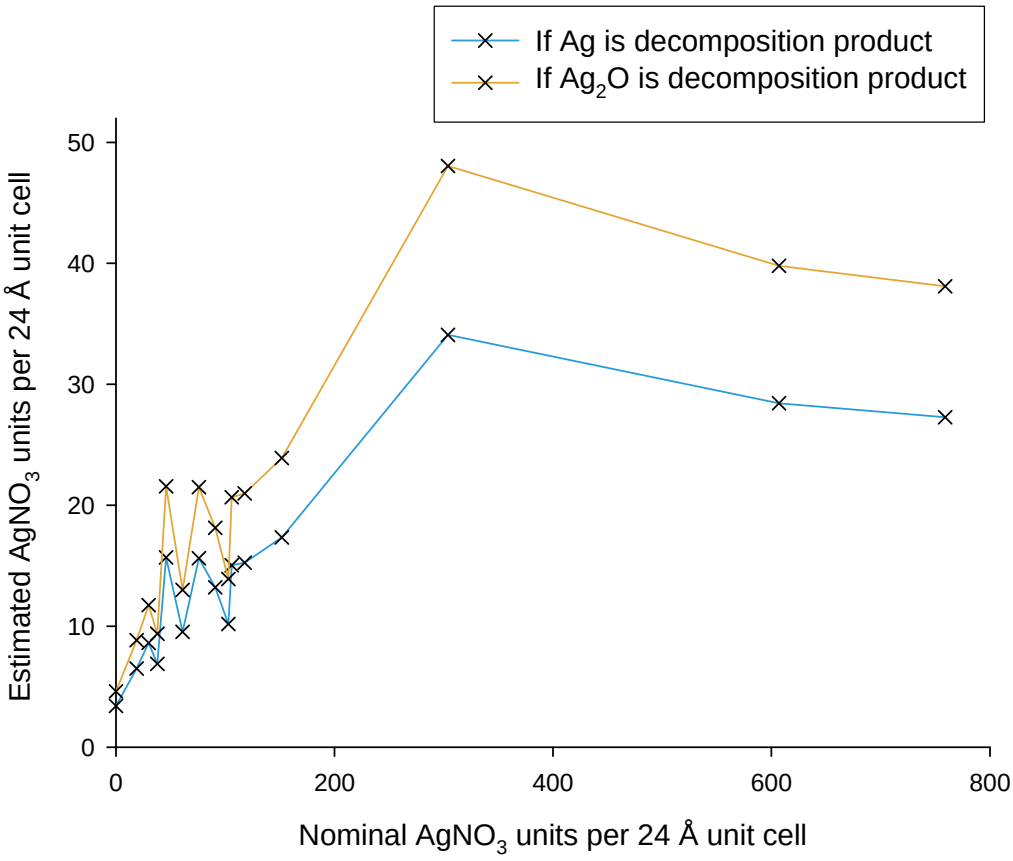

Figure 4.21: Corrected number of ions per 24 Å unit cell of zeolite A after washing estimated from TGA data

The fluctuations seen at low occlusion levels are believed to be a result of inconsistent washing removing varying levels of silver nitrate. It should be noted that according to Barrer and Meier[9] no more than 72 ions can be accommodated per 24 Å unit cell. The above plot demonstrates how little of the silver nitrate in the reaction mixture actually remains occluded in the zeolite A framework after washing.

In terms of the corrected estimated data, the superlattice is seen for occlusion levels

equivalent to ≥ 30 (if Ag only remains in the cell after the TGA process) or ≥ 40 (if Ag_2O remains) silver nitrate units per 24 Å unit cell. Samples prepared in the absence of water (i.e. dehydrated samples) only displayed superlattice peaks in XRD patterns for an occlusion level of ≥ 56 silver nitrate units per 24 Å unit cell[23].

It is likely that the TGA data has underestimated the true level of silver nitrate occluded, and it could in fact be closer to that seen in the dehydrated sample. It is also possible that the hydrated samples contain a greater concentration of occluded silver nitrate in their cores after washing (since the silver nitrate at the surface and edge of the crystals was removed) than that estimated from TGA data. However, the dehydrated samples are more likely to contain an even distribution of silver nitrate, and as a consequence a higher level is required to show a superlattice from the material as a whole.

4.4.2 Estimation of Superlattice Domain Size

The peaks seen in the powder XRD patterns which result from superlattice ordering are noticeably broader than the zeolite framework peaks. This reveals that the superlattice ordering is on a far shorter length than the zeolite crystal size. Applying the Scherrer equation (see section 2.1.4) to the broad superlattice peaks gives an estimate of the domain size. For the standard superlattice formation method (5 g $AgNO_3$ with 1 g Ag-zeolite A heated together at 260°C for 8 hours) the domain size was found to be approximately 260 Å, which is equivalent to a 3D domain covering ~9200 α-cages.

As has already been discussed in section 4.3.4, slower cooling steps were used to try and obtain longer range ordering of the superlattice. Figure 4.22 shows a plot representing how the cooling rates and holding steps affected the size of the superlattice domains.

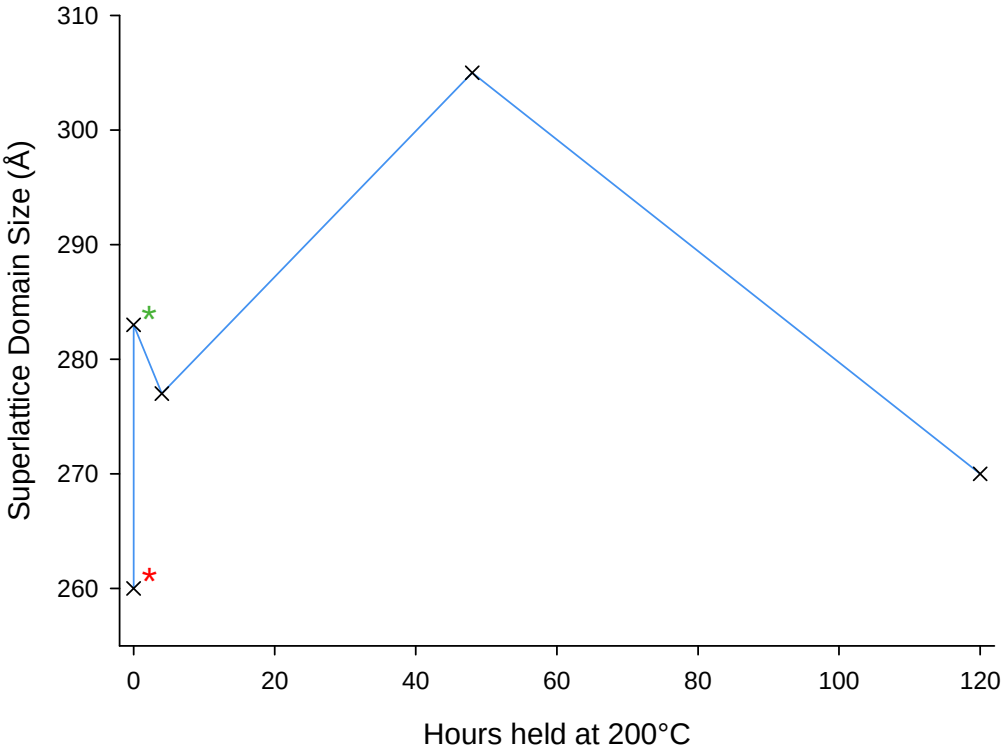

Figure 4.22: The effects of cooling rate on superlattice domain sizes.

* cooled from 260°C at 60°C/hr, no holding. * cooled from 260°C at 10°C/hr, no holding.

The graph seen in Figure 4.22 shows that slower cooling rates did result in larger superlattice domain sizes. However, the last sample (held at 200°C for 120 hours) had smaller domains, perhaps indicating that prolonged heating begins to destroy the superlattice ordering.

The first two points in the graph demonstrate that slowing the cooling rate (without the use of a holding step) from 60°C an hour to 10° an hour caused an increase in the superlattice domain size. The introduction of a holding step at 200°C, in addition to the slower cooling, caused the superlattice domain to increase further still. Overall, the increase in size of the domains observed is equivalent to growing from ~9200 α-cages to ~15600 α-cages.

Figure 4.23: Sequential powder XRD scans of the reaction between 1 g of silver nitrate and 1 g of silver-exchanged zeolite A

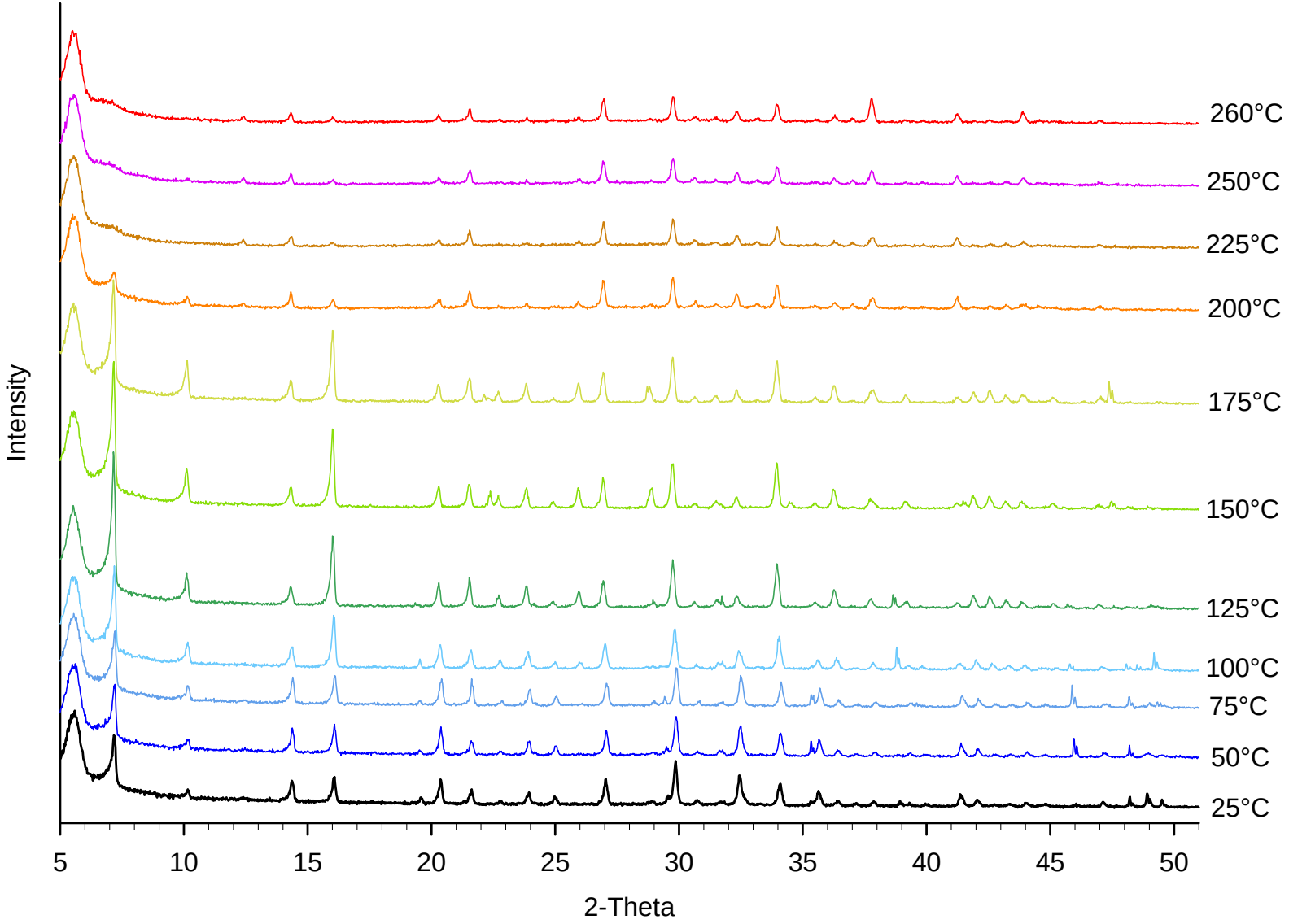

4.4.3 Examination of an Occlusion Reaction

A series of experiments examining the transformations undergone by the silver nitrate and silver-exchanged zeolite A mixture was conducted in the X-ray diffractometer. An occlusion mixture was prepared by grinding the zeolite and silver nitrate together before transferring the powder to an alumina sample holder, which was positioned on a heating stage in the X-ray diffractometer. The heating and scanning of the sample was controlled via a computer.

Figure 4.23 on the previous page shows scans which ran for 3 hours as the mixture of 1 g of silver nitrate and 1 g of silver-exchanged zeolite A were heated from room temperature to 260°C.

There is a shift towards lower values of 2-theta as the temperature is increased (i.e. the lattice parameter is increasing). This is best seen in the form of a plot of lattice parameters versus temperature.

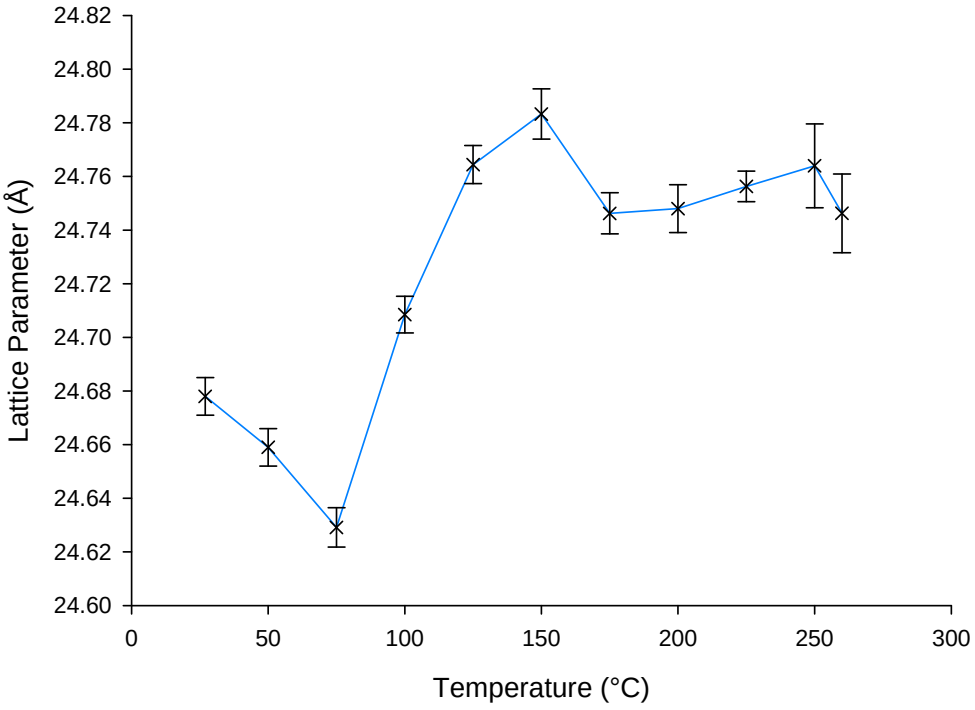

Figure 4.24: The effect of temperature on the lattice parameter of zeolite A

The shape of the curve in Figure 4.24 shows that between 75 and 125°C there is a sharp increase in the lattice parameter. Either side of these temperatures the lattice parameter is effectively constant. The sudden increase in the size of the unit cell could be a result of the start of the occlusion process. Whilst the temperature is below that of the melting point of silver nitrate, it is known that at temperatures between the boiling point of water and the melting point of silver nitrate the two chemicals can coexist in a liquid phase[8]. This could enable some occlusion to occur before the melting point of silver nitrate is reached. There are some small, yet noticeable, changes to peak intensities at lower temperatures (approximately ~100°C) which may be due to occlusion of silver nitrate beginning or dehydration of the zeolite. These changes to the zeolite are the cause of the increase in lattice parameters.

Table 4.5 lists the peaks seen in the powder XRD patterns in Figure 4.23. The 2-theta values listed are approximate due to a slight shift towards lower 2-theta on increasing temperature. Where there was ambiguity for a given 2-theta value due to zeolite A and silver nitrate sharing a peak position (highlighted in pale yellow), assignment has been made based on the constancy of peak intensity. This is because there is a phase change for silver nitrate at 159°C, and it is assumed that silver nitrate peak positions and intensities will differ between these phases.

Table 4.5: Interpretation of high temperature X-ray diffraction data (as illustrated in Figure 4.23) for the occlusion reaction between 1 g $AgNO_3$ and 1 g zeolite A

Approximate 2-theta	Peak Assignment	Comments
7.0	A 2 0 0	Intense peak, lost between 200°C and 225°C
10.2	A 2 2 0	Peak lost between 200°C and 225°C
12.5	A 2 2 2	Appears at 200°C with low intensity
14.5	A 4 0 0	Fairly steady intensity throughout reaction
16.0	A 4 2 0	Rapid decrease in intensity between 175°C and 200°C
19.5	$AgNO_3$	Room temperature phase, lost by 150°C (phase change at 159°C)
20.5	A 4 4 0	Intensity gradually reduces throughout reaction
21.5	A 4 4 2	As intensity steady at all temperatures, most likely A 4 4 2 not $AgNO_3$
22.8	A 6 2 0	Low intensity peak, lost above 200°C. $AgNO_3$ could cause split at 150°C
24.0	A 6 2 2	Intensity loss occurs at 175°C. Peak could be due to $AgNO_3$
25.0	A 4 4 4	Intensity lost by 175°C
26.0	A 6 4 0	Appears at 100°C, intensity increases then diminishes to low intensity
27.0	A 6 4 2	Steady intensity at all temperatures
29.0	A 8 0 0	Small at all temperatures, except for 150°C where it reaches a maximum
29.8	A 8 2 0	As intensity is steady the peak is most likely zeolite A not $AgNO_3$
30.7	A 8 2 2	Low intensity for all diffraction patterns
31.5	A 6 6 2	Low and steady intensity
32.5	A 8 4 0	Intensity does not vary, therefore the peak is most likely zeolite A not $AgNO_3$
34.0	A 8 4 2	Intensity does not vary, therefore the peak is most likely zeolite A not $AgNO_3$
35.5	A 8 4 4	Broad peak with low intensity
36.5	A 10 0 0	Steady intensity
37.0	A 10 2 0	Constant intensity
41.5	A 8 8 0	Steady intensity
42.0	A 10 4 4	Vanished at temperatures over 200°C
42.5	A 8 6 6	Lost at temperatures above 200°C
43.5	A 10 6 2	Very low intensity above 200°C
44.0	A 12 0 0	Very small intensity over 200°C

The majority of zeolite peaks which lose intensity during the reaction do so at around 200°C. As the silver nitrate melts at 212°C significant levels enter the zeolite and this greatly affects the intensity of peaks seen in the X-ray diffraction pattern. The peaks most significantly affected upon occlusion are those at low 2-theta (high d-spacing).

Trace 1 in the graph in Figure 4.25 is a plot of the relative intensity values of the 200 peak (traditionally the most intense peak in the zeolite A XRD pattern) when compared to the peak with maximum intensity in the given diffraction pattern, as a function of occlusion levels. The relative intensities used are calculated from the peak counts as a percentage of the counts of the most intense peak (counts themselves are not used for plotting the graph here, as these values vary according to scan durations and are therefore not suitable for comparisons). A second trace in the figure shows the relative intensity of the 200 peak compared to the average of relative peak intensities for the 642, 820 and 664 peaks. These three particular peaks were chosen because their intensities did not fluctuate dramatically across the range of occlusion reactions studied.

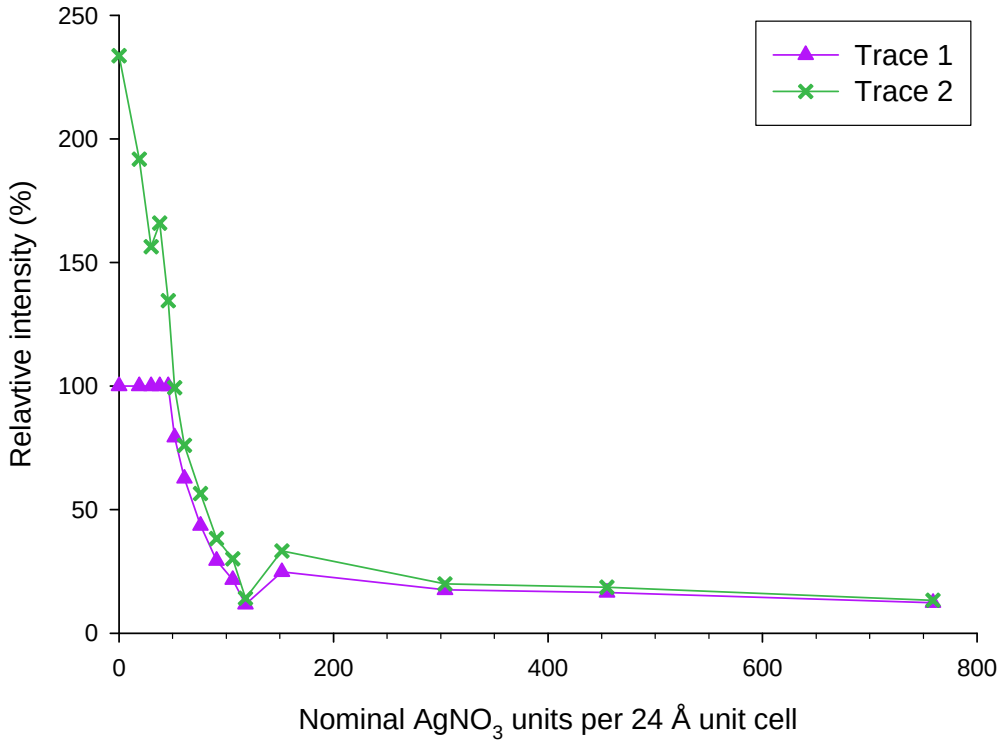

Figure 4.25: Relative intensity of the 200 peak in powder XRD patterns for washed silver occluded samples.

Empirically, the loss in relative intensity of low angle peaks is a reliable indicator of the extent of salt occlusion in all systems studied. In simple terms this can be rationalised in terms of the large d-spacings of low angle peaks. D-spacings relate to the distance between parallel planes in the structure which are hit by in-phase X-rays. For d-spacings above ~4 Å information is being obtained over a relatively long characteristic length scale within the zeolite, in effect contrasting the framework with void spaces further away. For shorter d-spacings, the comparison is over a much shorter length scale. For unoccluded samples, the α-cage contains some low atomic mass ions and water, and the contrast between the framework and the α-cage is significant. However, for silver-occluded samples, there are now high atomic mass ions within the α-cage and there is a loss of contrast with the zeolite framework. This is shown in the loss of intensity for the low 2-theta reflections. Interestingly, the same pattern is also seen following the ion-exchange of zeolite A with caesium nitrate (see section 5.3.4 in Chapter 5). In this case the heavy caesium ions sit well recessed into the zeolite cages in order to have suitable Cs–O bond distances with framework oxygen atoms. This effect was well modelled by the Poudrix simulations of ion-exchanged zeolites (section 5.3.4).

4.4.4 Superlattice Structure Interpretation

From this section onwards, interpretation shall be performed using the 12 Å cell, and so the hkl values of peaks are half that of those for the 24 Å cell. It has been demonstrated, through the use of thermogravimetric analysis and powder X-ray diffraction, that when occlusion reactions were performed between zeolite A and silver nitrate, the salt entered the zeolite

framework. Samples were subjected to powder XRD before and after ion exchange and salt occlusion, and the relative peak intensities were compared. The dramatic changes seen (see Figure 4.26) were a result of the heavily scattering silver nitrate occupying voids which previously held only weakly scattering water. In terms of the relative intensities to other peaks in the powder X-ray diffraction pattern, Table 4.6 lists the changes seen when the sodium zeolite A is first ion exchanged, and then filled with occluded silver nitrate.

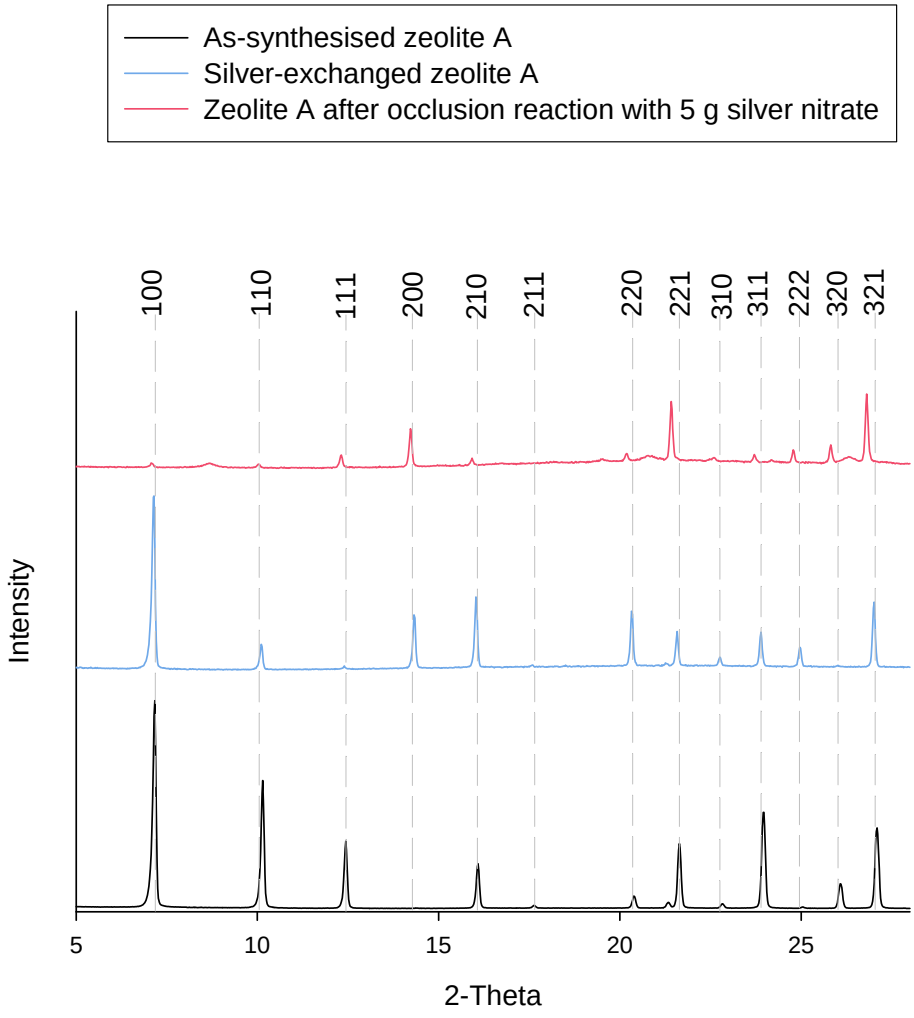

Figure 4.26: Comparison of powder XRD patterns for zeolite A before and after reactions with silver nitrate. Peaks have been indexed using the 12 Å unit cell.

Table 4.6: Comparison of peak intensities in XRD patterns for zeolite A when ion exchanged and filled with occluded silver nitrate

Peak hkl[a]	As synthesised NaA	Silver-exchanged A	Silver occluded A
100	very strong	very strong	weak
110	very strong	medium/ weak	weak
111	strong	very weak	medium
200	very weak	medium	medium/ strong
210	strong	medium	medium/ weak
211	weak	weak	-
220	medium	medium	medium/ weak
221	strong	medium	strong
310	weak	weak	weak
311	strong	medium	medium/ weak
222	weak	medium/ weak	medium
320	medium	very weak	medium
321	strong	medium/ strong	strong
400	weak	weak	medium/ weak

Note a) The hkl values listed are based on the 12 Å unit cell.

It is interesting to note the hkl values of the zeolite A peaks that increase or decrease in relative intensity following the occlusion reaction. It is interesting that peaks that increase in intensity have hkl values which are all even (the 200, 222 and 400) and those that lose intensity following occlusion have a mix of odd and even hkl values (the 100, 110, 210 and 211). This trend would indicate a face centred arrangement of silver nitrate within the zeolite, as the face centred structure has systematic absences for hkl values which are a mixture of odd and even numbers.

Close examination of the peaks in Figure 4.26 also reveals how the peaks move to lower 2-theta values following the ion exchange and occlusion of silver nitrate. This indicates an increase in the lattice parameter as more silver nitrate is accommodated within the zeolite framework. This is reinforced by the data analysis performed using CELL[24].

It has been noted that a superlattice was formed within zeolite A following a reaction with

excess silver nitrate. Samples which contained a superlattice showed extra peaks in their powder XRD patterns, and these were a consequence of a regular ordering of the silver nitrate within the zeolite framework. For samples where a superlattice was present, the superlattice peaks appeared at the same 2-theta values regardless of the sample preparation. This means that there is a preferred arrangement of silver nitrate within the zeolite framework, and that this arrangement is adopted no matter what the occlusion method.

A typical powder XRD pattern showing all the superlattice peaks is shown in Figure 4.27.

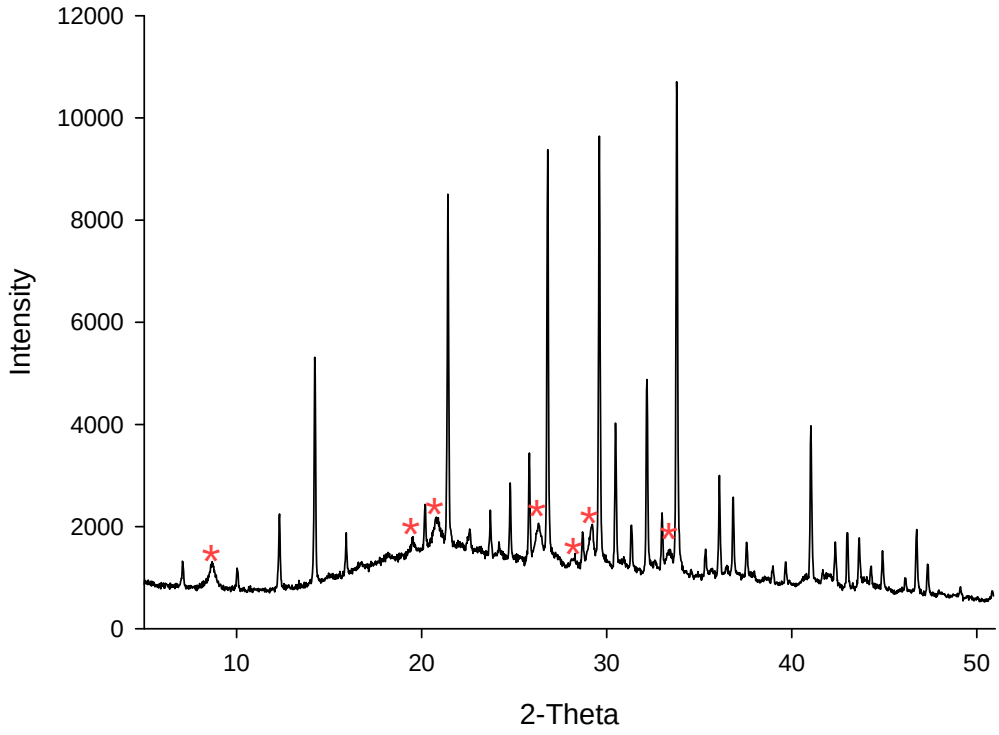

Figure 4.27: Powder XRD pattern showing superlattice peaks (*) for zeolite A following an occlusion reaction with 5 g silver nitrate (equivalent to 95 ions per 12 Å unit cell)

The data for the highlighted peaks are given in Table 4.7.

Table 4.7: Powder XRD data for superlattice peaks

2-Theta	d (Å)	Intensity %
8.675	10.18473	12.2
19.529	4.54168	16.8
20.814	4.26419	20.4
26.325	3.38263	19.3
28.142	3.16822	12.6
29.194	3.05641	19.1
33.371	2.68279	14.5

Information about face centring of scattering density in the zeolite framework provides a starting point for identifying where the silver nitrate may be located.

The structure of zeolite A is shown in Figure 4.28, with the α and β cages marked. Note that the silicon/aluminium atoms are located at the intersection of the black lines which represent bonds. For clarity the oxygen atoms are not shown, but are positioned approximately half way along the bonds.

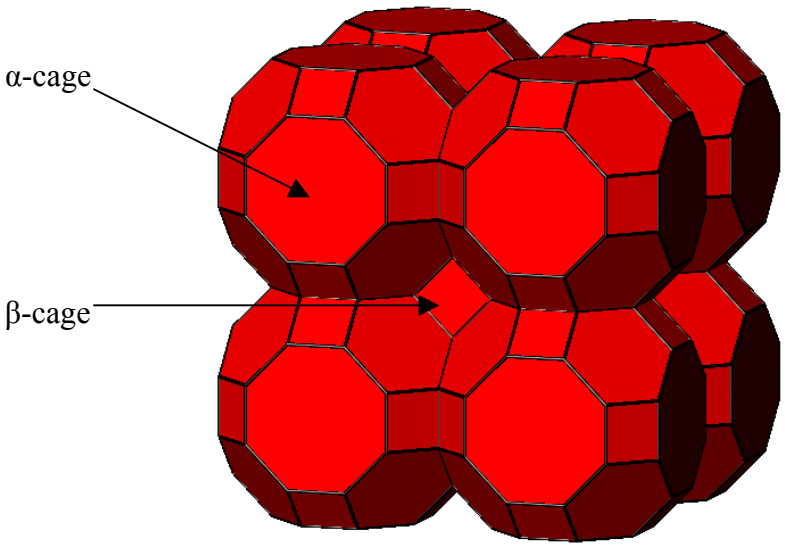

Figure 4.28: Structure of one 24 Å unit cell of zeolite A

This structure can be simplified and illustrated is in Figure 4.29.

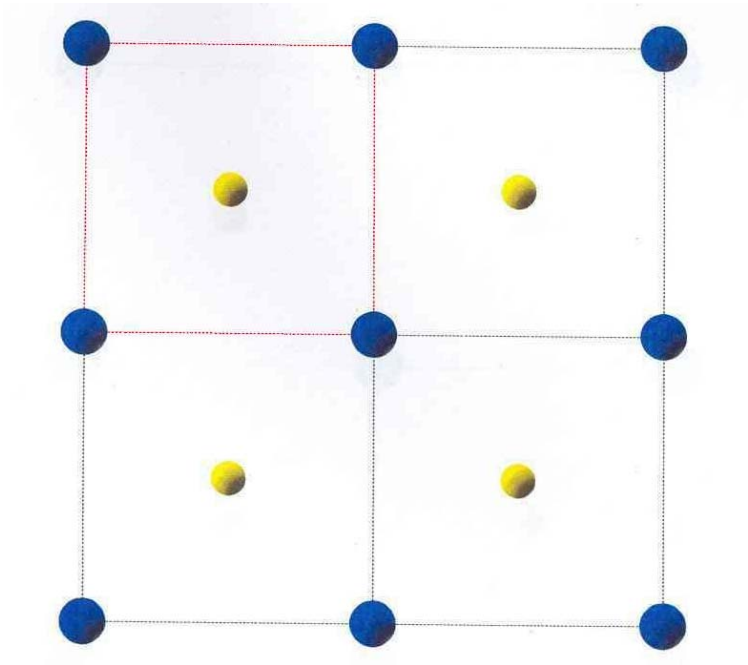

Figure 4.29: Representation of zeolite A.

Blue spheres represent the 8-ring of the α-cages and yellow spheres represent the centre of the β-cages. The red lines outline one 24 Å unit cell, as previously shown in Figure 4.28.

This simplified drawing of zeolite A clearly shows the face-centred arrangement of β-cages with respect to the 8-rings of the α-cages. If the heaviest scatterers (i.e. silver cations) were located in both sites, this might account for the changes seen in peak intensities in the powder XRD patterns, which suggested a pseudo face-centred arrangement. However, whilst this model accounts for the change in intensities, such a structure would not produce new peaks in the powder X-ray diffraction pattern.

To accommodate extra peaks, a larger unit cell size must be considered. Barrer and Meier[9] considered many theoretical cells and found a tetragonal cell with $a' = 2a$ and $c' = a$ best fitted their data. However, this is very much larger than the original unit cell, and it is possible that a smaller cell could be used. Therefore the unit cell considered had lattice parameters of $a' = \sqrt{2}\,a$ and $c' = a$. A cell with these parameters (illustrated in Figure 4.30) has half the volume of that considered by Barrer and Meier[9].

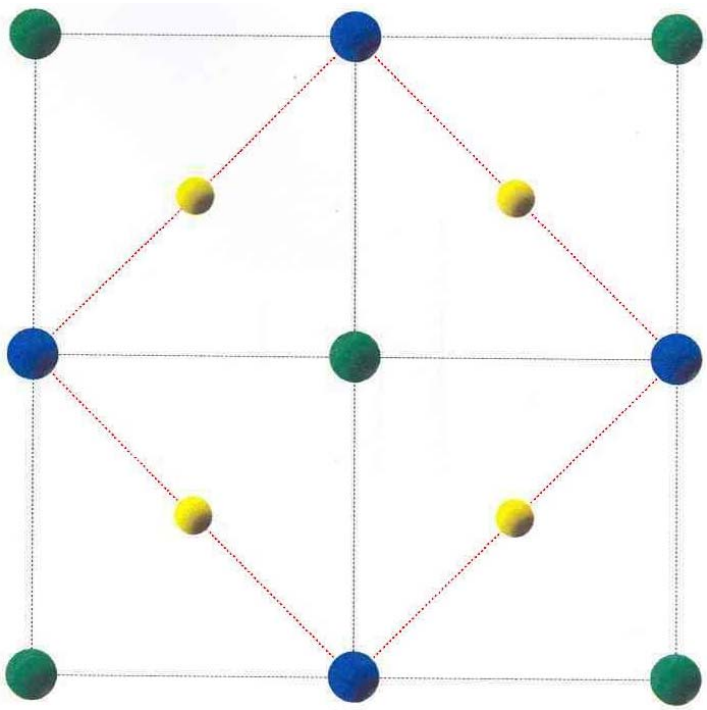

Figure 4.30: Representation of the new unit cell in two dimensions.

Blue spheres represent 8-rings (type I) and the green spheres represent 8-rings (type II).

Yellow spheres represent β-cages. The red lines outline the new unit cell.

As indicated in the description of Figure 4.30, there must now be different "types" of 8-ring. This is because there are no face-centred tetragonal cells, but as can be seen the proposed cell appears to be face-centred. By assuming that the 8-rings differ in some way, as yet unknown, the cell is no longer face-centred.

There is some further supporting evidence for the tetragonal unit cell in the powder XRD patterns. After storing for some time, samples had a second powder XRD pattern recorded, and there was evidence of peak splitting (indicated by the * Figure 4.31). This could well be a consequence of slow ordering of the silver nitrate over time into a tetragonal superlattice. An example of a powder X-ray diffraction pattern with evidence of peak splitting is shown in Figure 4.31. The peaks at higher values of 2-theta are most significantly affected.

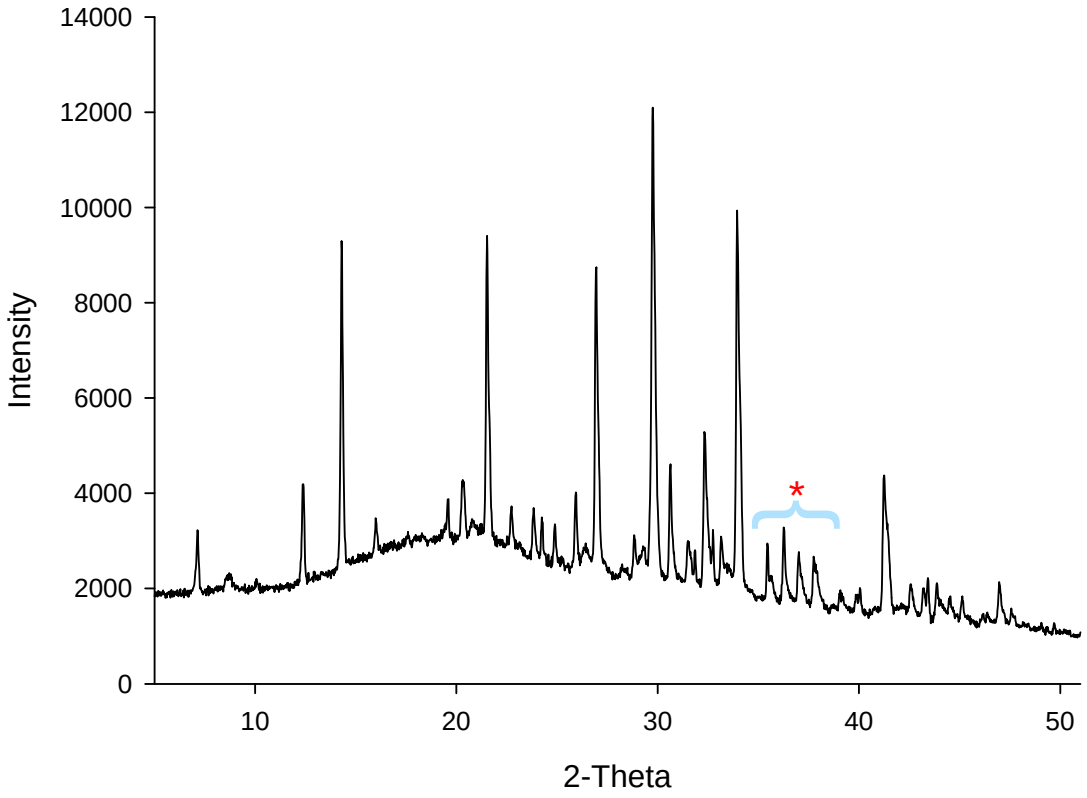

Figure 4.31: Powder X-ray Diffraction pattern of zeolite A with occluded silver nitrate (equivalent to 95 ions per 12 Å unit cell) which shows peak splitting

All the evidence put forward so far suggests that the new unit cell which describes the superlattice is tetragonal. There are many tetragonal space groups, so the most logical starting point is to examine groups related to that of zeolite A, since the framework remains unaltered.

It has been reported[23] that the superlattice data can be fitted to the group P4/nmm, which is related to the $Fm\bar{3}c$ space group of the 12 Å zeolite A unit cell. It should be emphasised that the space group reported is a proposal based on the fact that the data fits the space group, but no other evidence for (or indeed, against) has been found. Electron diffraction would usually assist structure determination, but in this case silver nanowires are known to grow from the samples studied[8].

4.5 Conclusion

Occlusion reactions between zeolite A and silver nitrate were seen to be successful by examination of changes to the lattice parameter, differences in relative peak intensities and from TGA weight loss data. A significant change in lattice parameters was seen to occur for both washed and unwashed occluded samples at an occlusion level of between 38 and 46 ions per 24 Å unit cell. Below 38 ions per unit cell the lattice parameter remained steady at approximately 24.55 – 24.57 Å. Above 46 ions per unit cell the lattice parameter was consistently found to be larger at ~24.72 Å. At this same loading level, thermogravimetric analysis data showed a distinct change in the amount of water present in the zeolite. With increasing quantities of silver nitrate, there was a reduction in water until this reached a steady amount, while there was an increase in nitrate levels within the zeolite. It is believed that there may be some supersaturation of silver nitrate occurring which would account for the sudden steps in both lattice parameter and TGA data.

The use of unexchanged zeolite A proved successful in the formation of a superlattice, although again, only with high levels of silver nitrate. It is believed that some of the occluded salt performed a molten ion exchange, thereby reducing the relative quantity of silver nitrate for the occlusion stage, therefore, the same mass of silver nitrate with exchanged and unexchanged zeolite A was not equivalent to the same number of ions per unit cell. The mass of Ag-zeolite A and Na-zeolite A are also different which leads to a different number of ions per unit cell for reactions with equivalent masses of silver nitrate.

When dehydrated Ag–zeolite A is used in occlusion reactions, a far lower level of silver nitrate is required to form a superlattice. It is believed that this is because the presence of water either hinders superlattice formation or dissolves the superlattice.

The temperature the reaction was carried out at was not significant, provided that occlusion was performed above the melting point of silver nitrate. For samples known to form a superlattice, cooling rates were also investigated. It was hoped that the broad peaks, thought to be caused by short-range order of the superlattice domains, could be improved to a more ordered form by altering the duration and rate of sample cooling. Various sequences of cooling, annealing and holding steps were used, but the overall appearance of the superlattice peaks was not improved.

There are many factors to be considered in the occlusion reaction between silver nitrate and zeolite A which can influence whether a superlattice will form. The most significant of these parameters was the mass of silver nitrate mixed with the zeolite. It was noted that a vast excess was necessary for a superlattice to form – a mass equivalent to 455 ions per 24 Å unit cell was required. It is believed that if a superlattice does form below this level, any washing the sample undergoes destroys the superlattice and therefore no peaks are observed in powder X-ray diffraction patterns for washed samples. However, even with lower levels of silver nitrate, occlusion was seen to occur from the changes in peak intensities in the XRD patterns.

Overall, attempts to form superlattices in silver zeolite A proved successful. Attempts to promote ordering of the superlattice (as distinguished by the broad peaks in the powder XRD patterns) did not improve upon that formed in the original sample. The best combination of reaction conditions involved the use of silver-exchanged zeolite A, mixed with an excess of silver nitrate and a heating temperature of 260°C for 8 hours.

A preliminary proposal has been made of a possible space group for the superlattice. This space group is P4/nmm and has been found to fit in with data recorded in the course of studying samples containing a superlattice.

Chapter 5: Occlusion Reactions with Other Nitrates

5.1 Introduction

A general introduction to the processes of ion exchange and occlusion has already been provided in chapter 4. This section is concerned with the ion exchange and occlusion of zeolites ZK-4 (LTA) and rho (RHO) with silver nitrate, and of zeolite A (LTA) with monovalent group 1 metal nitrates, i.e. $LiNO_3$, $RbNO_3$ and $CsNO_3$.

5.1.1 Zeolites and Salts Investigated

Chapter 4, inspired by the original Barrer and Meier paper[1], found that occlusion of silver nitrate in zeolite A (LTA) occurred, and in the process a superlattice formed. It was decided to investigate whether occlusion and superlattice formation occurred for other zeolite structures in the presence of silver nitrate.

ZK4 also has the LTA structure, but has a different Si:Al ratio to zeolite A due to the presence of large tetramethylammonium cations, which means that there are fewer corresponding aluminium TO_4 units included in the structure. After calcination under O_2, the TMA^+ is lost, thus clearing the channels of this bulky ion. It has been noted that ion exchange will not occur unless the TMA^+ ion is removed[2]. Although the structure will have a lower cation exchange capacity due to the lower quantity of aluminium which accounts for the negative framework charge, once the TMA^+ has been removed, the channels will be more open than in zeolite A. It was hoped, therefore, that the ZK4 structure would be able to accommodate more neutral salt units per unit cell upon occlusion with a metal nitrate salt.

Zeolite rho (RHO) has a structure related to zeolite A, but slightly more open and flexible due to the presence of double 8 rings (instead of the single 8 rings in zeolite A). It was hoped that

silver nitrate would be occluded within these spacious voids, although there was a risk that washing excess silver nitrate from the sample would remove the occluded salt if it was not sufficiently "trapped".

Barrer and Meier[1] reported reactions with silver nitrate in which superlattice formation was observed. It was decided to see whether other monovalent cations, as part of a nitrate salt, could produce a superlattice in the zeolite framework as was seen with silver nitrate. The other salts investigated were lithium, caesium and rubidium nitrates. Nitrates are commonly chosen as a result of their melting points being in a favourable temperature range for reaction with zeolites[3].

5.1.2 Lithium Reactions with Zeolites

Ion exchange and occlusion reactions with lithium salts have mainly focused on the use of lithium chloride[4-6]. For low silica zeolite X (FAU), it was found that the amount of lithium chloride occluded varied with the reaction temperature[6]. At higher temperatures, more salt was occluded, however, this had an adverse affect on the crystallinity of the sample. It is thought the LiCl used damaged the zeolite framework, and hence more damage was seen when more salt was occluded by the zeolite. Another interesting finding from this work was that the occlusion reaction occurred at a quicker rate if excess salt was used.

Yoshida *et al*[6] discussed the possible sites occupied by lithium and chloride ions in dehydrated low silica X. They suggested that each unit cell could accommodate up to 104 Li^+ ions and 8 Cl^- ions, since each sodalite cage has space for only one lithium chloride unit.

5.1.3 Rubidium Reactions with Zeolites

Many studies have examined the reactions between zeolites and rubidium[7-11]. Song and co-workers[7] performed an ion exchange between dehydrated zeolite A (LTA) and rubidium vapour, and studied the location of rubidium ions. The rubidium ions were found to occupy four different crystallographic sites, with 12 Rb ions per unit cell.

Firor[8], Pluth[9] and Igarashi[10] agree that there is only a 90% level of ion exchange between zeolite A and rubidium solutions (hydroxide[8,9] and chloride[10]) meaning there are 11 rubidium ions per unit cell. The former[8,9] also present structural analysis to determine the location of the rubidium ions within the zeolite.

5.1.4 Caesium Reactions with Zeolites

The uptake of caesium by zeolites is of considerable interest, due to the presence of ^{137}Cs in nuclear waste[12]. Whilst clinoptilolite is primarily used for the removal of caesium from nuclear waste, other zeolites will exchange and occlude caesium.

Of the many studies of ion exchange between caesium ions and zeolites[4,13-18], only one has examined zeolite A[13], and only two have used caesium nitrate[13,14]. Lima *et al*[13] found that in reactions with zeolite A, the concentration and salt type (caesium chloride, nitrate or acetate) had no effect upon the location of caesium ions in the sample (although differences in location were seen for zeolite X).

5.1.5 Occlusion Reactions

All of the papers discussed in sections 5.1.3 – 5.1.4 have been concerned with the ion

exchange reactions: none have looked at whether occlusion reactions occur or what effect this has on the zeolite. Therefore, the method used by Barrer and Meier[1] for the occlusion of silver nitrate with zeolite A has been followed. That is, heating an ion-exchanged zeolite with an excess of metal nitrate at a temperature roughly 40–50°C above the melting point of the salt. Whilst occlusion can occur at the melting point of the salt, temperatures above the melting point were employed to be consistent with Barrer and Meier's work[1]. A duration of 8 hours and heating and cooling rates of 60°C per hour were employed. Full reaction details are given in the following section.

5.2 Reactions

5.2.1 Zeolite Synthesis

5.2.1.1 Zeolite A

Zeolite A was synthesised using 0.723 g sodium hydroxide (AnalaR 99 % pellets, BDH) which was dissolved in 80 ml of deionised water. This solution was divided into two portions. To the first, 8.258 g of sodium aluminate (Strem Chemicals) was added and dissolved. In the second measure, 15.48 g of sodium metasilicate pentahydrate was dissolved with heating and stirring. The two solutions were then recombined and immediately heated at 99°C in a conventional oven. The zeolite powder was recovered by filtration and was washed and dried at ~ 50°C.

5.2.1.2 Zeolite ZK4

30 g of tetramethylammonium hydroxide (25 % with water, Aldrich) was stirred with 10 g of colloidal silica (SiO_2, 40 % with water, Dupont Ludox HS40) for 30 minutes. In a separate container, 2.06 g sodium aluminate was dissolved in 54.4 g deionised water, before being added to the initial solution. The gel was aged for 48 hours before being heated at 100°C for 24 hours. The solid zeolite was recovered by filtration and dried in air overnight at 50°C.

To remove the tetramethylammonium ion, the ZK4 product was heated under oxygen at a temperature of 500°C for 24 hours. The resulting product was then ready for either ion exchange or salt occlusion.

5.1.2.3 Zeolite Rho

A solution of sodium hydroxide was prepared by dissolving 18 g of sodium hydroxide (AnalaR 99 % pellets, BDH,) in 25 ml of deionised water. 7.25 g of alumina (Catapal B,

Vista) were added to this solution, which was heated and stirred to aid dissolution. 18 g of caesium hydroxide (50 wt.% with water, Aldrich) and 150 g of colloidal silica (SiO_2, 30 wt.% with water, Dupont Ludox HS 30) were then added to the solution. The resulting gel was aged for 24 hours before heating for 6 days. Zeolite rho was filtered and washed before drying at ~ 50°C.

5.2.2 Ion Exchange

5.2.2.1 Silver Ion Exchange

A 250 ml, 0.1 M solution of silver nitrate was prepared by dissolving 4.25 g of $AgNO_3$ (99+%, Aldrich) in deionised water. 5 g of zeolite rho or 4 g of calcined ZK4 were added and the mixture was stirred at room temperature for 24 hours. As silver nitrate is light sensitive the flask was wrapped in aluminium foil to prevent light affecting the reaction.

The solution was filtered after the 24 hours, and was washed and dried at 60°C. The resulting powder was stored in a sample container covered with aluminium foil to prevent light affecting the product.

5.2.2.2 Lithium Ion Exchange

A 0.1 M solution of lithium nitrate was made by adding 1.72 g $LiNO_3$ (Aldrich) to a flask of 250 ml deionised water. This was stirred with 4 g sodium zeolite A at 60°C for 24 hours. The solution was then filtered, washed and dried at 60°C. The powder collected was then ion-exchanged again until it had been reacted in this way six times.

5.2.2.3 Rubidium Ion Exchange

This method has been adapted from Edmondson[19]. 3.68 g of rubidium nitrate (99.7 %,

Aldrich) was dissolved in 250 ml of deionised water to make a 0.1 M solution. Zeolite A (4 g) was added, and the solution stirred for a 24 hour period. The ion exchange was carried out six times, the first two at 50°C and the next four at 80°C. The samples were collected by suction filtration and dried in air.

5.2.2.4 Caesium Ion Exchange

A 0.1 M solution was prepared from 4.87 g of caesium nitrate (99.99 %, Aldrich) dissolved in 250 ml deionised water. 4 g of zeolite A was stirred at 80°C for 24 hrs. The solution was filtered and dried in air. This ion exchange was only carried out once in accordance with the method used by Bonelli *et al*[14].

5.2.3 Occlusion Reactions

The majority of samples were prepared from metal exchanged zeolite A and the corresponding monovalent metal nitrate (all supplied by Aldrich – as noted in the section on exchange). The appropriate quantities of zeolite A and metal nitrate were ground together and placed in an alumina reaction vessel before heating in a furnace. See Table 5.1 on the next page for compositions made.

Typical heating programs involved a heating and cooling rate of 60°C/hour, and holding at a temperature approximately 40–50°C above the melting point of the metal nitrate for a minimum of 8 hours, as these conditions were similar to those set out by Barrer and Meier[1].

The melting points of silver nitrate, lithium nitrate, rubidium nitrate and caesium nitrate are known to be 212, 264, 310 and 414°C respectively so occlusions were carried out at 260, 300, 350 and 450°C accordingly.

Table 5.1: Occlusion Reactions Performed

Zeolite[a]	Salt	Mass of Salt (g)[b]	Ions per 24 (Å) Unit Cell	Temperature (°C) & Duration (hrs) of occlusion	Cooling Rate (°C/hr)
Ag-ZK4	$AgNO_3$	5	708	260, 8	60
Ag-Rho	$AgNO_3$	5	104	260, 8	60
Ag-Rho	$AgNO_3$	24	500	260, 8	60
Li-A	$LiNO_3$	5	917	300, 8	60
Li-A	LiNO3	2	367	300, 8	60
Rb-A	$RbNO_3$	5	798	350, 8	60
Rb-A	$RbNO_3$	5	798	350, 24	60
Cs-A	$CsNO_3$	5	720	450, 8	60
Cs-A	CsNO3	5	720	450, 24	60

Note:

a) All reactions used zeolites which had previously been ion exchanged with the appropriate metal nitrate salt.

b) Mass of salt quoted is per 1 g of zeolite.

All samples produced were split into two portions – the first was stored as made, and the second was washed with deionised water.

Powder XRD patterns were obtained for all samples to examine whether there was any evidence of superlattice formation and to what extent occlusion may have occurred.

To verify the claim that ion exchange and occlusion have occurred the computer program Poudrix was again used. An explanation of this program has been given in section 4.2.5.

5.3 Results and Discussion

All powder X-ray diffraction patterns and samples discussed in this section were washed, since the unwashed samples showed only the metal nitrate pattern.

5.3.1 Silver Nitrate Reactions

5.3.1.1 Zeolite ZK4 Reactions

Silver occlusion reactions with zeolite A were successful in terms of superlattice formation. Since zeolite ZK4 is iso-structural with zeolite A, and differs only in its silicon to aluminium ratio, it was thought that reactions under similar conditions might also yield a superlattice. Zeolite ZK4 was synthesised, calcined to remove the organic template and then ion-exchanged with silver nitrate to obtain the silver form.

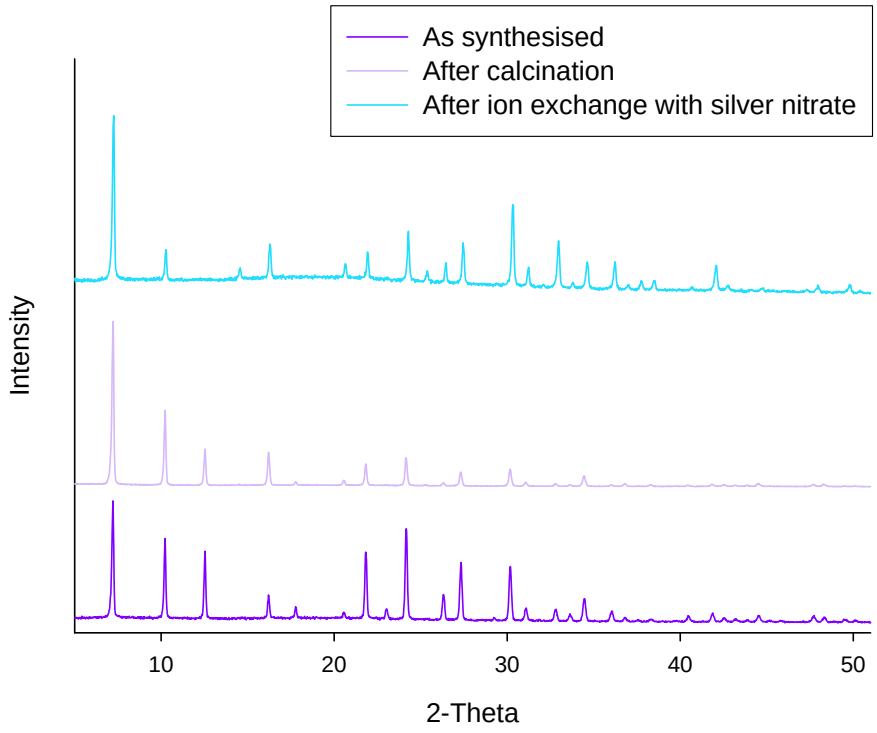

Figure 5.1: Comparison of powder XRD patterns from zeolite ZK4 samples

The relative intensities of many peaks can be seen to have altered after each reaction as a consequence of changing cell contents. Further changes to the powder X-ray diffraction

pattern were observed upon occlusion of silver nitrate, as seen in Figure 5.2.

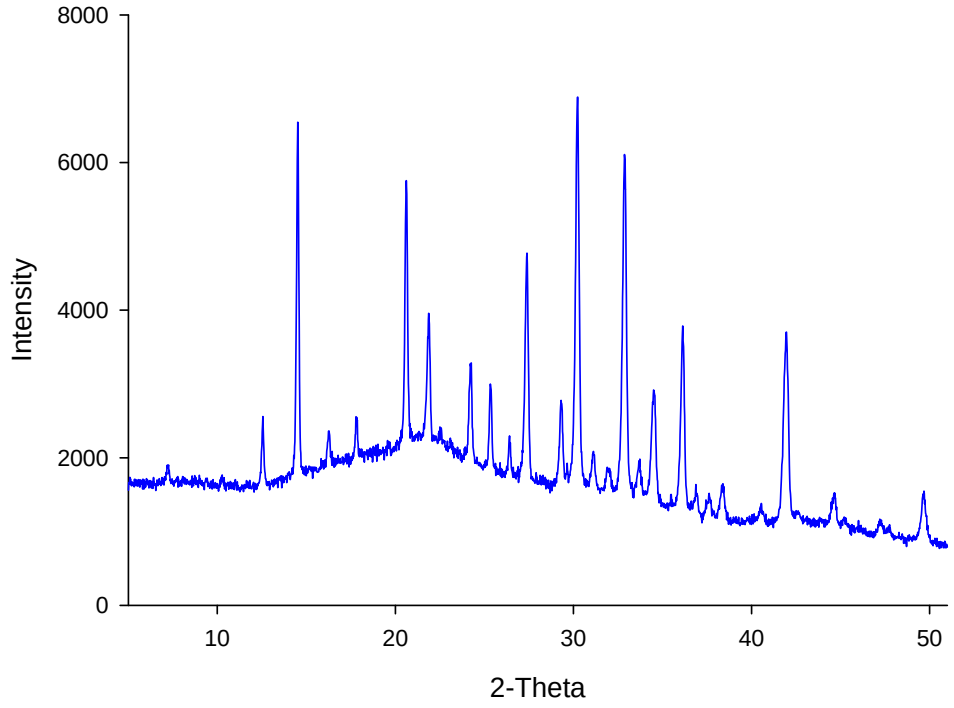

Figure 5.2: Powder XRD pattern of zeolite ZK4 after occlusion reaction with 5 g of silver nitrate

As was seen for the zeolite A samples, there was a dramatic loss in intensity for the peaks at low two theta, which shows that silver nitrate has entered the zeolite, i.e. the occlusion of silver nitrate by zeolite ZK4 is successful. There is also an increase in lattice parameter upon salt occlusion. However, in contrast to the zeolite A reactions, there do not appear to be any extra peaks caused by a superlattice in the powder XRD pattern in Figure 5.2 above. It is possible that this is a result of the amorphous background obscuring any small superlattice peaks.

5.3.1.2 Zeolite Rho Reactions

The structure of zeolite rho is related to that of zeolite A. Whereas in zeolite A the α-cages are linked by 8 rings, in zeolite rho they are linked by *double* 8 rings. This results in a framework that is more flexible than that of zeolite A. Reactions were conducted to see if

silver nitrate could be occluded and whether a superlattice could form within zeolite rho.

From the loss of peak intensity in the occluded zeolite rho sample, it can be concluded that silver nitrate entered the zeolite pores, i.e. occlusion was successful. Whilst there are peaks present in the powder X-ray diffraction pattern of the sample with occluded salt which were not evident in the other samples, these could be indexed to zeolite rho and are merely the result of a change of intensity and are not attributable to any superlattice. All zeolite rho samples (as-synthesised, silver-exchanged and silver-occluded) could be indexed with the $Im\bar{3}m$ unit cell.

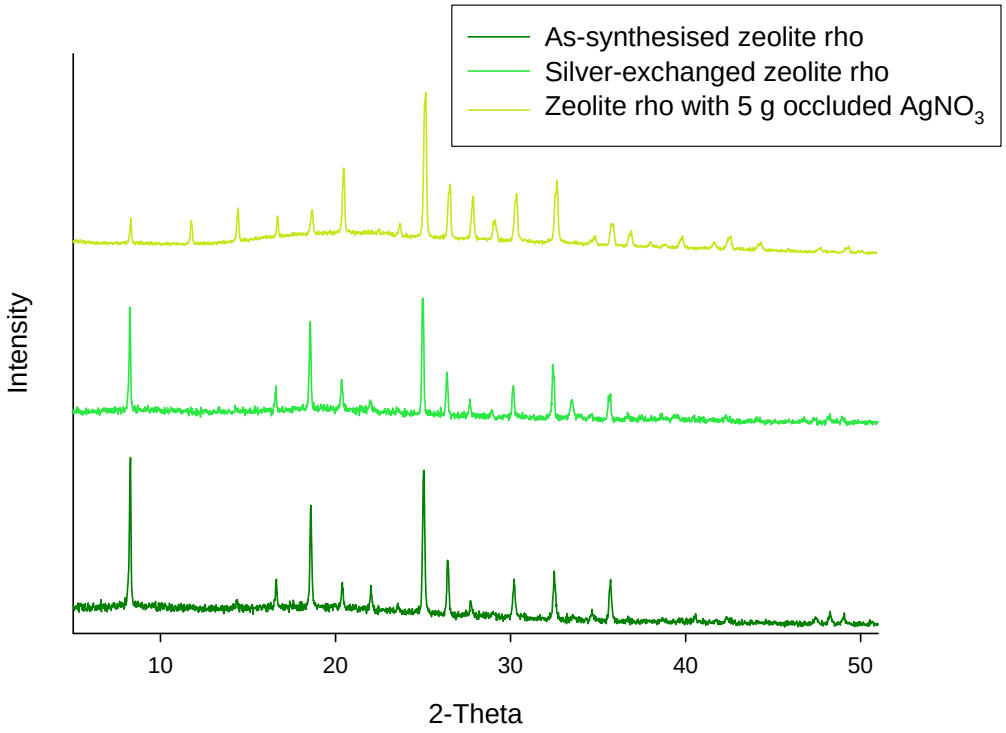

Figure 5.3: Powder XRD patterns of zeolite rho

Although zeolite rho was reacted with 5 g of silver nitrate, this was only equivalent to 104 Ag^+ and NO_3^- ions per unit cell, and at these levels superlattices were not observed for zeolite A. As with zeolite A, it is possible that washing not only removed excess silver nitrate, but may have destroyed any superlattice within the crystals.

Silver-exchanged zeolite rho was also reacted with an excess of silver nitrate, equivalent to 500 ions per unit cell. At this level of occlusion for zeolite A, as can be seen in Figure 5.4, there are peaks which could not be indexed to the zeolite rho structure. It is possible that these peaks could indicate the presence of a superlattice.

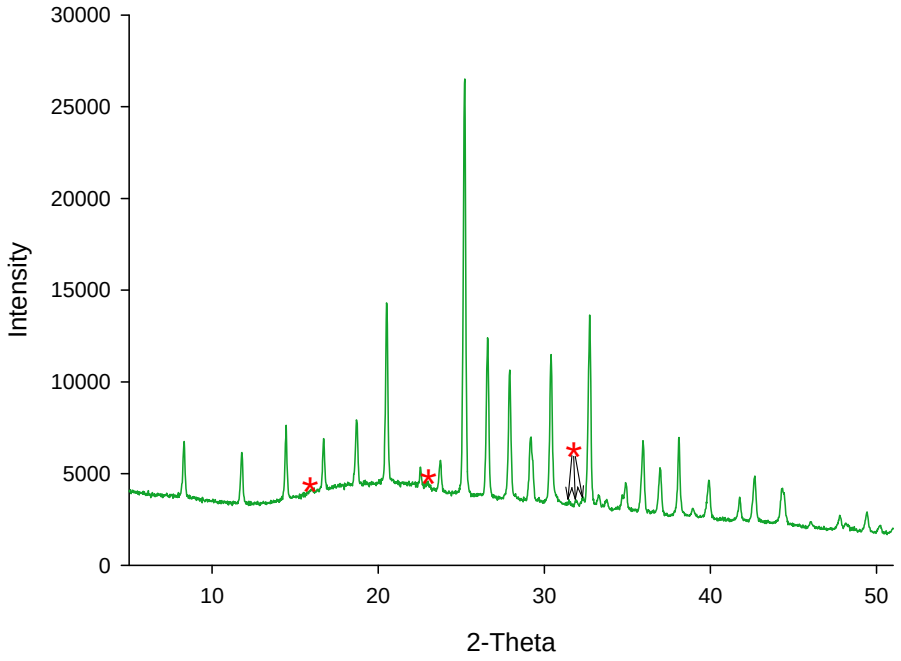

Figure 5.4: Powder XRD pattern of zeolite rho after occlusion with 500 ions per unit cell of silver nitrate.

* indicates 5 unindexable peaks which do not match zeolite rho or silver nitrate.

5.3.1.2.1 Investigation of Possible Space Groups for the Silver Superlattice in Zeolite Rho

The presence of extra peaks in the X-ray diffraction pattern of the silver-occluded zeolite rho indicates a change of symmetry may have occurred. The lattice parameter of the sample was found using the program CELL to be a = 14.98 Å, and enabled a trial and error examination of space groups to be conducted using the computer program Chekcell, which is described on the next page.

In Chekcell the user enters the known data for the sample, such as lattice parameters, and then selects a space group from a list. The program then calculates where peaks should be seen

for the chosen space group. These peaks can be compared to the XRD pattern which can be imported into the program. The user can then go through all the space groups within a crystal system and judge which groups best match the XRD pattern.

After eliminating potential impurities (such as chabazite and pollucite which can co-form in zeolite rho syntheses, and excess silver nitrate) the next course of action is to examine other space groups which may account for the extra peaks. It is known that zeolite rho has the space group $Im\bar{3}m$, however, if the sample is dehydrated it can adopt a lower symmetry space group of $I\bar{4}3m$[20]. As the zeolite rho containing occluded silver nitrate was prepared at a temperature of 260°C and was formed in the presence of a large excess of silver nitrate, it is reasonable to assume that the sample may not contain as much water as the as-synthesised zeolite rho.

Cubic, tetragonal, orthorhombic and rhombohedral space groups were considered. Table 5.2 summarises the space groups examined and the lattice parameters used in the computer program Chekcell.

From the data obtained in Chekcell, it appears that body centred unit cells, whilst not being a good fit by any means, fit the data better than primitive or face centred unit cells. None of the space groups examined, however, predicted extra peaks which fitted with those seen in the powder X-ray diffraction pattern obtained in the laboratory.

Whilst common impurities have been considered, it is possible that the peaks seen, which do not index well with other space groups, arise from some other source of impurity.

Table 5.2: Space Groups and Lattice Parameters Examined for the Silver Superlattice in Zeolite Rho

Cell Type	Space group Number	Space group Symbol	Lattice Parameters (Å)			θ (°)	Number of peaks predicted for 5 - 50°	Quality of Peak Fit
			a	b	c			
Cubic	229	Im3m	14.98	14.98	14.98		48	Good, but no extra peaks
Cubic	217	I43m	14.98	14.98	14.98		48	Good, but no extra peaks
Tetragonal	75-142	All	14.98	14.98	29.96		226	Poor matches, with body centred groups better than primitive
Tetragonal	75-142	All	29.96	29.96	14.98		416	Poor matches, with body centred groups better than primitive
Tetragonal	75-142	All	14.98	14.98	21.18		161	Poor matches, with body centred groups better than primitive
Orthorhombic	16-74	All	14.98	14.94	15.00		206	No extra peaks predicted. Body centred groups match best.
Rhombohedral	Various	R groups only	14.98	14.98	14.98	10 - 90	19 - 232	Very poor fits

Notes

1. There were 40 peaks observed between 5 and 50° in the powder XRD pattern for the zeolite rho sample containing a silver superlattice.
2. The number of predicted peaks contains multiples of peaks in the same position, and is therefore greater than the number of peaks actually observed.

5.3.2 Lithium Nitrate Reactions

Barrer and Meier[1] also reported in their work with silver nitrate that superlattice peaks were observed in X-ray powder photographs of samples of zeolite A reacted with lithium nitrate. Experiments using lithium nitrate were performed with zeolite A only, as this was so far the only zeolite in which evidence of a superlattice had been observed.

Ion exchange with lithium nitrate was carried out six times before an occlusion reaction was performed. A comparison of powder X-ray diffraction patterns, before and after ion exchange and occlusion reactions, are shown in Figure 5.5.

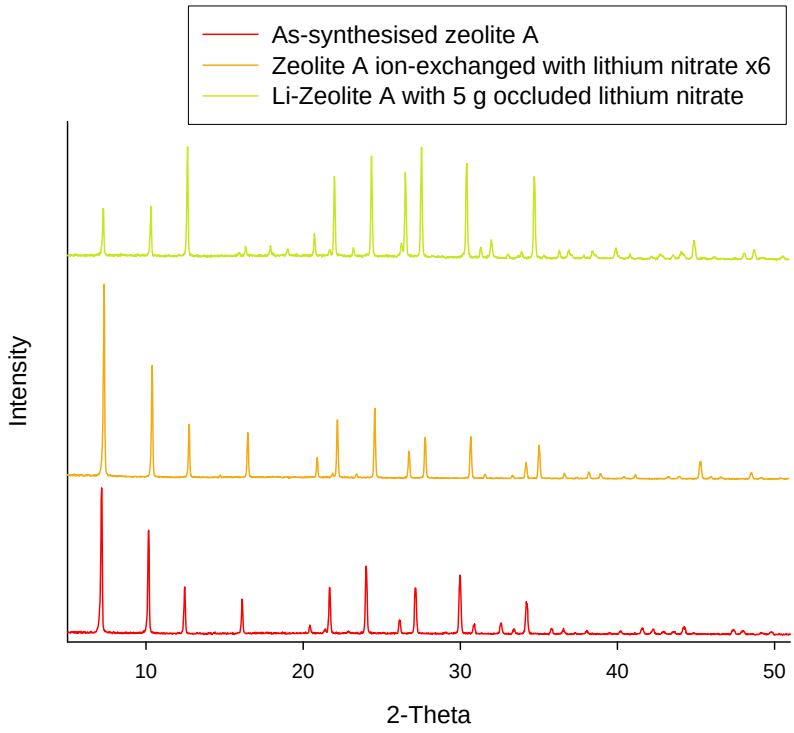

Figure 5.5: Comparison of samples reacted with lithium nitrate

Although more peaks are seen for the sample with occluded salt, these can be indexed to zeolite A, and are a consequence of the changing peak intensities. Lattice parameters were greatly affected by the ion exchange and occlusion reactions. The initial, sodium form of zeolite A had a lattice parameter of 24.605 Å. After the six ion exchange steps, the lattice

parameter had decreased to 23.989 Å. When the exchanged sample was reacted with the equivalent of 917 ions per 24 Å unit cell (5 g of lithium nitrate) the resulting sample had a lattice parameter of 24.203 Å.

Although changes in peak intensities were observed for the sample with occluded salt, indicating a successful occlusion reaction, there was no evidence of superlattice peaks. In the case of silver nitrate containing samples, the cation is a more significant scatterer of X-rays than the zeolite framework or the nitrate ion, and therefore it is the scattering power of the cation which enables the superlattice peaks to be seen in powder XRD patterns. In the work with lithium, it is possible that a similar superlattice could be present, but due to lithium being such a light element which would only weakly scatter the X-rays when surrounded by the more strongly scattering zeolite A framework, any superlattice present might not be observed. Therefore, work with other, heavier, group one nitrates was undertaken to see if these can produce a superlattice and whether this could be identified through powder X-ray diffraction.

5.3.3 Rubidium Nitrate Reactions

Reactions between zeolite A and rubidium nitrate were carried out. After six ion exchanges, the rubidium-exchanged zeolite A had undergone an increase in lattice parameter from 24.623 Å to 24.695 Å. This sample was then heated with rubidium nitrate and after indexing the peaks was found to have a lattice parameter of 24.665 Å, which was slightly smaller than the rubidium-exchanged zeolite.

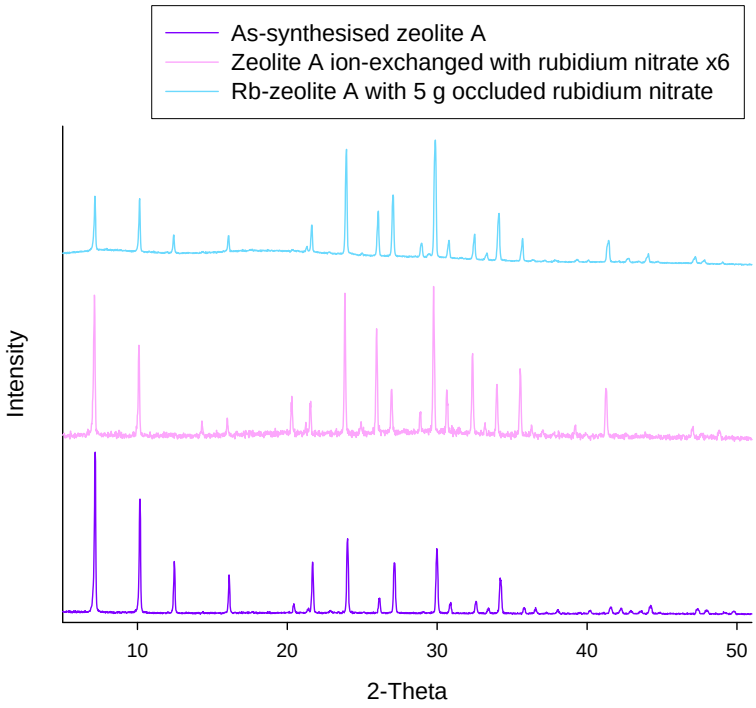

Figure 5.6: Powder X-ray diffraction patterns of samples reacted with rubidium nitrate

A change in the peak intensities for samples with occluded salt was observed, but there was no sign of any peaks due to a superlattice. Figure 5.6 above charts the changes seen in powder XRD patterns at different stages of the reaction. From changes in peak intensities and lattice parameters, it was concluded that occlusion had taken place.

5.3.4 Caesium Nitrate Reactions

The last monovalent nitrate to be examined in reactions with zeolite A was caesium nitrate. Following the method used by Bonelli *et al*[14] the ion exchange was performed once at 80°C and the powder X-ray diffraction pattern shown in Figure 5.7 can be seen to be greatly altered with respect to the original zeolite A. From the sodium to the caesium form of zeolite A there was a slight decrease in the lattice parameter from 24.615 Å to 24.567 Å.

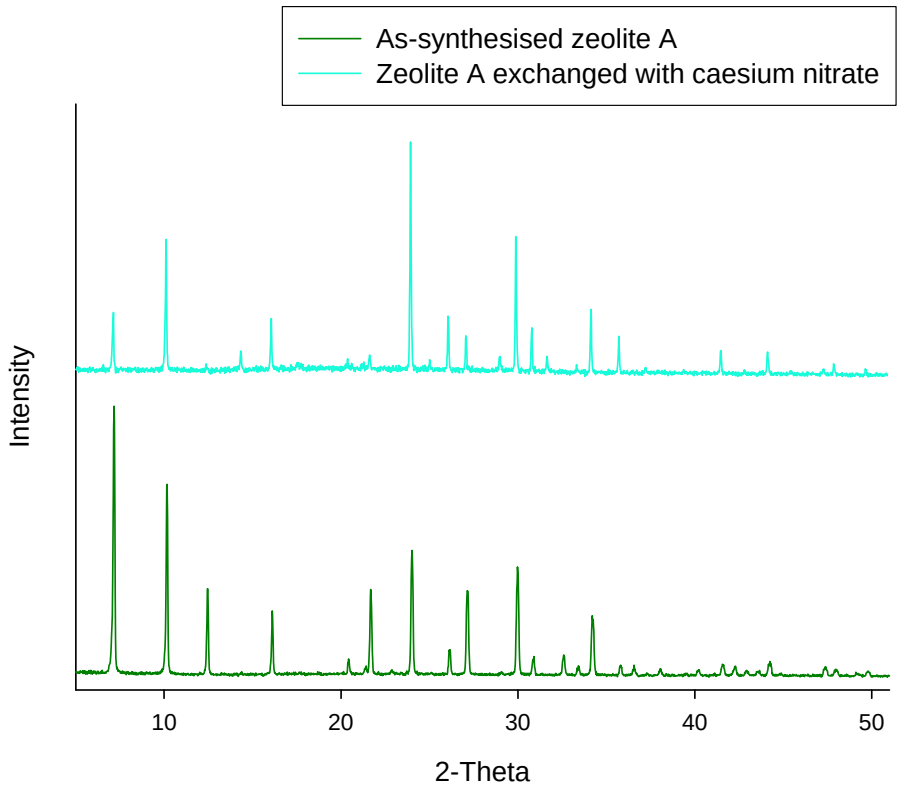

Figure 5.7: Comparison of sodium and caesium forms of zeolite A

The dramatic alteration in peak intensity seen upon ion exchange is similar to what would be expected for an occluded sample. It is thought that due to the large size of caesium, the exchanged ions do not sit in the plane of the 6-rings as sodium would, but are instead pushed further towards the centre of the α-cage. This helps maintain a distance between the caesium ion and the framework oxygen atoms. Having the heavy caesium ion located more in the α-cage than the 6-ring plane would reduce the contrast between the two regions, thus diminishing the intensity of the early peaks in the powder XRD pattern.

Poudrix was used to look at the predicted powder XRD pattern of hydrated caesium-exchanged zeolite A. Figure 5.8 shows the pattern generated by Poudrix when data was entered for caesium ions. The atom co-ordinates used were taken from the paper by Heo *et al*[21].

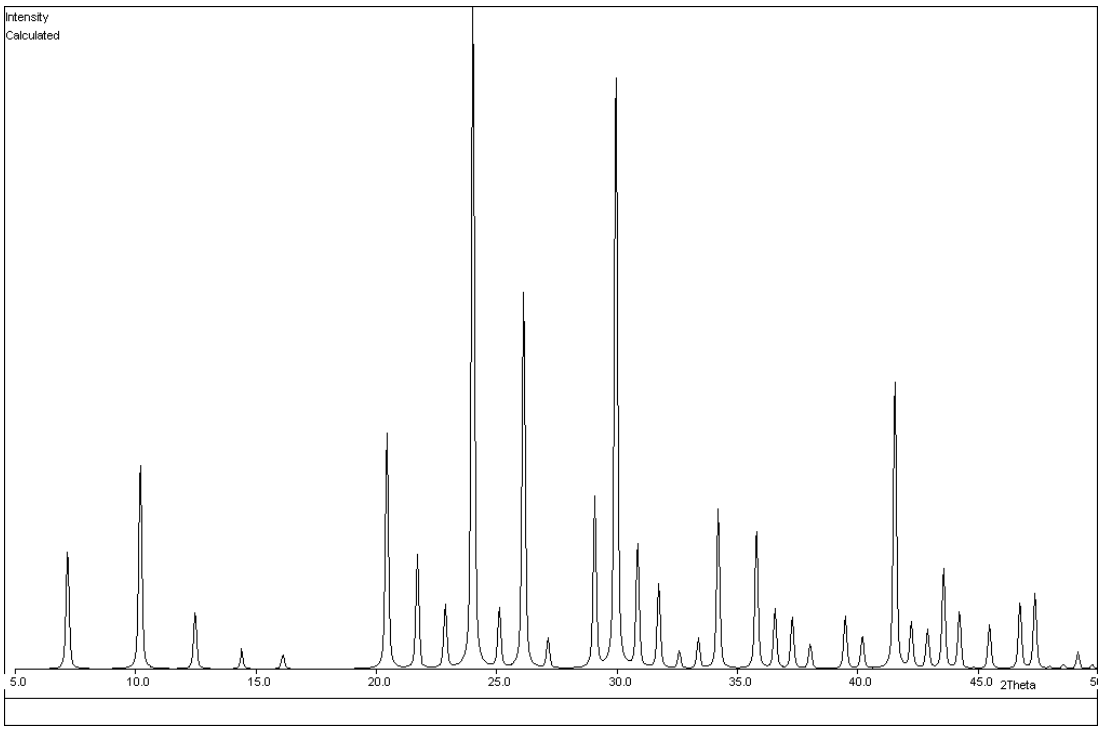

Figure 5.8: Predicted powder XRD pattern for caesium-exchanged zeolite A

The simulated and real patterns correspond reasonably well, although both differ from their Na-A and Ag-A counterparts. The first two peaks at ~7 and ~10° two theta are in the same 1:2 proportions in each of the patterns. The peak with largest intensity in both XRD patterns is at ~24° two theta.

The exchanged sample was then subjected to an occlusion reaction which caused the lattice parameter to increase to 24.583 Å. Despite repeated washings, a trace amount of caesium nitrate was still observed in the powder XRD pattern of the occluded sample, but these peaks were of low intensity. There were also some small peaks present which could not be assigned to zeolite A or caesium nitrate, which could indicate the presence of a superlattice.

It is believed that the level of caesium occlusion is quite low compared to that of silver, since further peak intensity changes are small. This may be caused by the comparatively larger Cs atomic radii (1.81 Å compared to 1.29 Å for silver).

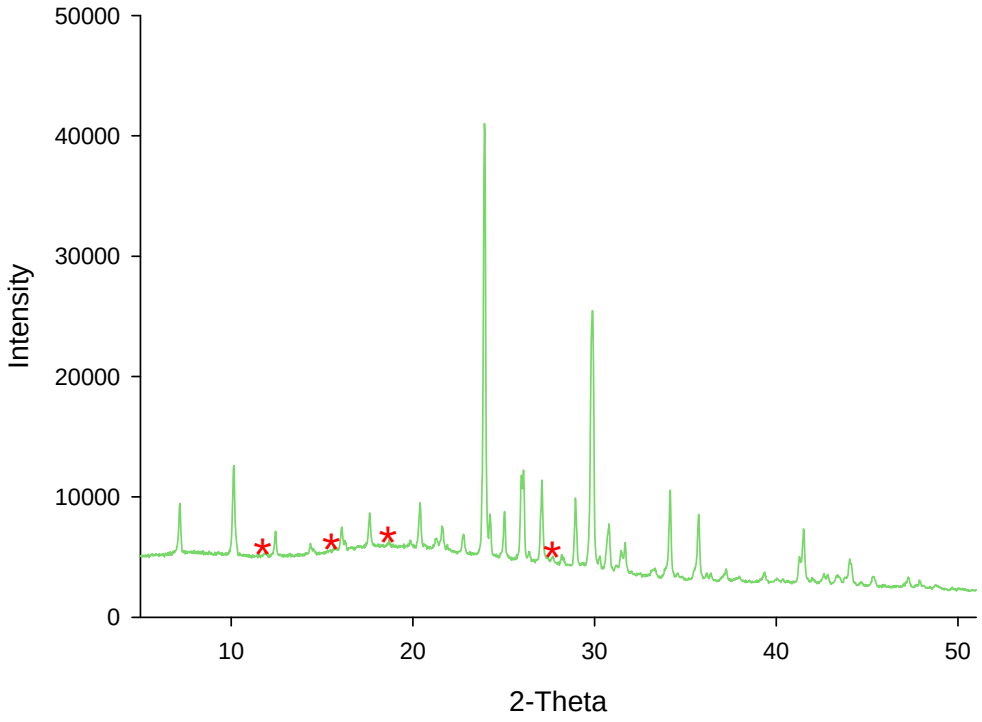

Figure 5.9: Powder XRD pattern of caesium exchanged zeolite A occluded with 5 g $CsNO_3$ at 450°C. * indicates unindexable peaks.

There was also evidence of peak splitting at higher 2 theta values. This could be the result of a second (possibly superlattice-containing) phase being present. It is possible that the four peaks which are marked with asterisks on Figure 5.9 were due to ordering of the caesium nitrate within the zeolite A, i.e. a superlattice, although it should be noted that these were not in similar positions to the superlattice peaks observed for zeolite A containing occluded silver nitrate. However, as the peaks were so small in relation to the zeolite A peaks, a full analysis would be very difficult.

5.3.4.1 Investigation of Possible Space Groups for the Caesium Superlattice

One possible explanation for the extra peaks in the X-ray diffraction pattern of zeolite A containing occluded caesium nitrate is a change in symmetry. As a consequence, potential new space groups must be considered which take account of the extra peaks. By analogy

with zeolite A containing silver nitrate, the first space groups considered were based closely on the original zeolite A structure: angles α, β and γ at 90°, and lattice parameters a, b and c related to the initial zeolite A unit cell measurement of a = 12.29 Å were examined. Cubic, tetragonal and orthorhombic space groups were considered. Table 5.3 details the space groups examined and the lattice parameters used. Analysis of the data was performed using the computer program Chekcell.

The orthorhombic groups were immediately dismissed as poor matches, whilst the cubic space groups did not predict any of the superlattice peaks. The tetragonal groups showed much more promise, and of those the best lattice parameters were found to be a = 12.29 Å and c = 17.38 Å. When going through the potential space groups, only the primitive lattices showed a good fit, i.e. the sample was not body centred.

Of the primitive tetragonal space groups, it is difficult to pick which best fits the data. The majority predict the extra peaks seen in the original diffraction pattern, but also predict more peaks which are not seen. It is possible that these peaks are not seen due to a high background (it has already been stated that the superlattice peaks which are seen are quite low in intensity).

This means that the potential space groups for the caesium superlattice are remarkably similar to that proposed for the silver superlattice. As has already been pointed out[22] the space groups for $(AgI)_n$-NaA and $(PbI_2)_n$-NaA are symmetrically related to the suggested space group of P4/nmm for $(AgNO_3)_9$-AgA, so it is not surprising that a similar space group would be appropriate for the caesium superlattice.

Table 5.3: Space Groups and Lattice Parameters Examined for the Caesium Superlattice

Cell Type	Space group Number	Space group Symbol	Lattice Parameters (Å)			Number of peaks predicted for 5 - 50°	Quality of peak fit
			a	b	c		
Cubic	221	Pm3m	12.29	12.29	12.29	54	Good, but no extra peaks
Cubic	226	Fm3c	24.58	24.58	24.58	70	Good, but no extra peaks
Tetragonal	75–142	All	12.29	12.29	24.58	250	Poor matches
Tetragonal	75–142	All	12.29	12.29	17.38	178	Only primitive groups offer a good match
Tetragonal	75–142	All	24.58	24.58	12.29	452	Poor matches
Orthorhombic	16–74	All	12.29	12.10	12.34	228	All very poor

Notes

1. There were 41 peaks observed between 5 and 50° in the powder XRD pattern for the sample containing a caesium superlattice.
2. The number of predicted peaks contains multiples of peaks in the same position, and is therefore greater than the number of peaks actually observed.

5.3.5 IR Analysis

Infrared spectroscopy was carried out on all samples, except those containing silver nitrate. The IR method used was the KBr disc technique, and due to the reaction between KBr and silver nitrate, samples occluded with this salt could not be studied.

The as-synthesised, sodium form of zeolite A was studied first. The IR spectrum (Figure 5.10) shows two water peaks, the largest at 3468 cm^{-1} and the other at 1654 cm^{-1}. The framework peaks are at lower wavenumbers, and include the intense TO_4 stretch at 1007 cm^{-1}.

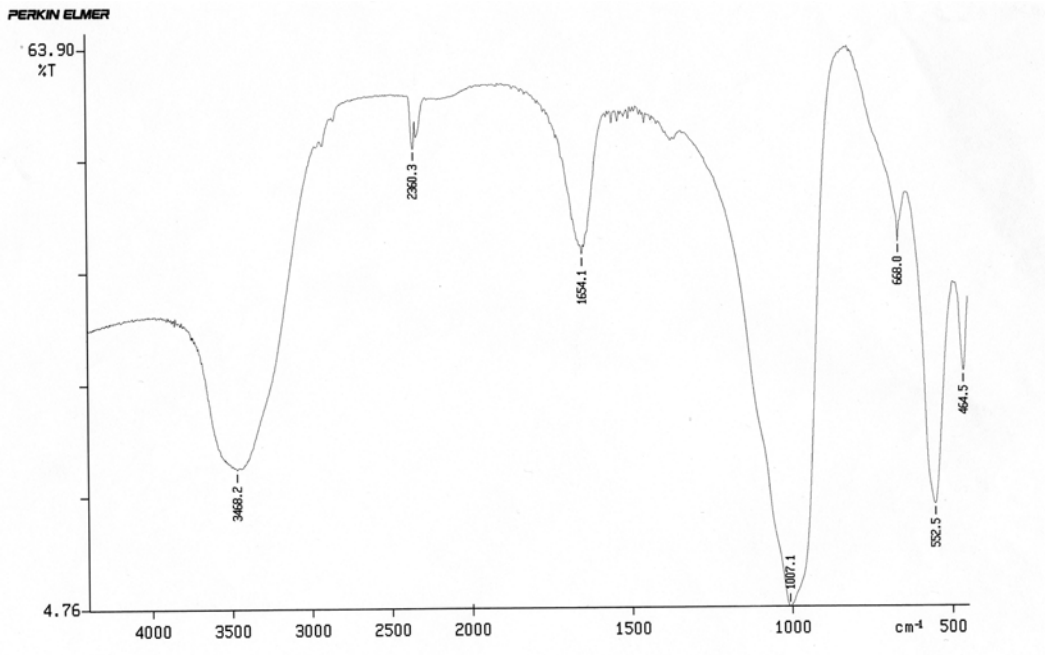

Figure 5.10: IR spectrum of as-synthesised zeolite A

The IR spectra of ion-exchanged samples appeared to be little different from the sodium zeolite A spectrum as the water peaks and the TO_4 stretch still appeared with a similar intensity and position. The reason no significant changes were observed in the spectra is most probably because the cations do not significantly affect the zeolite structure or water content. An example of one such spectrum is shown below for the rubidium-exchanged form

of zeolite A.

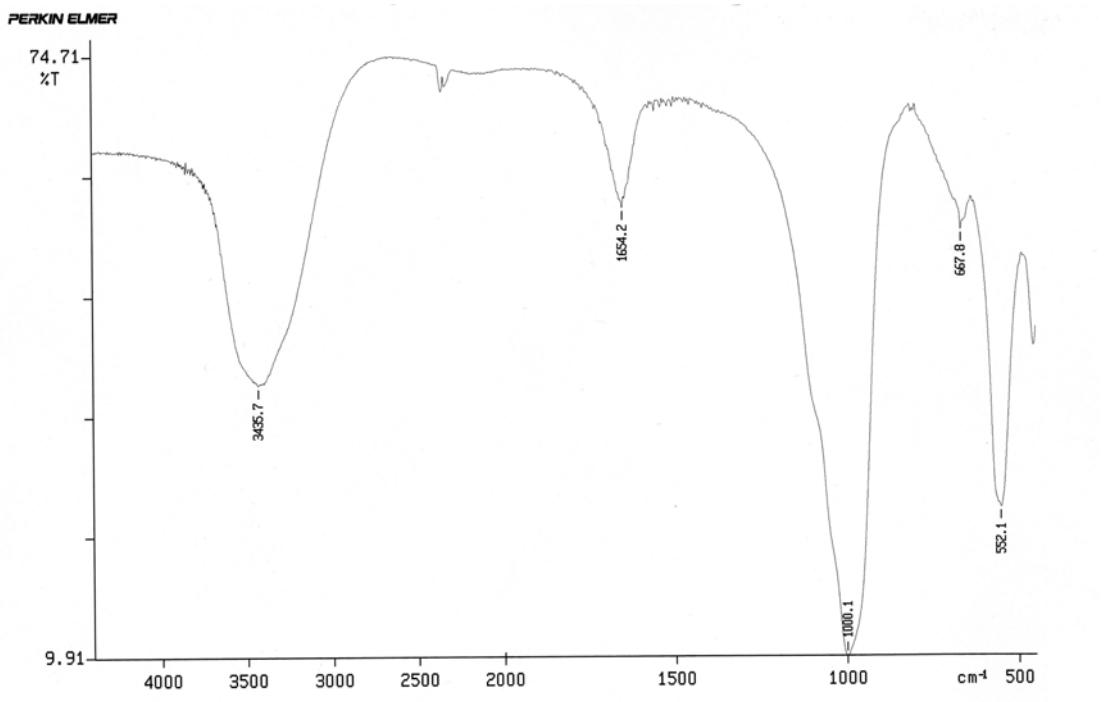

Figure 5.11: IR spectrum of rubidium-exchanged zeolite A.

Water peaks can be seen at 3436 cm^{-1} and 1654 cm^{-1}.

The framework peaks at lower wavenumbers include the major TO_4 stretch at 1007 cm^{-1}.

After occlusion reactions were performed with the lithium, rubidium and caesium nitrates, IR spectra were taken of the samples. In all cases, the intense water peak at 3468 cm^{-1} was greatly reduced in size. This shows that the incoming salts had caused a reduction in the level of water within the zeolite pores. The framework peaks remained the most intense, especially the TO_4 stretch at c.1000 cm^{-1}. In addition to the peaks seen for the original zeolite A, there are a couple of peaks arising from the presence of the nitrate anion, in particular a medium intensity peak at c.1384 cm^{-1}. The fact that there is a loss of intensity in the water peak and that there are peaks associated with the NO_3^- ion indicates that occlusion has occurred for all the samples examined. Figure 5.12 shows an IR spectrum for zeolite A

containing rubidium nitrate.

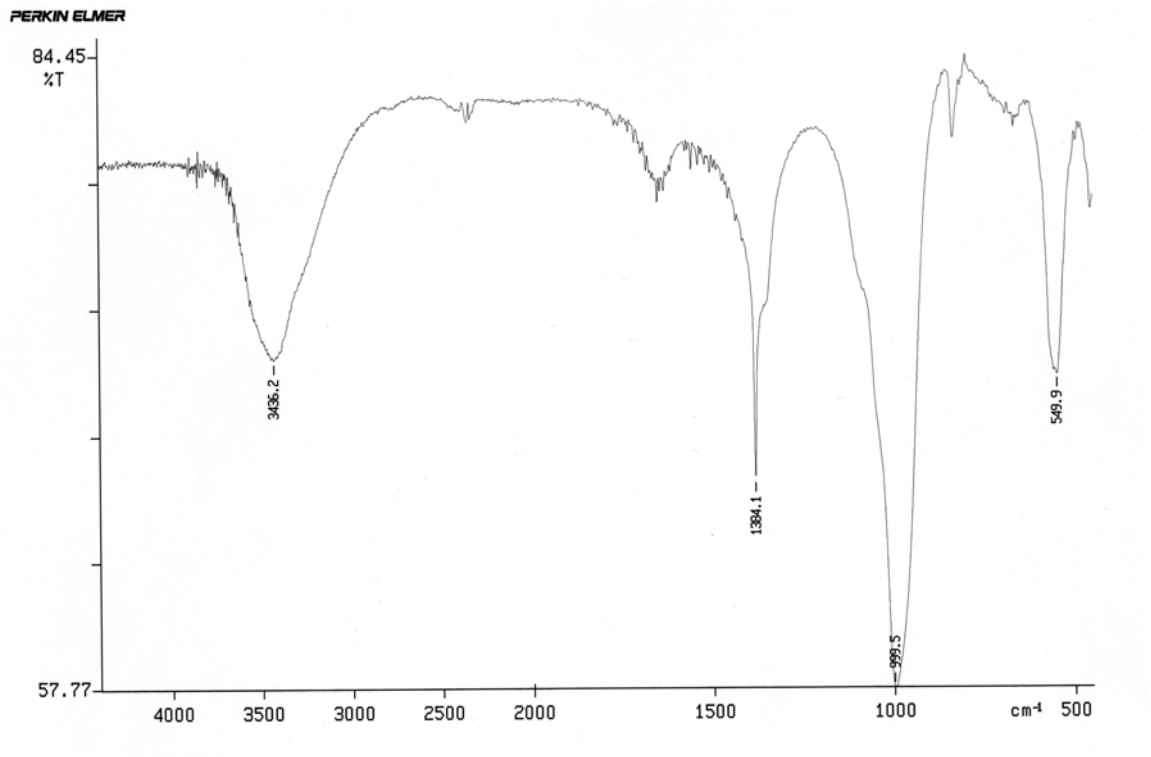

Figure 5.12: IR spectra of zeolite A after occlusion with rubidium nitrate.

The water peaks at 3436 cm^{-1} and 1654 cm^{-1} are reduced in size.

The framework TO_4 stretch at 1000 cm^{-1} remains the most intense peak in the spectra.

The new peak at 1384 cm^{-1} indicates the presence of a nitrate group within the zeolite.

The IR spectra for the caesium and lithium forms of zeolite A show similar trends in the peak intensities, as can be seen in Figures 5.13 and 5.14 on the following page. From these spectra it can be concluded that occlusion was successful and that the salts entered the zeolite framework.

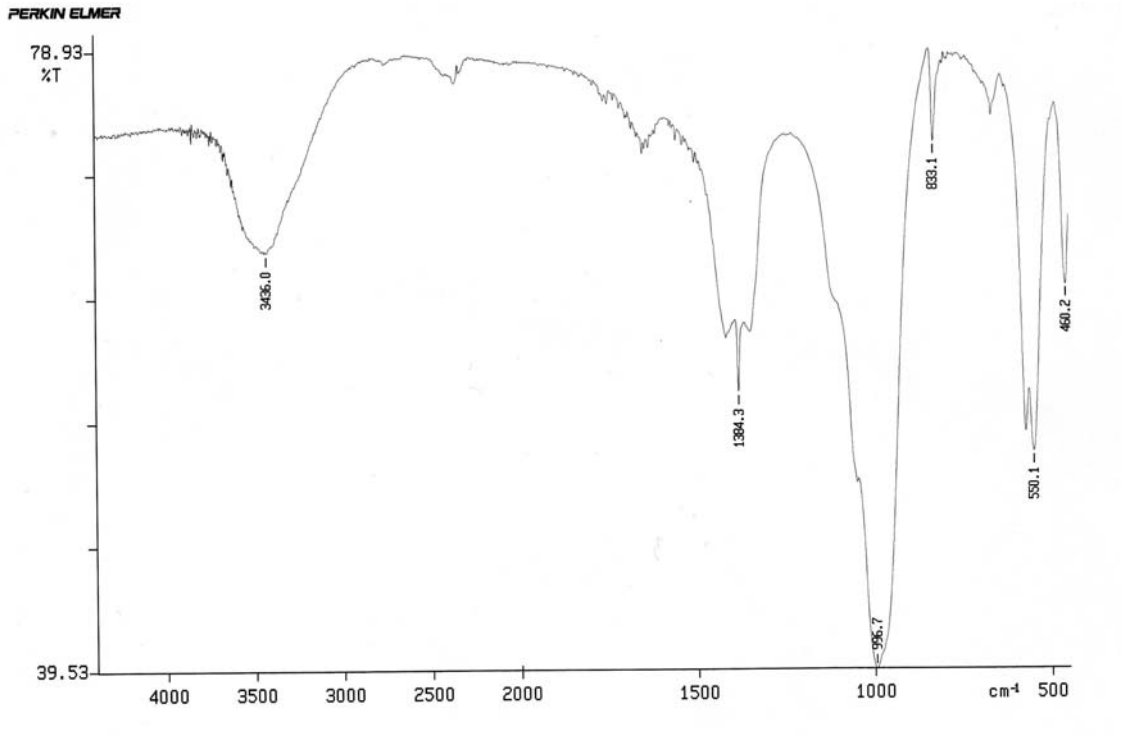

Figure 5.13: IR spectra of zeolite A after occlusion with caesium nitrate.

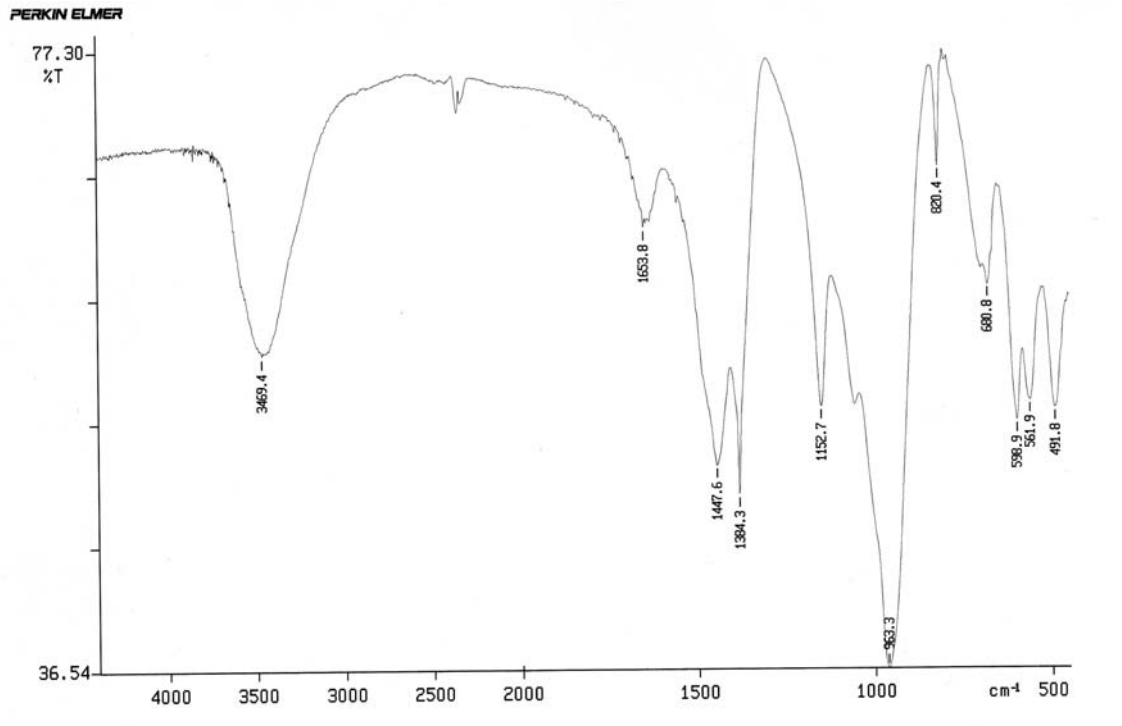

Figure 5.14: IR spectra of zeolite A after occlusion with lithium nitrate.

5.4 Conclusions

Work with different metal nitrate salts and zeolites has been performed to establish whether superlattice formation is a phenomenon seen in many reactions or whether it is unique to zeolite A and silver nitrate.

Unwashed samples showed only the metal nitrate pattern in their powder X-ray diffraction patterns. This was most likely due to the sample containing more salt than zeolite, and as a result the excess salt gave stronger peak intensities than the zeolite framework.

As zeolite ZK4 has an identical structure to zeolite A, and differs only in the amount of silicon and aluminium in the zeolite framework, it was thought that a superlattice might form on occlusion of silver nitrate. That occlusion did occur was seen in the relative peak intensities in the powder XRD patterns. However, despite identical reaction conditions being used, no extra peaks were observed in the powder X-ray diffraction pattern.

Given that the only difference between zeolite A and zeolite ZK4 is the quantity of aluminium in the framework, it is believed that this must in some way influence the formation of a superlattice. In theory, zeolite A, with its lower Si:Al ratio, should have more cations within the framework to counter the negative aluminium tetrahedra. As a consequence, there would be less void space to accommodate the silver nitrate units, so they may be forced into a particular orientation throughout the zeolite structure which would give rise to the superlattice.

The converse of the above argument is that zeolite ZK4, with its lower quantity of AlO_4 tetrahedra, cannot exchange as many cations as zeolite A. Whilst this would leave a greater

void space for the occluded salt units to occupy, the silver which is occluded must be accompanied by an equal number of nitrate ions. In zeolite A there are more silver cations present before the arrival of the occluded pairs of silver and nitrate ions, meaning that zeolite A has a greater proportion of silver to nitrate than zeolite ZK4. As it is the silver ions which contribute most to the powder X-ray diffraction pattern (and hence the superlattice peaks), perhaps there is not sufficient silver present in zeolite ZK4 to contribute to superlattice peaks.

When zeolite rho was used in the reaction with silver nitrate, unindexed peaks were observed if excess salt was used. These peaks did not correspond to zeolite rho, silver nitrate or known potential impurities. It is possible that these peaks were due to a superlattice formed by the silver nitrate. No extra peaks were seen when low levels of silver nitrate were used. This could be a result of washing removing some of the ions necessary for superlattice formation. However, it can be seen in the powder XRD pattern that some level of occlusion must have occurred, even at this low mass of silver nitrate, due to the alteration in relative peak intensities.

Other monovalent metal nitrates including those of lithium, rubidium and caesium were reacted with zeolite A in a series of ion exchange and occlusion reactions. When occluded, changes were observed in relative peak intensities in the powder XRD patterns, and these showed that occlusion of the salt had occurred. Only caesium nitrate caused the presence of unindexed peaks, but the relative intensities of the peaks were very low. Such low intensity peaks could imply that only in a part of the sample was a superlattice present.

Salt occlusion was confirmed to have occurred by IR spectroscopy for all except the silver nitrate-containing samples. The presence of nitrate peaks, and the reduction in intensity of the water peaks, indicated that the nitrate salts had entered the zeolitic framework. The

alteration in peak intensities in powder X-ray diffraction patterns also revealed that occlusion had been successful.

Further Work

Microwave synthesis of zeolites is a popular area of research and work is continually being published in this field. There are many reagent combinations which could be tried, as well as a whole range of zeolites yet to be synthesised in a microwave oven. Despite significant reductions in reaction times for some of the zeolites examined in this thesis, however, to date improvements have been insufficient to lead to the widespread adoption of microwave heating in the synthesis of zeolites on a laboratory or an industrial scale.

In this work, levels of silver occlusion in the samples of zeolite A occluded with silver nitrate have been estimated from TGA data, but this method has been shown to have limited reliability. To verify the true levels and assess the accuracy of TGA estimates, full chemical analysis should be carried out. A reduction in the relative intensity of low angle peaks on occlusion was found empirically to be a reliable indicator of the degree of salt occlusion in zeolites. Modelling studies could be carried out to place this observation on a sound theoretical basis.

Despite study spanning many decades, including a number of attempts at Rietveld refinement of powder neutron or powder X-ray diffraction data, the structure of silver nitrate in zeolite A remains unknown. Attempts to solve this problem using pair distribution function analysis are now in progress. Zeolites containing high levels of occluded silver ions are currently attracting interest for their potential bactericidal properties.

Work with other monovalent metal nitrates (lithium, rubidium and caesium) with a variety of zeolites (A, Rho and ZK4) appeared to be promising. The occlusion of caesium nitrate in a number of zeolites is currently being pursued in an attempt to tune the refractive index of

zeolite particles for optical applications. A wider “mix and match” approach could be taken, such that each zeolite is reacted with each metal nitrate. These experiments could be performed on both the hydrated and dehydrated zeolites. The work could also be expanded to examine other zeolites with a variety of other metals as nitrates, and with other anions.

The samples of zeolite rho with occluded silver nitrate, and zeolite A with occluded caesium nitrate showed non-framework peaks in their powder XRD patterns. Work to enhance the presence of these peaks and confirm the possible occurrence of superlattices in these compounds is planned.

References

References

Chapter 1: Introduction to Zeolites

1. Dyer, A.; "*An Introduction to Zeolite Molecular Sieves*", (1988) John Wiley & Sons, Inc.
2. Barrer, R.M.; *J. Chem. Soc.*, (1950) 2342–2350
3. Barrer, R.M.; "*Hydrothermal Chemistry of Zeolites*", (1982) Academic Press Inc., London.
4. Breck, D.W.; "*Zeolite Molecular Sieves*", (1974) John Wiley & Sons, Inc.
5. Smart, L.; Moore, E.; "*Solid State Chemistry: An Introduction*" 1st Edition, (1992) Chapman and Hall
6. Maxwell, I.E.; *Catal. Today*, **1** (1987) 385–413
7. Reháková, M.; Čuvanová, S.; Dzivák, M.; Rimár, J.; Gaval'ová, Z.; *Curr. Opin. Solid St. M.*, **8** (2004) 397–404
8. Li, Z.; *Micropor. Mesopor. Mater.*, **61** (2003) 181–188
9. http://www.zeoinc.com/zar1.shtml accessed in June 2006
10. http://www.atzzeoliti.it/applications.htm accessed in June 2006
11. Ozin, G.; *Adv. Mater.*, **4(10)** (1992) 612–649
12. Kühl, G.; in "*Verified Syntheses of Zeolitic Materials*", Robson, H. (Ed.) 2nd Edition (2001) Elsevier Science B.V. 19–20
13. Aiello, R.; Barrer, R.M.; *J. Chem. Soc. A*, (1970) 1470–1475
14. Lechert, H.; in "*Verified Syntheses of Zeolitic Materials*", Robson, H. (Ed.) 2nd Edition (2001) Elsevier Science B.V. 33–38
15. Jansen, J.C.; *Stud. Surf. Sci. Catal.*, **137** (2001) 205–211
16. Slangen, P.M.; Jansen, J.C.; van Bekkum, H.; *Microporous Mater.*, **9** (1997) 259–265
17. Freund, E.F.; *J. Cryst. Growth*, **34** (1976) 11–23

18. Davis, M.E.; Lobo, R.F.; *Chem. Mater.*, **4** (1994) 756–768

19. Kerr, G.T., Kokotailo, G.T.; *J. Am. Chem. Soc.*, **83** (1961) 4675

20. Kerr, G.T.; *Inorg. Chem.*, **5(9)** (1966) 1537–1539

21. Ikeda, T.; Kodaira, T.; Oh, T.; Nisawa, A.; *Micropor. Mesopor. Mater.*, **57** (2003) 249–261

22. Milton, R.M.; *US Patent No. 2,882,244*, (1959)

23. Breck, D.W.; *US Patent No. 3,130,007*, (1964)

24. Bieniok, A.; Hammonds, K.D.; *Micropor. Mesopor. Mater.*, **25** (1998) 193–200

25. Robson, H.E.; *US Patent No. 3,904,738*, (1975)

26. Edmondson, M.J.; *PhD Thesis, The University of Birmingham, UK*, (2002)

27. Robson, H.E.; Shoemaker, D.P.; Ogilvie, R.A.; Manor, P.C.; "*Molecular Sieves*" American Chemical Society "Advances in Chemistry" series **101**, (1973) 106–115

28. Callanan, L.H.; O'Connor, C.T.; van Steen, E.; *Micropor. Mesopor. Mater.*, **35–36** (2000) 163–172

29. MacLaren, I.; Cirre, J.; Ponton, C.B.; *J. Am. Ceram. Soc.*, **82(11),** (1999) 3242–3244

30. Yanagisawa, H.; Kanahara, S.; Nishioka, M.; Yamasaki, N.; *J. Nucl. Sci. Technol.*, **21(7)**, (1984) 558–560

31. Gallagher, S.A.; McCarthy, G.J.; *J. Inorg. Nucl. Chem.*, **43** (1981) 1773–1777

Chapter 2: Experimental Techniques

1. Cheetham, A.K; Day, P; *"Solid State Chemistry Techniques"*, Oxford, 5th Edition (1995)
2. Cullity, B.D.; *"Elements of X–ray Diffraction"*, Addison–Wesley Publishing Company, Inc., 3rd Edition (1967)
3. Hammond, C.; *"Introduction to Crystallography"*, Oxford University Press, Revised Edition (1992)
4. Atkins, P.W.: *"Physical Chemistry"*, Oxford University Press, 6th Edition, (2000)
5. West, A.R.; *"Basic Solid State Chemistry"* John Wiley and Sons Ltd. (1991)
6. Klinowski, J.; Ramdas, S.; Thomas, J.M.; Fyfe, C.A.; Hartman, J.S.; *J. Chem. Soc. Farad. T. 2*, **78** (1982) 1025–1050
7. Mägi, M.; Lippmaa, E.; Samoson, A.; Engelhardt, G.; Grimmer, A.–R.; *J. Phys. Chem. – US*, **88(8)** (1984) 1518–1521
8. Thomas, J.M.; Fyfe, C.A.; Ramdas, S.; Klinowski, J.; Gobbi, G.C.; *J. Phys. Chem. – US*, **86** (1982) 3061–3064
9. Breck, D.W.; *"Zeolite Molecular Sieves"*, Wiley (New York) (1974)
10. Watt, I.M.; *"The Principles and Practice of Electron Microscopy"*, Cambridge University Press (1997)
11. Amelinckx, A.; van Dyck, D; van Landuyt, J.; van Tendeloo, G. (Eds); *"Electron Microscopy: Principles and Fundamentals"*, VCH (1997)
12. Šušić, M.V.; Petranović, N.A.; Mioč, D.A.; *J. Inorg. and Nucl. Chem.*, **33** (1971) 2667–2675
13. Petranović, N.; Mioč, U.; Šušić, M.; Demitrijević, R.; Krstanović, I.; *J. Chem. Soc. Farad. T. 1*, **77** (1981) 379–389
14. Barrer, R.M. and Meier, W.M.; *J. Chem. Soc.*, (1958) 299–304

Chapter 3: Microwave Synthesis

1. Randall, J.T., Boot, H.A.H.; *US Patent No. 2,542,966*
2. Randall, J.T., Boot, H.A.H.; *US Patent No. 2,648,028*
3. Roussy, G.; Chenot, P.; *J. Phys. Chem.–US*, **85** (1981) 2199–2203
4. Chu, P.; Dwyer, F.G.; Vartuli, J.C.; *US Patent No. 4,778,666* (1988)
5. Jansen, J.C.; Arafat, A.; Barakat, A.K.; van Bekkum, H.; in "*Synthesis of Microporous Materials Vol. 1: Molecular Sieves*", Occelli, M.C. and Robson, H. (Eds.), (1992) 507–521, Van Nostrand Reinhold, New York
6. Slangen, P.M.; Jansen, J.C.; van Bekkum, H.; *Microporous Mater.*, **9** (1997) 259–265
7. Xu, X.; Yang, W.; Liu, J.; Lin, L.; *Sep. Purif. Technol.*, **25**, (2001) 241–249
8. Bonaccorsi, L.; Proverbio, E.; *J. Cryst. Growth*, **247**, (2003) 556–562
9. Arafat, A.; Jansen, J.C.; Ebaid, A.R.; van Bekkum, H.; *Zeolites*, **13** (1993) 162–165
10. De Araújo, L.R.G.; Cavalcante Jr., C.L.; Farias, K.M.; Guedes, I.; Sasaki, J.M.; Freire, P.T.C.; Melo, F.E.A.; Mendes–Filho, J.; *Mater. Res.*, **2(2)** (1999) 105–109
11. Katsuki, H.; Furuta, S.; Komarneni, S.; *J. Porous Mat.*, **8** (2001) 5–12
12. Zhao, J.P., Cundy, C., Dwyer, J.; *Stud. Surf. Sci. Catal.*, **105** (1997) 181–187
13. Park, M.; Komarneni, S.; *Micropor. Mesopor. Mater.*, **20**, (1998) 39–44
14. Jhung, S.H., Chang, J–S., Hwang, J.S., Park, S–E.; *Micropor. Mesopor. Mater.*, **64**, (2003) 33–39
15. Girnus, I., Jancke, K., Vetter, R., Richter–Mendau, J., Caro, J.; *Zeolites*, **15** (1995) 33–39
16. Cundy, C.S.; Plaisted, R.J.; Zhao, J.P.; *Chem. Commun.*, (1998) 1465–1466
17. Jansen, J.C.; *Stud. Surf. Sci. Catal.*, **137** (2001) 205–211
18. Mintova, S.; Valtchev, V.; *Micropor. Mesopor. Mater.*, **55**, (2002) 171–179
19. Li, Q.; Mihailova, B.; Creaser, D.; Sterte, J.; *Micropor. Mesopor. Mater.*, **40**, (2000) 53–62

20. Hamilton, K.E., Coker, E.N., Sacco Jr., A., Dixon, A.G., Thompson, R.W., *Zeolites*, **13**, (1993) 645–653

21. Lechert, H.; in "*Verified Syntheses of Zeolitic Materials*", Robson, H. (Ed.) 2nd Edition (2001) Elsevier Science B.V., 33–38

22. Donahoe, R.J.; Liou, J.G.; *Geochim. Cosmochim. Ac.*, **49** (1985) 2349–2360

23. Kodaira, T.; Miyazawa, K.; Ikeda, T.; Kiyozumi, Y.; *Micropor. Mesopor. Mater.*, **29** (1999) 329–337

24. Barrer, R.M., Mainwaring, D.E.; *J. Chem. Soc. Dalton*, (1972) 1254–1259

25. Connor, W.C.; Tompsett, G.; Lee, K–H.; Yngvesson, S.; *J. Phys. Chem. B*, **108** (2004) 13913–13920

26. Galema, S.; *Chem. Soc. Rev.*, **26** (1997) 233–238

27. Mingos, D.M.P.; Baghurst, D.R.; *Chem. Soc. Rev.*, **20**, (1991) 1–47

28. Rao, K.J., Vaidhyanathan, B., Ganguli, M., Ramakrishnan, P.A.; *Chem. Mater.* **11** (1999) 882–895

29. Cundy, C.S.; *Collect. Czech. Chem. C.*, **63** (1998) 1699–1723

30. Edmondson, M.J.; PhD Thesis, The University of Birmingham, UK. (2002)

31. Robson, H.E., Shoemaker, D.P., Ogilvie, R.A., Manor, P.C.; in "*Molecular Sieves*", eds. Meier, W.M. and Uytterhoeven, J.B.; *Adv. Chem. Ser.*, **121**, (1973) 106–115

32. Yanagisawa, K., Kanahara, S., Nishioka, M., Yamasaki, N.; *J. Nucl. Sci. Technol.*, **21**(7) (1984) 558–560

33. Tompsett, G.A., Connor, W.C., Yngvesson, K.S.; *ChemPhysChem*, **7**, (2006) 296–319

34. Gallagher, S.A., McCarthy, G.J.; *J. Inorg. Nucl. Chem.*, **43** (1981) 1773–1777

35. Data taken from www.iza–online.org

36. MacLaren, I., Cirre, J., Ponton, C.B.; *J. Am. Ceram. Soc.*, **82**(11) (1999) 3242–3244

37. Kormarneni, S. and White, W.B. in "*Scientific Basis for Nuclear Waste Management*", Moore, J.G. (Ed.) Volume 3 (1981) 387–396, Plenum, New York

38. Querol, X., Alastuey, A., Lopez–Soler, A., Plana, F., Andrés, J.M., Juan, R., Ferrer, P., Ruiz, C.R.; *Environ. Sci. Technol.*, **31** (1997) 2527–2533

39. Sathupunya, M., Gulari, E., Wongakasemjit, S.; *J. Eur. Ceram. Soc.*, **22** (2002) 2305–2314

Chapter 4: Occlusion Reactions with Silver Nitrate

1. Pabalan, R.T. and Bertetti, F.P., in "*Reviews in Mineralogy and Geochemistry – Volume 45*", eds. Bish, B.L. and Ming, D.W. Mineralogical Society of America, Washington D.C., (2001) 453–518
2. Dyer, A.; "An Introduction to Zeolite Molecular Sieves" John Wiley and Sons Ltd. (1988)
3. Colella, C.; *Miner. Deposita*, **31** (2001) 554–562
4. Park, M.; Choi, C.L.; Kim, J.S.; Lee, D.H.; Kim, K.S.; Heo, N.H.; Choi, J.; *Micropor. Mesopor. Mater.*, **62** (2003) 1–7
5. Park, M.; Shin, S.C.; Choi, C.L.; Lee, D.H.; Lim, W.T.; Kormarneni, S.; Kim, M.C.; Choi, J.; Heo, N.H.; *Micropor. Mesopor. Mater.*, **50** (2001) 91–99
6. Reháková, M.; Čuvanová, S.; Dzivák, M.; Rimár, J.; Gaval'ová, Z.; *Curr. Opin. Solid St. M.*, **8** (2004) 397–404
7. Li, Z.; *Micropor. Mesopor. Mater.*, **61** (2003) 181–188
8. Edmondson, M.J., Zhou, W., Sieber, S., Jones, I.P., Gameson, I., Anderson, P.A., Edwards, P.E.; *Adv. Mater.*, **13(21)** (2001) 1608–1611
9. Barrer, R.M. and Meier, W.M.; *J. Chem. Soc.*, (1958) 299–304
10. Yoshida, S., Harada, A., Kamioka, K., Nakano, M.; *B. Chem. Soc. Jpn.*, **77** (2004) 387–391
11. Kodaira, T., Ikeda, T., Takeo, H.; *Chem. Phys. Lett.*, **300** (1999) 499–503
12. Kodaira, T., Ikeda, T., Takeo, H.; *Eur. Phys. J. D*, **9** (1999) 601–604
13. Kodaira, T., Ikeda, T.; *Eur. Phys. J. D*, **24** (2003) 299–302
14. Petranović, N., Mioč, U., Šušić, M., Dimitrijević, R., Kristanović, I.; *J. Chem. Soc. Farad. T1*, **77** (1981) 379–389
15. Pavlovskaya, G.E., Horton-Garcia, C.F., Dybowski, C., Corbin, D.R., Meersmann, T.; *J. Phys. Chem. B*, **108** (2004) 1584–1589

16. Sun, T., Seff, K.; *Chem. Rev.*, **94(4)** (1994) 857–870

17. Matsuoka, M., Ju, W-S., Yamashita, H., Anpo, M.; *J. Photoch. Photobio., A*, **160** (2003) 43–46

18. Thomas, R.L., Sarkar, A.K., Kohata, K., Abbas, S.A., Matta, K.L.; *Tetrahedron Lett.*, **31 (20)** (1990) 2825–2828

19. Laugier, J. and Bochu, B.; *Poudrix version 2*, © U.D.Altermatt and I.D.Brown

20. *Zeolites*, **16** (1996) 330–802

21. Barrer, R.M., Meier, W.M.; *T. Faraday Soc.*, **54** (1958) 1074–1085

22. Kim, Y., Seff, K.; *J. Phys. Chem.*, **82** (1978) 1071–1077

23. Viertelhaus, M., Taylor, A.E., Kloo, L., Gameson, I., Anderson, P.A.; *J. Chem. Soc. Dalton*, (2006) 2368–2373

24. "*CELL*", M.F. Pye, ICL, The University of Oxford (modified by C. Greaves, School of Chemistry, The University of Birmingham)

Chapter 5: Occlusion Reactions with Other Nitrates

1. Barrer, R.M. and Meier, W.M.; *J. Chem. Soc.* (1958) 299–304
2. Kerr, G.T.; *Inorg. Chem.*, **9(5)** (1966) 1537–1539
3. Park, M.; Choi, C.L.; Kim, J.S.; Lee, D.H.; Kim, K.S.; Heo, N.H.; Choi, J.; *Micropor. Mesopor. Mater.*, **62** (2003) 1–7
4. Kovacheva, P., Arishtirova, K., Davidova, N.; *Appl. Catal. A – Gen.*, **149** (1997) 277–287
5. Lexa, D. and Johnson, I.; *Metall. Mater. Trans. B*, **32B** (2001) 429–435
6. Yoshida, S., Harada, A., Kamioka, K., Nakano, M.; *B. Chem. Soc. Jpn.*, **77** (2004) 387–391
7. Song, S.H., Kim, U.S., Kim, Y., Seff, K.; *J. Phys. Chem.*, **96** (1992) 10937–10941
8. Firor, R.L. and Seff, K.; *J. Am. Chem. Soc.*, **99** (1977) 1112–1117
9. Pluth, J.J. and Smith, S.V.; *J. Am. Chem. Soc.*, **105** (1983) 2621–2624
10. Ciraolo, M.F., Hanson, J.C., Grey, C.P.; *Micropor. Mesopor. Mater.*, **49** (2001) 111–124
11. Igarashi, M., Kodaira, T., Ikeda, T., Itoh, M., Shimizu, T., Goto, A., Nozue, Y.; *Physica B*, **327** (2003) 72–78
12. Dyer, A.; "*An Introduction to Zeolite Molecular Sieves*" (1988) John Wiley & Sons, Inc.
13. Lima, E.J., Ibarra, I.A., Vera, M.A., Lara, V.H., Bosch, P., Bulbulian, S.; *J. Phys. Chem. B*, **108** (2004) 12103–12110
14. Bonelli, B., Ribeiro, M.F.; Antunes, A.P.; Valange, S.; Gabelica, Z.; Garrone, E.; *Micropor. Mesopor. Mater.*, **54(3)** (2002) 305–317
15. Ryu. K.S., Bae. M.N., Kim. Y., Seff. K.; *Micropor. Mesopor. Mater.*, **71** (2004) 65–75
16. Monticelli, O., Loenders, R., Jacobs, P.A., Martens, J.A.; *Appl. Catal. B – Environ.* **21** (1999) 215–220

17. Simon, A., Köhler, J., Keller, P., Weitkamp, J., Buchholz, A., Hunger, M.; *Micropor. Mesopor. Mater.*, **68** (2004) 143–150

18. Doskocil, E.J. and Davis, R.J.; *J. Catal.*, **188(2)** (1999) 353–364

19. Edmondson, M.J.; *PhD Thesis*, The University of Birmingham, Birmingham, UK (2002)

20. Bieniok, A.; Hammonds, K.D.; *Micropor. Mesopor. Mater.*, **25** (1998) 193–200

21. Heo, N-H., Dejsupa, C., Seff, K.; *J. Phys. Chem.*, **91** (1987) 3943–3944

22. Viertelhaus, M., Taylor, A.E., Kloo, L., Gameson, I., Anderson, P.A.; *J. Chem. Soc. Dalton*, (2006) 2368–2373

Appendices

Appendices

Appendix 1

Table of lattice parameters calculated for samples with occluded silver nitrate

Mass of $AgNO_3$ (g)[a]	Ions per 24 Å unit cell	Washed?	a (Å)	ESD
5	759	No	$AgNO_3$ pattern	
5	759	Yes	24.864	0.004
4	607	No	$AgNO_3$ pattern	
4	607	Yes	24.723	0.005
3	455	No	$AgNO_3$ pattern	
3	455	Yes	24.715	0.004
2	304	No	$AgNO_3$ pattern	
2	304	Yes	24.709	0.004
1	152	No	$AgNO_3$ pattern	
1	152	Yes	24.737	0.007
0.78	118	No	$AgNO_3$ pattern	
0.78	118	Yes	24.773	0.006
0.7	106	No	24.726	0.007
0.7	106	Yes	24.695	0.007
0.6	91	No	24.694	0.006
0.6	91	Yes	24.663	0.005
0.5	76	No	24.718	0.01
0.5	76	Yes	24.687	0.004
0.4	61	No	24.692	0.009
0.4	61	Yes	24.513	0.019
0.34	52	No	24.698	0.012
0.34	52	Yes	24.706	0.013
0.3	46	No	24.71	0.006
0.3	46	Yes	24.685	0.005
0.25	38	No	24.565	0.008
0.25	38	Yes	24.563	0.007
0.2	30	No	24.56	0.006
0.2	30	Yes	24.554	0.005
0.13	19	No	24.571	0.004
0.13	19	Yes	24.563	0.004
0	0[b]	No	24.589	0.004
0	0[b]	Yes	24.558	0.004

Notes:

a). Mass given is per gram of silver-exchanged zeolite A.

For all experiments listed, the heating and cooling were both 60°C/hour and the reaction was performed at 260°C for 8 hours

b). The reaction with 0 g $AgNO_3$ involved heating zeolite A alone.

Appendix 2

Table of TGA data used to plot graphs in Section 4.4

Mass of $AgNO_3$ (g)	Ions per 24 Å unit cell	Washed?	% total weight loss	% water	$\%NO_3^-$
Na-Zeolite A	-	-	19.19	19.19	-
Ag-Zeolite A	-	-	12.76	12.76	-
5.00	759	No	-	-	-
5.00	759	Yes	7.97	3.14	4.83
4.00	607	No	-	-	-
4.00	607	Yes	9.58	2.99	6.59
3.00	455	No	-	-	-
3.00	455	Yes	14.18	5.14	9.04
2.00	304	No	-	-	-
2.00	304	Yes	9.43	3.51	5.92
1.00	152	No	15.52	1.77	13.74
1.00	152	Yes	6.05	2.68	3.37
0.78	118	No	12.65	2.06	10.58
0.78	118	Yes	5.92	3.00	2.92
0.70	106	No	10.24	2.45	7.79
0.70	106	Yes	6.02	3.02	3.00
0.60	91	No	8.60	2.65	5.95
0.60	91	Yes	5.62	2.99	2.63
0.50	76	No	7.33	2.79	4.54
0.50	76	Yes	5.58	2.44	3.14
0.40	61	No	8.93	2.95	5.98
0.40	61	Yes	7.58	5.65	1.93
0.34	52	No	-	-	-
0.34	52	Yes	7.27	5.21	2.06
0.30	46	No	7.08	2.81	4.26
0.30	46	Yes	5.80	2.73	3.07
0.25	38	No	8.67	6.80	1.88
0.25	38	Yes	8.88	7.46	1.41
0.20	30	No	9.77	7.89	1.88
0.20	30	Yes	9.33	7.58	1.76
0.13	19	No	9.44	8.71	0.73
0.13	19	Yes	10.67	9.33	1.34
0.00	0	No	12.62	11.94	0.68
0.00	0	Yes	12.61	11.90	0.71

Appendix 3

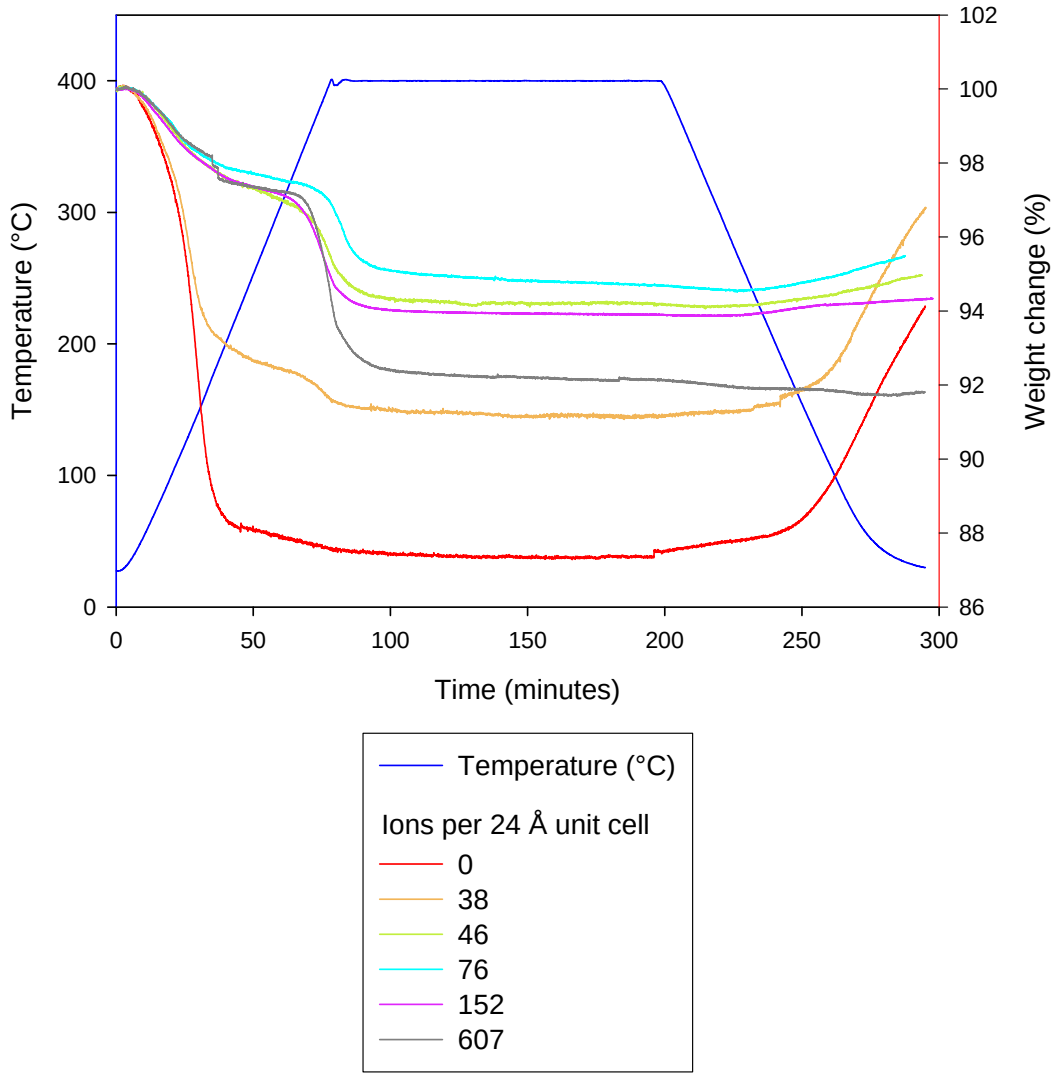

Figure A.1: TGA traces from washed samples of zeolite A following occlusion with silver nitrate ions

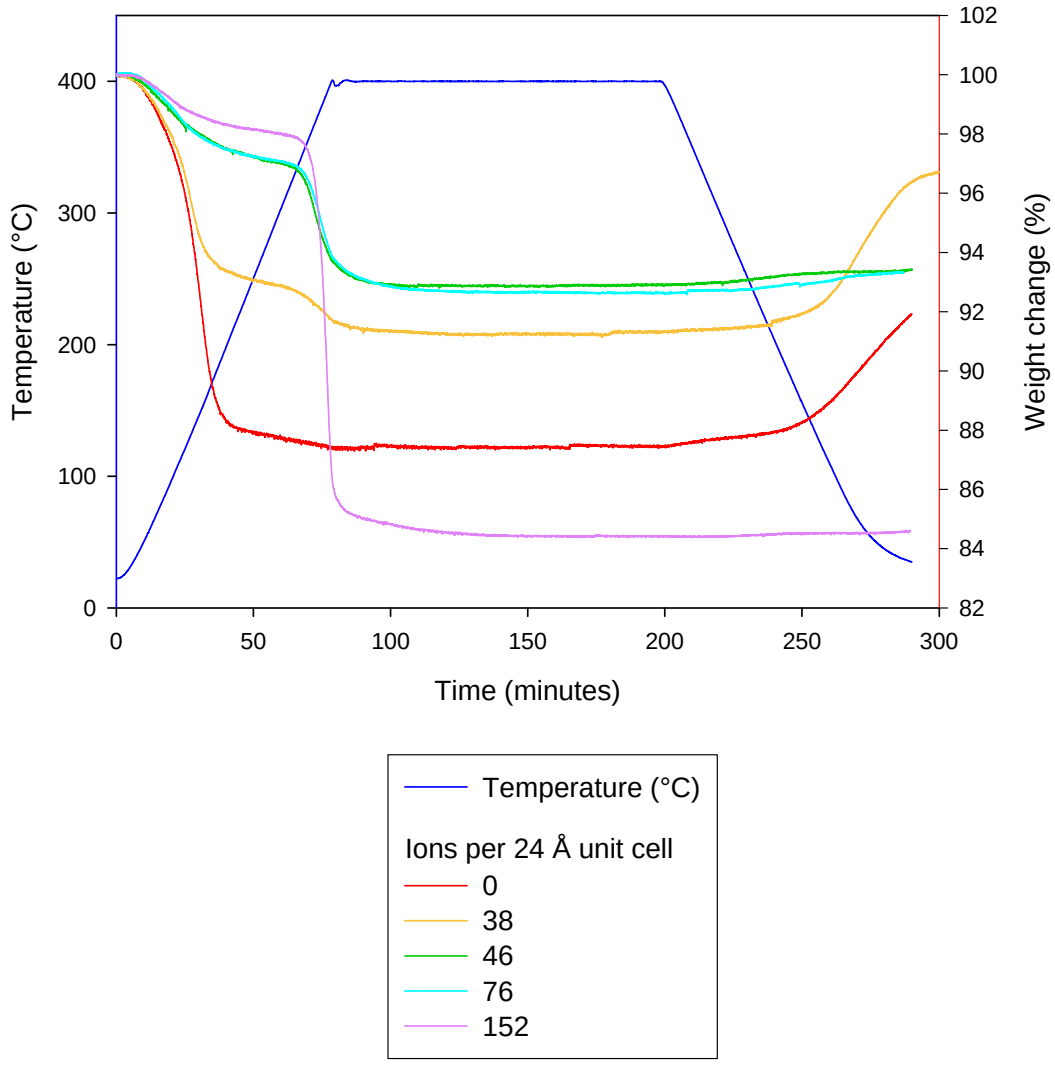

Figure A.2: TGA traces from unwashed samples of zeolite A following occlusion with silver nitrate ions